


GEOLOGICAL MODELING AND RESERVOIR SIMULATION OF UMIAT:

A LARGE SHALLOW OIL ACCUMULATION

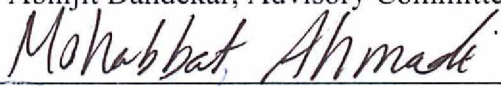
By

Iman Oraki Kohshour

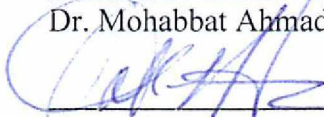
RECOMMENDED:



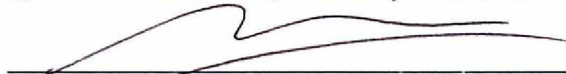
Dr. Abhijit Dandekar, Advisory Committee Member



Dr. Mohabbat Ahmadi, Advisory Committee Chair



Dr. Catherine Hanks, Advisory Committee Co-Chair

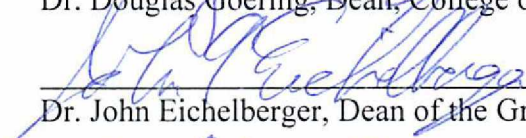


Dr. Abhijit Dandekar, Department Chair, Petroleum Engineering

APPROVED:



Dr. Douglas Goering, Dean, College of Engineering and Mines



Dr. John Eichelberger, Dean of the Graduate School



Date

**GEOLOGICAL MODELING AND RESERVOIR SIMULATION OF UMIAT:
A LARGE SHALLOW OIL ACCUMULATION**

A
THESIS

Presented to the Faculty
of the University of Alaska Fairbanks

in Partial Fulfillment of the Requirements
for the Degree of

MASTER OF SCIENCE

By
Iman Oraki Kohshour, M.S.

Fairbanks, Alaska

May 2013

Abstract

Current high oil price and availability of new technologies allow re-evaluation of oil resources previously considered uneconomic. Umiat oil field is one such resource: a unique, shallow (275–1055 feet), low-pressure (200–400 psi) reservoir within the permafrost zone located north of the Arctic Circle, 80 miles west of Trans Alaska Pipeline System (TAPS) with an estimated 1.5 billion barrel of oil-in-place.

This thesis presents a reservoir model that incorporates recently identified permeability anisotropy patterns within the Cretaceous Nanushuk sandstone reservoir to evaluate various potential mechanisms such as horizontal wells and immiscible gas injections. The simulation model focuses on the Lower Grandstand which is identified as a better reservoir rock. The reservoir temperature is assumed at 26 °F and gas is injected at the same temperature to maintain equilibrium with the permafrost and prevent any well integrity problems.

An optimum horizontal well length of 1500 ft was found and applied for all simulation cases. The simulation results show that with 50 years of lean gas injection, recovery factors for the base case and case of 600 psi injection pressures are 12% and 15%, respectively, keeping all other parameters constant.

Table of Contents

	Page
Signature Page	i
Title Page	v
Abstract	iii
Table of Contents	iv
List of Appendices.....	viii
List of Figures	viii
List of Tables	xiv
Disclaimer	xvi
Acknowledgments	xvii
Chapter 1 Introduction	1
1.1 Overview.....	1
1.2 Objective of the Study	4
Chapter 2 Background.....	6
Abstract	iii
Table of Contents	iv
Chapter 1 Introduction	1
Chapter 2 Background.....	6
2.4.1 Incentives for Reservoir Simulation	14
2.4.2 Designing the Simulation Model	15
2.5 Horizontal Wells.....	17

2.6 Gas Injection.....	19
	Page
2.7 Gas Hydrate	21
Chapter 3 Geologic Modeling, Methodologies, and Sources of Data.....	24
3.1 Petrophysical Property Modeling	24
3.2 Permeability Anisotropy	31
3.3 Optimal Geologic Grid Design for Simulation.....	33
3.4 Model Geometry.....	37
3.5 Modeling of Water Saturation: Concepts and Challenges.....	40
3.6 Application of Petrophysical Cut-offs.....	47
3.7 Monte Carlo Estimation of OOIP.....	51
3.8 Uncertainty Parameter Ranking by Multiple Realizations	53
Chapter 4 Simulation Model: Preparation of Input Data for Dynamic Model	59
4.1 Rock and Fluid Data	59
4.1.1 Relative Permeabilities to Oil and Gas	59
4.1.2 Relative Permeabilities to Oil and Water	67
4.1.3 Capillary Pressure.....	68
4.1.4 Fluid Properties.....	68
4.2 Initializing Model Based on Initial Reservoir Conditions.....	70
4.3 Design of Production and Injection Wells.....	71
Chapter 5 Results.....	79
5.1 Oil Recovery by Gas Injection (base case).....	79
5.2 Grid Size Optimization	80

	Page
5.3 Parameter Optimization	82
5.3.1 Horizontal Well Length	82
5.3.2 Injection Pressure	85
5.4 Sensitivity Analysis	87
5.4.1 Permeability Anisotropy	87
5.4.2 Relative Permeability and End Points Saturations	92
5.4.3 Producing GOR	101
5.5 Discussion	104
Chapter 6 Conclusions and Recommendations	107
6.1 Conclusions	107
6.2 Recommendations	110
References	112
Nomenclature	117

List of Appendices

	Page
Appendix A. Optimal Layer Design Algorithm	119
Appendix B. New Well Pick Data	123
Appendix C. Kelly Bushing Depths and Tie-in Points	126
Appendix D. Economic Model	128
Appendix E. Digital Project Archive	132

List of Figures

	Page
Figure 1: Lithology log of Umiat well #11 (Godabrelidze, 2010).....	3
Figure 2: Umiat field location (Gates and Caraway 1960).....	6
Figure 3: Location of Umiat wells (modified from Gates and Caraway 1960).....	8
Figure 4: Total uncertainty analysis in reservoir modeling	14
Figure 5: Schematic of a horizontal & vertical well drainage area (Joshi, 1990).....	18
Figure 6: Different stages of oil recovery with approval of SPE technical committee (modified from oil & gas journal, March 20, 2000)	19
Figure 7: Umiat reservoir temperature and pressure conditions superimposed on the hydrate equilibrium curves (Modified from Sloan and Koh, 2007).....	22
Figure 8: Horizon model of the previous Umiat geologic model (Levi-Johnson, 2010) and the updated horizon model with LGS divided into three sub-formations.....	25
Figure 9: New workflow for the entire modeling procedure	26
Figure 10: Porosity variogram result of sand in the LGS in X-Y directions (Axes in feet)	28
Figure 11: Permeability variogram result of sand in the LGS in X-Y directions (Axes in feet)	28
Figure 12: 2D distribution of porosity in uppermost Layer of LGS formation for one realization.....	29
Figure 13: 2D distribution of porosity in uppermost Layer of LGS formation	30
Figure 14: Histogram analysis for the permeability in the LGS formation	30
Figure 15: Histogram analysis for the porosity in the LGS formation	31

	Page
Figure 16: Permeability anisotropy ratio data versus depth for the well #9 (data collected from Shimer, G, personal communication, 2012).....	32
Figure 17: Permeability distribution in vertical direction, K (md) in layer #1 of LGS	33
Figure 18: Relation between heterogeneity and number of layers in Z direction.....	34
Figure 19: Histogram distribution for layer thickness in LGS formation	35
Figure 20: Grid view of permeability in x direction for layer #1 with grid dimensions of 600 ft * 600 ft.....	36
Figure 21: Grid view of permeability in x direction for layer #1 with grid dimensions of 400 ft * 400 ft.....	36
Figure 22: Grid view of permeability in x direction for layer #1 with grid dimensions of 200 ft * 200 ft.....	37
Figure 23: a (left): Inconsistencies in model caused by new data	38
Figure 23.b (right): Inconsistencies in model caused by new data.....	38
Figure 24: Design of structural framework incorporating new well pick data; note that the circles show the well pick data and the blue surface shows the uppermost layer of the Middle LGS formation which is layer #19	39
Figure 25: Grid view of the full field model with 500,000 active cells and 90*70*78 dimensions. The colors represent the grid cell thickness.....	40
Figure 26: Semi-log plot of (K/Φ) vs. Φ in the LGS formation	41
Figure 27: Oil-water capillary pressure data	44
Figure 28: Using a simplified look-up function to incorporate Sw height functions	45
Figure 29: Water saturation height function for different rock types.....	46

Figure 30: Modeling of water saturation in Umiat reservoir by use of capillary height function in upper part of LGS.....	47
	Page
Figure 31: Application of porosity cut-off and its effect on the oil in place.....	49
Figure 32: Application of porosity cut-off and its effect on OOIP by use of RIR parameter.....	49
Figure 33: Application of porosity cut-off and its effect on actnum by use of CIR parameter.....	50
Figure 34: Maximizing the exclusion of non-reservoir rocks from the model, the circles show the area hit by application of cut-offs	51
Figure 35: Graphical representation of Monte Carlo simulation for 10,000 runs for LGS	53
Figure 36: Uncertainty in fault interpretation (Poete, 2012)	54
Figure 37: Uncertainty to oil water contact in Umiat reservoir.....	55
Figure 38: Uncertainty parameter ranking in terms of contribution to STOOIP.....	58
Figure 39: Relative permeability to gas in presence of ice for core 60	60
Figure 40: Relative permeability to gas in presence of oil for core 60.....	60
Figure 41: Relative permeability to gas after including the non-Darcy effect	61
Figure 42: Relative permeability to oil & gas after Including the non-Darcy effect.....	62
Figure 43: Input relative permeability to oil & gas for rock type #1 as input to simulator	66
Figure 44: Input relative permeability to oil & gas for rock type #2 as input to simulator	66

Figure 45: Input relative permeability to oil and gas for rock type #3 as input to simulator	67
	Page
Figure 46: Relative permeability to oil & water as input to simulator for all three rock types	68
Figure 60: Average reservoir pressure and field producing gas oil ratio for different anisotropy ratios.....	
Figure 47: The proposed well pattern for the Umiat drilling program (modified from Linc Energy, 2012).....	72
Figure 48: Well targeting and trajectory design in RMS Irap TM (courtesy of Roxar manual guide).....	75
Figure 49: The design of well model	76
Figure 50: The final well profile model. The well lines have been magnified for better visualizations. Note the blue line show the production wells and the red line shows the injection wells.....	77
Figure 51: Producing GOR for two grid systems with different dimensions	81
Figure 52: Well oil rate for two grid systems with different dimensions	81
Figure 53: Field cumulative oil production and field oil production rates for two different horizontal well lengths.....	83
Figure 54: Pressure drop vs. oil rates for two different horizontal well lengths	84
Figure 55: Field cumulative oil production, field oil production rates, and producing GOR for different gas injection pressures.....	86
Figure 56: Average reservoir pressure for different gas injection pressures	86

Figure 57: A vertical view with a horizontal well and different configurations of well drainage area with respect to permeability anisotropy (GEKEngineering.com).....	87
Figure 58: Natural fractures and their orientation with respect to permeability anisotropy in horizontal wells (Modified after Hanks et al., 2012; Ayan et al., 1994).....	89
	Page
Figure 59: Field cumulative oil production and field oil production rates for different permeability anisotropy ratios.....	91
Figure 60: Average reservoir pressure and field producing gas oil ratio for different anisotropy ratios.....	92
Figure 61: Field cumulative oil production and field oil production rates for case #1: change in S_{or} for all the rock types.....	95
Figure 62: Average reservoir pressure and field producing gas oil ratio for case #1: change in S_{or} for all the rock types.....	95
Figure 63: Field cumulative oil and oil production rates for case #2: change in S_{gc} for the rock type #2 and #3	96
Figure 64: Average reservoir pressure and field producing gas oil ratio for case #2: change in S_{gc} for the rock type #2 and #3	97
Figure 65: Field cumulative oil production and field oil production rates for case #3: change in K_{rg} for rock type #1. The red curves underlie the blue curves	98
Figure 66: Average reservoir pressure and field producing gas oil ratio for case #3: change in K_{rg} for rock type #1.....	99
Figure 67: Field cumulative oil and oil production rates for case #4: change in K_{rg} for rock type #1.....	99
Figure 68: Average reservoir pressure and field producing gas oil ratio for case #4: change in K_{rg} for the rock type #2 and #3	100
Figure 69: Comparison of the cumulative oil productions for Case#1 though Case# 4 with the base case. The base case and Case# 3 are overlying each other. Case 1: change in S_{or}	

for all the rock types. Case 2: change in S_{gc} for the rock types #2 and #3. Case 3: change in K_{rg} for the rock types #1. Case 4: change in K_{rg} for the rock types #2 and #3.....101

	Page
Figure 70: Field cumulative oil production and field oil production rates for different producing GOR constraints.....	103
Figure 71: Average reservoir pressure and field producing GOR for different producing GOR constraints.....	104
Figure A.1: Workflow for layer coarsening scheme in the geologic model	120
Figure A.2: Step by step illustration of layer coarsening algorithm.....	121
Figure A.3: The relationship between degree of heterogeneity and the layer coarsening based on porosity modeling	122
Figure C.1: RKB configuration with respect to well pad	126

List of Tables

	Page
Table 1: Umiat well test production data (Gates and Caraway, 1960).....	7
Table 2: Oil recovery experiments at 75°F and 26°F (Baptist, 1960)	9
Table 3: Input parameters for volumetric calculation (Levi-Johnson, 2010).....	10
Table 4: Range values in the variogram for the sand bodies in the LGS formation.....	27
Table 5: Layer Information in the Umiat geologic model	34
Table 6: Different grid resolutions of the geologic model	37
Table 7: Well data from geologist	38
Table 8: Different rock types in the Umiat reservoir.....	43
Table 9: Oil and water density at reservoir conditions	44
Table 10: Different variable ranges used as input to Monte Carlo simulation.....	52
Table 11: STOOIP estimations for each zone in the LGS formation.....	52
Table 12: P quantiles for resource estimation.....	53
Table 13: The Input uncertainty parameters for multiple realizations workflow	57
Table 14: Different rock types and their corresponding lithology factor. It also shows how the pore size frequencies are relatively different from each other	65
Table 15: General fluid properties for reservoir simulation at surface conditions.....	69
Table 16: Fluid properties Input data to the simulator	70

Table 17: Reservoir parameters for initializing the simulation model	71
Table 18: Well model parameters used in the simulation model	78
Table 19: Simulation parameters used in the base case model	79
	Page
Table 19: Simulation parameters used in the base case model	79
Table 20: Run time and grid dimensions for two grid resolutions	82
Table 21: Relative permeability and saturation end points in the base case simulation...	93
Table 22: Relative permeability and saturation end points used in sensitivity runs.....	94
Table B.1: Well pick data for Chandler horizon in the updated model geometry	123
Table B.2: Well pick data for UGS horizon in the updated model geometry	123
Table B.3: Well pick data for Shale barrier horizon in the updated model geometry	124
Table B.4: Well pick data for upper LGS horizon in the updated model geometry	124
Table B.5: Well pick data for middle LGS horizon in the updated model geometry	125
Table B.6: Well Pick data for lower LGS hrizon in the updated model geometry	125
Table B.7: Well pick data for base Grandstand horizon in the updated model geometry	125
Table C.1: RKB depth and tie-in points for each well pad used in the model.	126
Table C.2: Tie-in depth for different wells used in the well designing	127
Table D.1: Financial metrics and economic model parameters	129
Table D.2: Project NPV and IRR for case with available gas supply	131

Disclaimer

This thesis was prepared as an account of work sponsored by an agency of the United States Government. Neither the United States Government nor an agency thereof, nor any of their employees makes any warranty, expressed or implied, or assumes any legal liability or responsibility for the accuracy, completeness, or usefulness of any information, apparatus, product, or process disclosed, or represents that its use would not infringe privately owned rights. References herein to any specific commercial product, process, or service by trade name, trademark, manufacturer, or otherwise does not necessarily constitute or imply its endorsement, recommendation, or favoring by the United States Government or any agency thereof. The views and opinions of authors expressed herein do not necessarily state or reflect those of the United States Government or any agency thereof.

Acknowledgments

This thesis is based upon work supported by the DOE under Award Number DE-FC26-08NT0005641. I would like to begin my acknowledgment by thanking the author of beauty, God, for His perfect creation of beauty and symmetry. Next, I'd like to thank my advisory committee, Dr. Catherine Hanks, Dr. Mohabbat Ahmadi and Dr. Abhijit Dandekar, for reviewing this work and giving me their valuable comments for improving my thesis. I am extremely grateful to my advisors, Dr. Mohabbat Ahmadi and Dr. Catherine Hanks, for all their useful technical suggestions and support while I was conducting this study.

I am indebted to Dr. Shirish Patil who encouraged me to apply to the UAF graduate program in the first place. I would also like to thank Dr. Jo Mongrain for her support during the first part of my thesis work. Special thanks go to Melody Hughes, Stephanie Knaebel, and Jennifer Hedrick, office managers of the Petroleum Engineering Department, for helping me to complete all administrative requirements. For their administrative support and technical cooperation, I would like to thank the following individuals: Grant Shimer, team geologist for providing geological interpretations; the Geologic Material Center (GMC) in Eagle River and the US DOE for providing much-needed core samples and financial assistance, respectively. Thanks also go to Paul Brown, Jawad Khalid, Sasan Ghanbari, Jezy Longoria, members of the joint project between Linc Energy and Renaissance Alaska, LLC and Linc Energy, with whom I had many interesting discussions.

I dedicate this work to my mother whose constant love has always sustained me throughout my life, to my father who has been the strongest pillar in our family, my brothers and sisters with their unconditional supports, my friends for their kindness over the course of my studies at the UAF and all of my teachers who took their time to instill me with a love of learning more. Without them, I wouldn't be who I am today.

Chapter 1 Introduction

1.1 Overview

The ever-increasing demand for energy requires efficient and economic exploitation of the remaining petroleum reserves. Much of the attention has been given to production from conventional oil and gas reservoirs as the main source of supplying energy in the world. Easy access, and continued production from such reservoirs resulted in a decline in oil recoveries throughout the world. In such conditions and with higher oil prices, exploring unconventional resources by applying new technologies such as IOR (improved oil recovery), and horizontal drilling is becoming imperative.

Umiat reservoir is a light oil accumulation (36° API gravity) that is at a very shallow depth (275–1055 feet) and has a low reservoir pressure (200–400 psi). It was discovered during exploration activities conducted by Department of Navy from 1944 through 1953 in the arctic region of Northwestern Alaska (Baptist, 1960). According to initial estimates of the resource, the recoverable reserve ranged from 30 to over 100 MM bbl with an average of 70 MM bbl of oil (Baptist, 1960).

The development plan to produce from Umiat started with 11 vertical wells and failed after a few months of unsuccessful operation. The lack of proper technology and the physical environment with unique conditions presented challenges that added to the complexity of production. These conditions include low temperature (20–35°F), low pressure, low quantity (70.5 scf/stb) of solution gas (Baptist, 1960), presence of permafrost, and remote location of the reservoir. The base of permafrost ranges from 770–1055 feet that if located in the reservoir section of the field would cause significant reduction in oil recovery (Venepalli, 2011).

To overcome field development barriers, a suitable production strategy must be planned. Recovery techniques such as thermal methods are ruled out as they would melt the permafrost causing the potential collapse of the well-bore. Water flooding might be a good candidate to maintain the reservoir pressure and help increasing oil recovery, but in Umiat, it would freeze and block future injectivity. Any gas injected above reservoir temperature would tend to thaw and then refreeze any interstitial water that came in contact with and would reduce the permeability to oil substantially. Therefore, cold gas injection was proposed by Renaissance as the preferred pressure maintenance development plan (Watt et al., 2010).

There are two main sandstone oil-producing intervals which vary in thickness and quality across the Umiat area. The main oil-producing zones in the Umiat field are in shallow marine sandstones of the Cretaceous Nanushuk Group (Baptist, 1960). These sandstones are referred to locally as the Grandstand sands. The Upper Grandstand (UGS) is separated from the Lower Grandstand (LGS) by 300 feet thick gray shale (the 'shale barrier') (Figure 1).

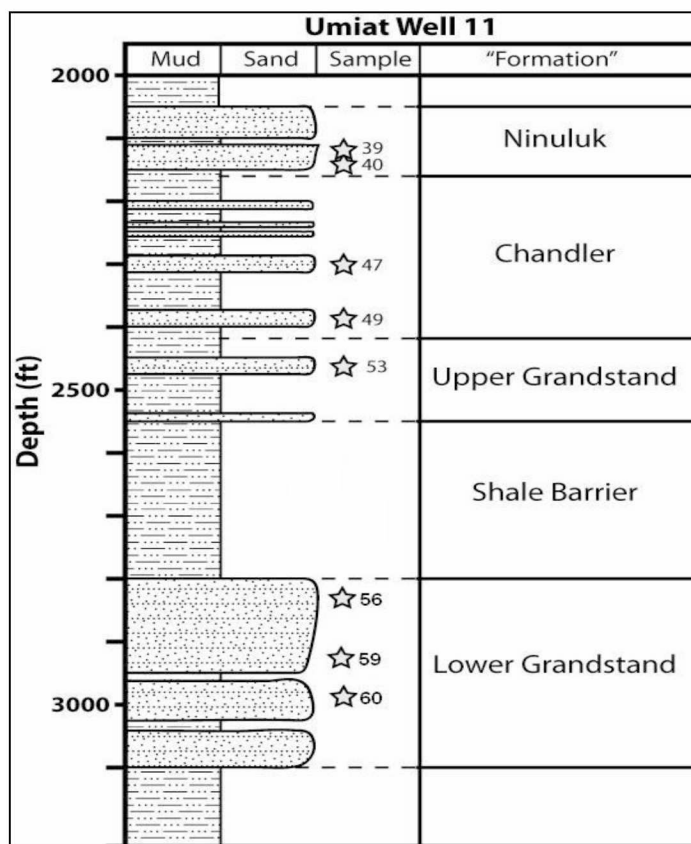


Figure 1. Lithology log of Umiat Well# 11 (Godabrelidze, 2010)

The average reservoir pressure is about 50 psi in the UGS and about 350 psi in the LGS. Most of the primary production will be due to solution gas drive. However, since the bubble point of the oil is 345 psi in the LGS (Shukla, 2011), the field is considered an undersaturated black oil field that needs immediate pressure support for efficient oil production. Immiscible gas injection is a mechanism of IOR (improved oil recovery) that can be used to maintain reservoir pressure and give incremental oil recoveries. A separate study was done by Joshi International Technology Inc. (2008) to evaluate oil recovery by comparing horizontal wells with vertical wells and gas injection with depletion drive mechanism. This study determined that horizontal wells had higher productivity compared to vertical wells. Furthermore, the gas injection resulted in 3-4 fold increase in oil recovery over the natural depletion mechanism. Since establishing equilibrium with

permafrost condition is more viable by isothermal gas injection than the water, gas injection was proposed as the production mechanism in this study.

In 1960, the Umiat was expected to be the largest oil field in Alaska (Watt et al., 2010). Now with more than 50 years after the initial discovery, advances in horizontal drilling technology and with higher oil prices, development of Umiat reservoirs seems more practical. Successful production from Umiat could lead to a better understanding of how to develop other oil fields located in permafrost and Arctic regions.

1.2 Objective of the study

New data acquisition is indispensable in development phase of any hydrocarbon field. A geological model is needed to build the static framework of the reservoir and to estimate volume of original oil in place. As more interpreted data comes in, the model will need updating. Based on new data, a more in-depth volumetric calculation can be made to estimate original oil in place (OOIP), with different degrees of certainty (e.g., P-10, P-50, and P-90). To evaluate oil recovery under a dynamic situation, the geologic model must be incorporated into a simulation model of the reservoir. The integrated simulation model must then be accompanied by appropriate rock and fluid data. Different production scenarios can then be conducted to determine which scenario adequately suits criteria imposed by the reservoir conditions.

The main objective of this study is:

- 1) To update a petrophysical property model for Umiat including:
 - a) Re-distribution of porosity and permeability across the field
 - b) Grid structure of the reservoir
 - c) Estimation of volume of oil in place
- 2) To use the petrophysical property model to build a simulation model and

3) To use the simulation model to investigate reservoir performance using the proposed production plan and determine the major factors that produce uncertainties in the results.

Chapter 2 Background

2.1 Field History and Location

In the early 1900s, field geologists from the United States Geological Survey (USGS) explored the National Petroleum Reserve of Alaska (NPR-A), a roadless area 200 miles north of the Arctic Circle (Gates and Caraway 1960, Baptist 1960). These geologists discovered several good shows of oil that prompted the establishment of Naval Petroleum Reserve No.4 (NPR4) in 1923. This area remained largely untouched until the conclusion of World War II.

The Umiat oil field is situated in the folded and thrust-faulted sedimentary rocks at the leading edge of the Brooks Range foothills of northern Alaska. Geographic location of the Umiat oil field is shown in Figure 2.

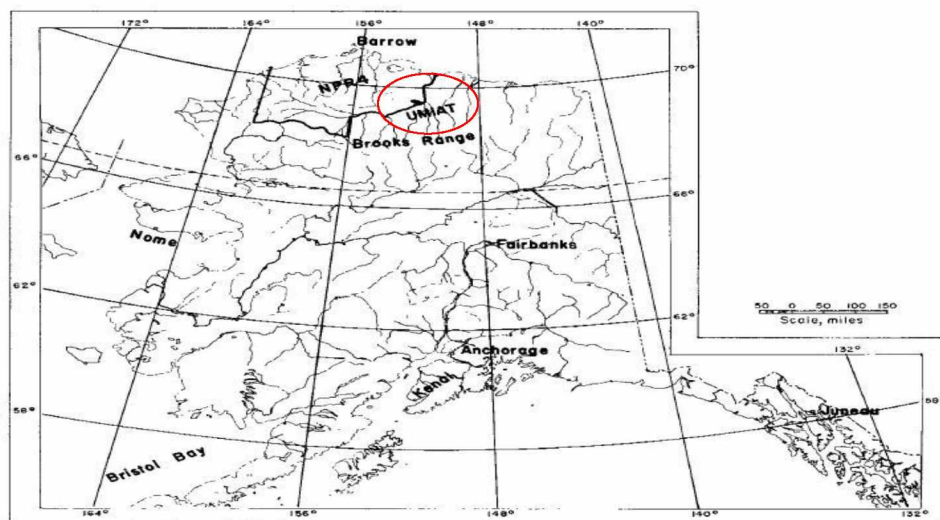


Figure 2. Umiat field location (Gates and Caraway 1960)

The Umiat field lies mostly within the continuous permafrost region. Permafrost depth ranges from 770 to 1055 feet. Oil was found at depths of 275 to 1100 feet (Baptist, 1960);

therefore, some of the oil is believed to be in the permanently frozen zone. For this reason, the Umiat field is considered unconventional.

The location of Umiat wells is shown in Figure 3. Of eleven wells drilled by the U.S. Department of the Navy, only six produced oil in varying amounts (Gates and Caraway 1960). The production test rates for the six wells are shown in Table 1. At first glance, these varying production levels suggest that we face a heterogeneous reservoir. Data from the 1950s is highly limited, but it was observed that wells drilled with either cable tools using brine or with rotary tools using oil or oil-based mud produced significantly more oil than those drilled with a rotary rig using water-based mud. For example, Well #2 and Well #5 are located at about the same elevation on the structure. Yet despite the short distance (200 feet) between them, Well #2 (which was drilled with a rotary rig using water-based mud) was abandoned as a dry hole, while Well #5 (drilled with cable tools) pumped 400 BOPD, the maximum capacity of the pump and possibly less than the well's capacity.

Table 1. Umiat well test production data (Gates and Caraway, 1960)

Well Number	3	4	5	6	8	9	10
Rate (bpd)	24	100	400	80	60	300	70
Length of test (days)	14	18	93	1	14	45	1

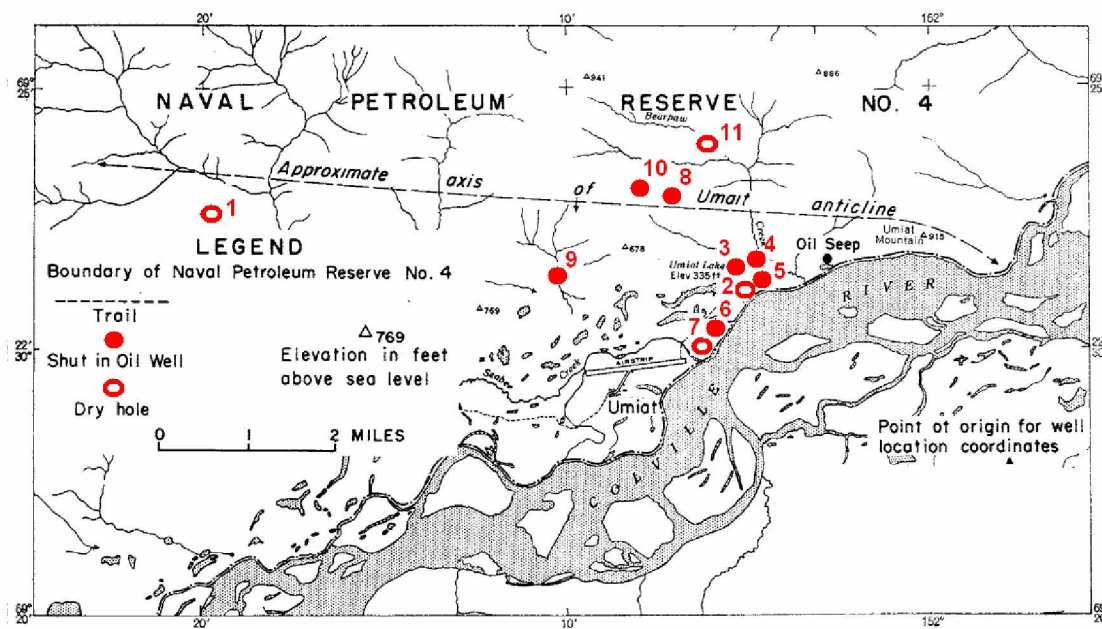


Figure 3. Location of Umiat wells (modified from Gates and Caraway 1960)

2.2 Previous Research

Initial studies of Umiat oil field began as early as the 1950s. Espach (1951) was first to estimate the original-oil-in-place (OOIP) in Umiat at 122 million barrels with an uncertain volume of gas. Collins (1958) provided some lithologic description based on porosity and permeability data from Umiat well test data.

Baptist (1960) was one of a few people who focused on production under permafrost conditions. He analyzed temperature and pressure gradients in Umiat wells to research the reduction of oil permeability and oil recovery due to freezing of interstitial water with a set of experiments run both at room condition (75°F) and simulated permafrost conditions (26°F). Experiments were also made on six radial samples to obtain a qualitative index of oil recovery by solution gas expansion and additional oil recovery by gas drive, as well as to investigate the effect of freezing on these two recovery processes. The average

recovery by solution gas expansion for the four samples tested at 75°F was 40%, while the same index for the same four samples tested at 26°F was only about 29%. The average irreducible water saturation for these four samples was about 41%. These results are summarized in Table 2.

Table 2. Oil recovery experiments at 75°F and 26°F (Baptist, 1960)

Well	Sand	Porosity (%)	Air permeability (md)	Initial saturation (%PV)		Solution-gas				Gas drive			
				Brine	Oil	Recovery (%)		Residual oil (%PV)		Recovery (%)		Residual oil (%PV)	
						26F	75F	26F	75F	26F	75F	26F	75F
Umiat-3	UGS	18.2	128	42	58	36	-	38	-	34	-	19	-
		17.7	134	38	62	31	50	43	34	26	23	27	16
		16.3	52	44	56	25	33	42	38	19	34	32	19
Umiat-2	LGS	16.5	196	37	63	34	48	42	33	21	20	28	20
		15.1	49	44	56	27	29	41	39	7	9	36	34
		14.6	92	41	59	17	-	49	-	28	-	33	-

To further investigate the effects of freezing of interstitial water, the oil-water relative permeability of two samples was tested at room temperature (70°F) and then at below the freezing point of the water (26°F) (Baptist, 1960). Permeabilities of the samples at 70°F and 26°F were 30 md and 23 md for the first sample (23.3% reduction) and 19 md and 13 md for the second sample (31.5% reduction) at an initial water saturation of 41%. Thus the average reduction in effective oil permeability due to freezing of irreducible water was about 27% (Baptist, 1960).

Some of the parameters that affect relative permeability include (Dandekar, 2006):

- 1) The pore space geometry (the distribution of large and small conduits and their sizes)
- 2) Viscosity of the fluid
- 3) Wettability of the mineral surface, and

4) Interfacial tension (IFT) (and/or surface tension) between the fluid phases and between each fluid phase and the minerals.

These parameters are the major factors in a 3-component system (oil-water-gas). With introduction of ice into the system, along with the above parameters, the freezing of water within porous media also has a significant effect in altering the relative permeability of each phase (Venepalli, 2011).

Despite the low price of oil in the 1960s and a high degree of uncertainty in production from a frozen reservoir, several scientists investigated the depositional environment and sedimentological history of the Umiat field. In 1966, Brosge (1966) believed that the relative cleanness of the sands in both Grandstand formations was a result of winnowing and reworking of the sediments in a part of the sedimentary basin that subsided quickly. Ahlbrandt (1979) concluded that in the Umiat area the Grandstand sands consist of a complexly inter-bedded delta-front and delta-plain facies called the Umiat Delta which prograded northeasterly with the source terrane southwest of Umiat. Others tried to narrow the high range of resource that was a huge uncertainty in the Umiat structure due to its fault systems. Their reports indicated a reserves estimate of 30 to 100 MM bbl, with an average value of 70 MM bbl (Molenaar, 1982; Potter and Moore, 2003).

Table 3. Input parameters for volumetric calculation (Levi-Johnson, 2010)

Parameter	Value
Porosity	Estimated from 3D porosity distribution
Water saturation	41% (third party report for Renaissance Alaska)
Oil water contact	783 feet (third party report for Renaissance Alaska)
GOR	71 scf/stb (Baptist, 1960)

In recent years, with oil prices significantly higher than in the 1950s, and with a tempting amount of relatively high quality crude (37° API) present in the Umiat system, attention again turned to development of the field, this time with a more rigorous approach. In 2008, Renaissance Alaska LLC shot a 3D seismic survey for more data and to facilitate decision-making with regard to business needs. Watt and others (2010) and Levi-Johnson (2010), proposed that Umiat could have OOIP of more than 1 billion stock tank barrels assuming variables listed in Table 3.

In 2011, Venepalli (2011) ran a series of core flood experiments of two clean Berea sandstone to evaluate sensitivity of end-point relative permeability to oil under a temperature range of 23°C to -10°C for different levels of connate water salinity (0–6467 ppm). Venepalli concluded that both cores showed maximum and minimum reduction in relative permeability to oil when saturated with deionized and highest salinity water, respectively. The results showed that high salinity water injection might be a good candidate for the efficient production from Umiat reservoir. However, the operator decided not to consider it because of lack of waterflooding infrastructure and remoteness of the field.

2.3 Geological Modeling

The geologic model or 3D geomodel is considered the backbone of a dynamic simulation study. It includes all of the static data such as porosity, absolute permeability, structural layers, faults, fractures, and formation anisotropies. A robust geological model is the product of many discussions among geologists, geophysicists, reservoir engineers, and petrophysicists about input data and model output and includes construction of many workflows to distribute petrophysical properties in the reservoir model.

In this study, the input parameters used in building the geologic model included seismic data, well log data, and core data and were obtained from the previous model (Levi-Johnson's model). The well tops and the well log data were provided by Renaissance Alaska and the lithologic description was obtained from Collins (1958). These data along with new permeability anisotropy and quantitative geologic information (Shimer, G, personal communication, 2012) were loaded into IRAP RMS and were used to build an updated petrophysical model of Umiat field detailing porosity, permeability, and water saturation.

The development of reservoir simulation models from high-resolution geologic models remains an active field of research (Darche et al., 2005). To reduce the total number of cells used for numerical reservoir simulation, a simulation grid is often generated instead of using the geological grid directly. A uniform simulation grid is used often for simplicity. The drawback is that reservoir heterogeneity cannot be maintained. The key ideas of simulation grid design include: (1) volume preservation; (2) similarity between geological grid and simulation grid; and (3) geological details preservation (Zhang et al., 2009). The common concern is that a simulation grid must keep the maximum amount of geological details captured by the geological grid as possible. In other words, only homogeneous geological grid cells should be combined. There are many ways to quantify reservoir heterogeneity and variation and optimization algorithms are often applied to simplify the workflow (Zhang et al., 2009). Particularly in Umiat reservoir, due to relatively large area of the reservoir, an optimum grid resolution must be selected that is acceptable to preserve the heterogeneity and will be executable in the simulation study.

Uncertainty will normally occur at two different levels during model construction: is the scenario correct and if so, how certain are we of the details? The importance of each level will vary and need to be investigated for their associated contribution to the model output (Roxar manual guide, 1994-2008). IRAP allows the user to incorporate both scenario level and parameter level uncertainty into the geologic model.

Scenario uncertainty: scenario level uncertainty may be addressed by looking at different values of critical variables, such as:

- The number of wells in the development plan
- Is the fault open or sealed for pressure maintenance

To fully understand the degree of uncertainty at this level, the simulation model should be run dynamically and the variable implications on any decisions be considered. The analysis for this type of uncertainty is discussed further in the next chapter.

Parameter ranking: The best way to address the impact of uncertainty in various parameters is to run multiple realizations in the geologic model for the importance of parameters such as:

- Geologic complexity (degree of shaliness, net to gross ratio, uncertainty in structure depth, etc...)
- Depth of fluid contacts, and
- Porosity

Total uncertainty: To paint a complete picture, these two levels need to be combined into a general scheme of uncertainty known as total uncertainty. It should be stressed that the uncertainty analysis should be linked together for a full assessment of reservoir modeling (Figure 4).

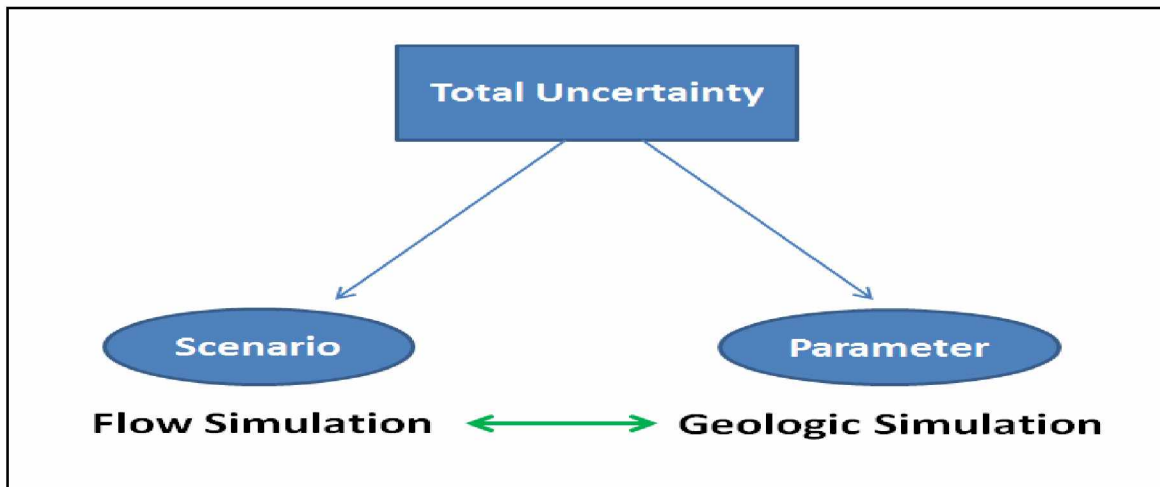


Figure 4. Total uncertainty analysis in reservoir modeling

2.4 Reservoir Simulation

Regardless of varying amounts of original hydrocarbon in place, important questions still remain: How much can be technically produced from the field? And at what rate they can be produced? Hopefully, the answers will be obtained by the end of this forecast simulation study.

2.4.1 Incentives for Reservoir Simulation

Our understanding of reservoir performance is increased through the study of fluid flow principles, a clear description of the reservoir geology, and the accurate use of appropriate reservoir simulators (Mattax and Dalton, 1990). This allows us to evaluate "what if" production solutions to produce the reservoir most efficiently and economically and predict future performance of the reservoir under different development strategies.

There are two important questions in simulating a reservoir:

- What is the impact of horizontal well's vertical placement (offset distance from the Water Oil Contact or WOC) on oil recovery and gas breakthrough times?
- What is the optimum horizontal well lateral length and its impact on oil recovery?

Simulation of a reservoir requires not only a good deal of software / hardware overhead and simulation engineers, but also a great deal of input data from other disciplines. Usually, in a simulation study there is production history that helps validate model performance. As there was no quantifiable amount of Umiat production data, our model output relied more on input data and more sensitivity analysis that could help the operator to include in development plan strategies to reduce the risk and enhance the quantity and quality of simulation input data in the future.

2.4.2 Designing the Simulation Model

Recent computer developments allow the quantification of sensitive parameters in appraisal phase of a reservoir using flow simulation. Such a procedure is normally implemented with a fixed production strategy because a variable strategy plan is very time consuming. The objective of this simulation study was to investigate the impact of a fixed production strategy (gas injection) on the ultimate oil recovery (the objective function). An optimization procedure was implemented to evaluate the most effective range of parameters. The methodology comprised of construction of a base simulation model, selection of the most critical attributes, simulation of all possible models and maximization of an objective function through a combination of the optimized parameters under a realistic operating conditions applicable to Umiat field development. At the end the changes in the objective functions from sensitivity analysis are compared and some conclusions and recommendations are made. The approach developed in this study is based on two points: 1) optimization such as well length, operating condition,

injection pressures and 2) sensitivity analysis on uncertain parameters such as permeability anisotropy, relative permeability end-points, residual saturation, critical saturation, and producing GOR constraint.

It should be also noted that simulation assessment of a field is not one directional. It has a cyclic flow of data and interpretation. Whenever more data become available, they should be converted into consistent scale of the model and this process is repeated. A technical report of simulation results will then tell business level decision makers which scenario is most efficient and more profitable.

A preliminary simulation study of Umiat field was carried out by Joshi Technologies International Inc. in 2008. This study yielded estimated recovery factors of 25 percent for the UGS and 45 percent for the LGS. Assumptions in this simulation study were (Joshi Technologies International, 2008):

- 1) A gas injection recovery mechanism.
- 2) An 80 acre spacing between the injection wells and producing well.
- 3) An injection pressure 100 psi over initial reservoir pressure.
- 4) An average permeability of 70 md for the UGS while the LGS has an average permeability of 40 md.

Since they had used simplified PVT model with constant values for porosity and permeability, their model did not accurately present the reservoir parameters, thus their simulation result carried high degrees of uncertainties.

In addition to a reliable geologic model and petrophysical properties, a fluid model is also needed to account for dynamic changes in the reservoir parameters including viscosity, density, compressibility and GOR as a function of pressure. The two most common types of reservoir fluid models are black oil models and compositional models. Black oil

models are based on the assumption that the saturated phase properties of two hydrocarbon phases (oil and gas) depend on pressure only. Compositional models also assume two hydrocarbon phases, but they allow the definition of many hydrocarbon components. In this study, a black-oil reservoir simulator (IMEXTM), developed by Computer Modeling Group (CMG) was used to evaluate the LGS reservoir performance under immiscible gas injection. A CMG black oil PVT fluid model had been built by WinProp CMG (Shukla, 2011) and was used in simulation model. Moreover, capillary pressures of oil, gas, and water as well as relative permeabilities to oil and gas were measured under reservoir conditions and provided as input to the simulator (Godabrelidze, 2010; Venepalli, 2011).

2.5 Horizontal Wells

Horizontal wells have become a common industry practice in many fields throughout the world in the terms of increased recovery/reserves and improved well production rates in comparison to vertical wells. On average, they produce two to three times the rate of the similar vertical well (Beliveau, 1995). The major benefits of drilling a horizontal production well are to enhance contact with the reservoir and prevent water and gas coning thereby providing higher well productivity (Joshi, 1990). As an injection well, more fluid can be injected into the reservoir through the large contact area with the reservoir which is highly desirable in EOR/IOR applications (Figure 5) (Joshi, 1990).

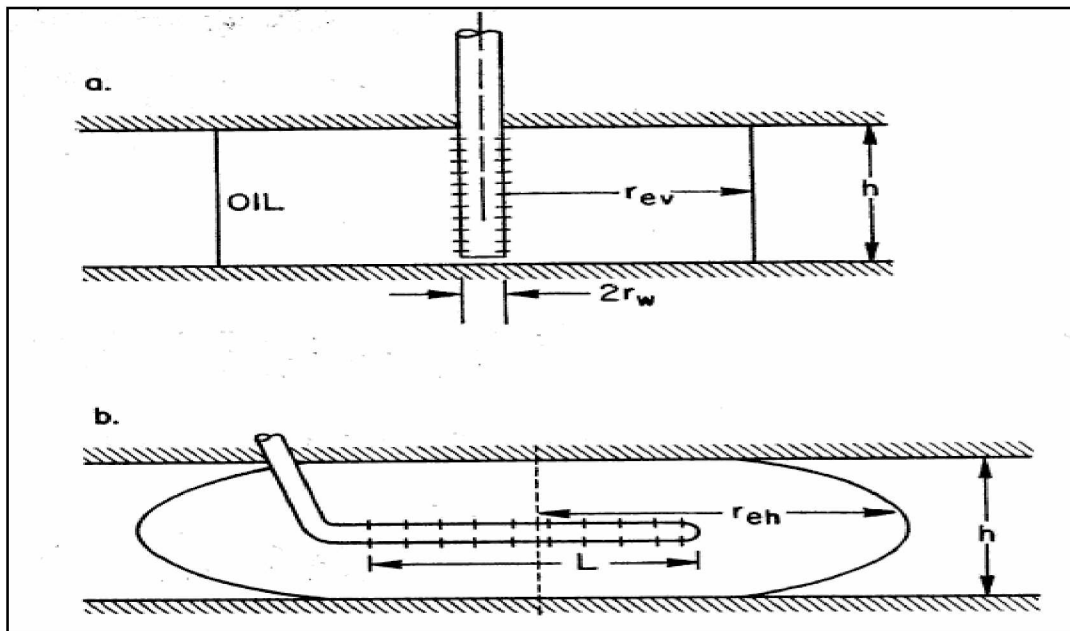


Figure 5. Schematic of a horizontal & vertical well drainage area (Joshi, 1990)

When the length of horizontal well increases, its drainage area increases. Today, horizontal wells are drilled with lengths up to several thousand feet long. The length of a horizontal well is not proportional to the well productivity (Cho and Shah, 2001). An increase in the production section causes friction pressure losses in the well-bore to increase and eventually a portion of the well would be unproductive (Cho and Shah, 2001). Since planning for horizontal and multi-lateral wells is more complicated and their completion is more expensive than the vertical wells, an optimum horizontal length must be drilled in order to make the project economically feasible.

Horizontal wells in Umiat would provide several benefits. The first one would be to access the entire reservoir while minimizing the surface footprint. The second benefit would be to provide segregated access to a large contact area of the sand bodies located in top and bottom of the formations. The third benefit is the rate benefit resulted from dual lateral legs of the horizontal wells (Watt et al., 2010).

2.6 Gas Injection

Primary depletion is not usually sufficient to optimize recovery from an oil reservoir. Incremental oil recoveries can be achieved by supplementing natural reservoir energy (Fanchi, 2001). The supplemental energy is provided using an external energy source, such as gas injection. Gas injection is a common process among oil recovery techniques (Hinderaker et al., 1996). Gas injection for pressure maintenance refers to secondary reservoir recovery processes that recover oil that was not produced by primary processes. Secondary recovery uses injectants to repressurize the reservoir and displace oil to producers focusing on rock/oil/injectant systems and the interplay of capillary and viscous forces. EOR (enhanced oil recovery) is a special type of IOR that focuses on the oil that has not been recovered by primary and secondary production methods (Figure 6).

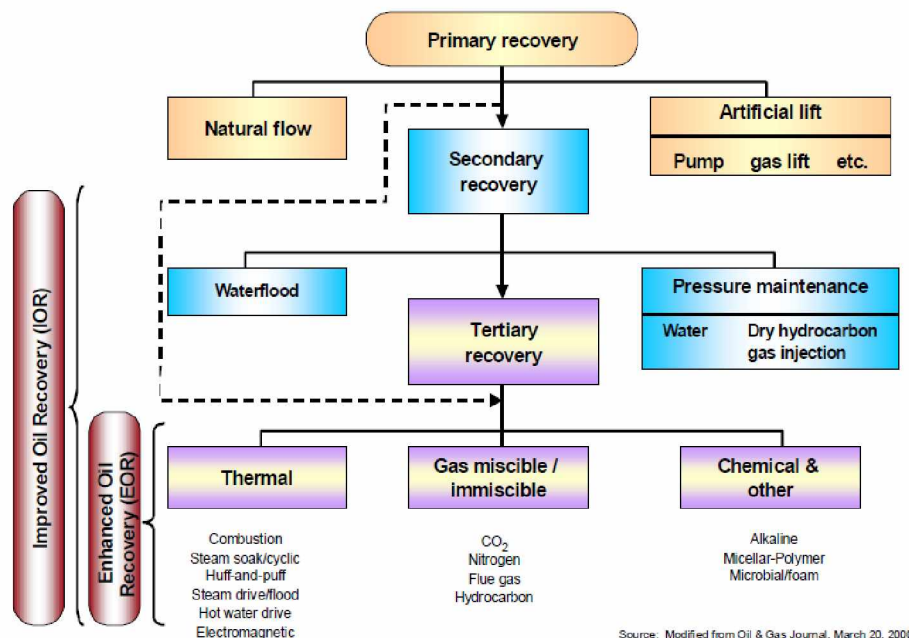


Figure 6. Different stages of oil recovery with approval of SPE technical committee (Modified from Oil & Gas Journal, March 20, 2000)

Since reservoir pressure in Umiat is low (200–400 psi), it is expected that good oil recovery can be achieved if reservoir pressure is maintained in order to increase the pressure gradient between reservoir and producing wells. Baptist (1960) claimed that even when the reservoir pressure is low, substantial amount of oil can be produced from the Umiat reservoir by piston-like displacement of oil by gas movements, but it was never proven by other references.

Gas-injection operations are generally classified into two distinct types depending on where in the reservoir, relative to the oil zone, the gas is introduced:

Dispersed Gas Injection: Dispersed gas-injection operations, frequently referred to as internal or pattern injection, normally use some geometric arrangement of injection wells for the purpose of uniformly distributing the injected gas throughout the oil-bearing portions of the reservoir (Roebuck, 1987). In practice, injection-well/production-well arrays vary from the conventional regular pattern configurations (e.g., five-spot, seven-spot, nine-spot) to patterns seemingly haphazard in arrangement with relatively little uniformity over the injection area.

External Gas Injection: External gas-injection operations, frequently referred to as crestal or gas-cap injection, use injection wells in the structurally higher positions of the reservoir-usually in the primary or secondary gas cap (Roebuck, 1987). This manner of injection is generally employed in reservoirs having significant structural relief and average to high vertical permeabilities. Injection wells are positioned to provide good areal distribution of the injected gas and to obtain maximum benefit of gravity drainage. The number of injection wells required for a specific reservoir will generally depend on the injectivity of each well and the number of wells necessary to obtain adequate areal distribution.

Regardless of location of gas injection wells at Umiat, one might think that gas injection in this situation would not be an EOR process, but an IOR one, as it is only for pressure maintenance. But despite that purpose, whether the process is considered EOR or IOR more or less depends on the type of injection gas. With pure methane, a dry gas, no miscibility will occur and the process will be classified as an IOR one. Under certain criteria, depending on the purity of injection gas, some mass transfer and solubility will occur that tends to include EOR applications for tertiary recovery.

For many conventional reservoirs with reservoir pressures higher than that at Umiat, secondary and tertiary oil recovery methods are not implemented until a few years into the producing life of the reservoir. The reason for this is that the primary depletion drive acts predominantly to produce the oil by use of reservoir's existing natural energy. This delay in implementation of secondary/tertiary operations results in obtaining more data and a better understanding of the reservoir characteristics and behavior and reduction of the risks of the many uncertainties associated with any of EOR or IOR operation. However, for the Umiat reservoir, there is no reason to delay: the lack of an active aquifer and low reservoir pressure means that there is no sufficient natural energy in the reservoir. Secondary oil recovery by gas injection is intended to maintain reservoir pressure and act as a supporting mechanism to primary drive to displace oil from the reservoir right from the start of production.

2.7 Gas Hydrate

Gas hydrates are basically a solid structure of water molecules like ice. They have a cavity in their structure where small molecules like methane can be trapped within the crystal structure built by water molecules. Gas hydrates tend to form in two geologic settings: (1) on land in permafrost regions, and (2) in the ocean sediments of continental margins (Pooladi-Darvish and Gerami, 2008).

Conditions for Occurrence: Gas hydrates occur under two conditions. They can be formed at high pressures or low temperatures where free water, methane and other light hydrate forming gases are present. A curve known as hydrate equilibrium curve is used to show the pressure and temperature conditions that hydrate can exist (Figure 7) (Sloan and Koh, 2007). As it can be seen in the diagram, the Umiat reservoir conditions do cross the hydrate phase equilibrium curve, indicating the potential of formation of hydrates during cold gas injection.

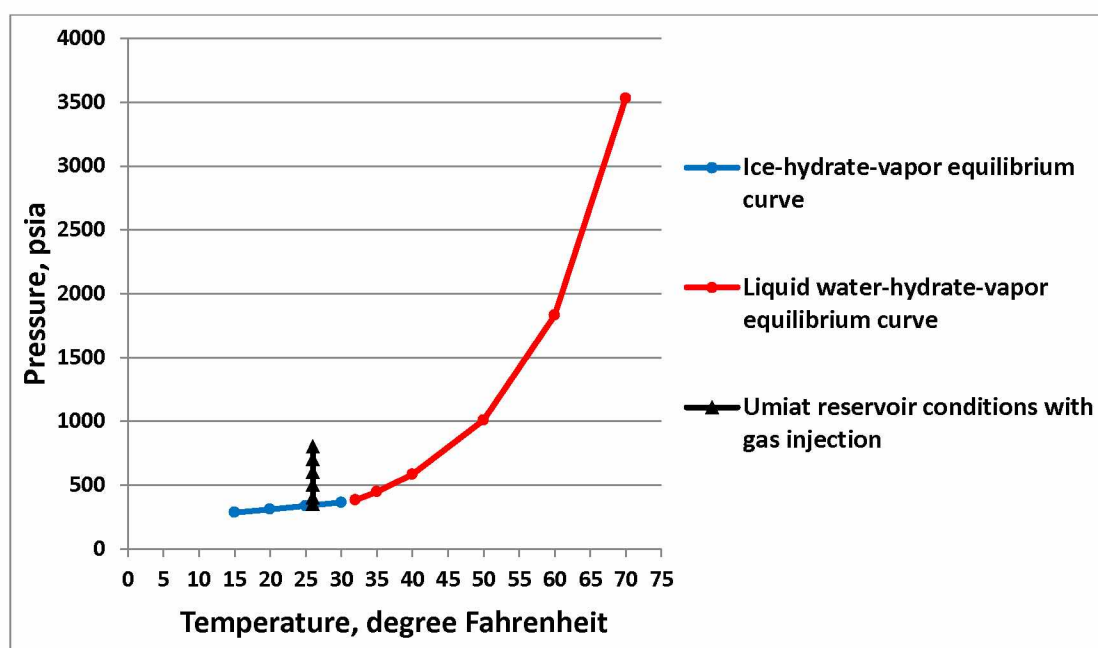


Figure 7. Umiat reservoir temperature and pressure conditions superimposed on the hydrate equilibrium curves. The plot shows that there is a possibility for hydrate formation. (Modified from Sloan and Koh, 2007)

Once formed, natural gas hydrates are difficult to remove (Zhang et al., 2002) and can plug the production zones. Presence of water and methane can cause hydrate to form in the reservoir which can reduce injectivity.

The key important factor is to locate hydrate bearing formations before the production begin. One of the common methods is to utilize measurement technologies to identify the precise location of the gas hydrate formations. Gas hydrates have certain characteristic petrophysical properties that can be identified by LWD (Logging While Drilling) tools.

Chapter 3 Geologic Modeling, Methodologies, and Sources of Data

3.1 Petrophysical Property Modeling

Reservoir modeling is the process of building and maintaining a reservoir model (Roxar manual guide, 1994-2008). A petrophysical property model for Umiat field had been built by Levi-Johnson (2010) using IRAP RMS geostatistical software. The Levi-Johnson model had been built for the entire Umiat field including both UGS and LGS and had large scale cell dimensions (600 ft * 600ft) and is shown here in Figure 7. It used a single value for the water saturation ($S_w=0.41$) and set the WOC depth at 783 ft in the volumetric calculations. Since one of the main purposes of geologic modeling is to provide reservoir engineers with a grid system for forecast simulation planning, the grid resolutions in the geologic model should be high enough to capture the heterogeneity in the reservoir and low enough for the computational capacity of the simulation. However, the grid dimensions in the Levi-Johnson model were too large for the reservoir simulation studies. Consequently, the grids had to be regenerated to higher resolutions for the use in subsequent grid optimization analysis in the reservoir simulator.

Because of the systematic approach in the petrophysical property modeling, when the model is re-gridded, all the parameters such as structure, horizon, porosity, and permeability must be modeled again and sampled into the new grid system. New geologic data, including permeability anisotropy (Shimer, G, personal communication, 2012) was incorporated into this new geologic model. In addition to permeability anisotropy and re-gridding, water saturation was mapped and incorporated into the analysis. After a series of meetings with the field operator, a value of 1500 ft was selected for the WOC depth in the geologic model.

This simulation study focused on the Lower Grandstand sand. Discussions with the geoscientists and the operator determined that the Lower Grandstand sand (LGS) should be considered the primary reservoir interval. The LGS consists of two thick (90-150 ft) upward-coarsening wave-influenced deltaic successions with an intervening 20-50 ft thick shale (Figure 8) (Hanks et al., 2012). Based on permeability trends and geologic information (Shimer et al., 2011), the LGS was divided into three sub-formations known as: the Upper LGS, the Middle LGS, and the Lower LGS. The Lower LGS is mostly mudstone impermeable layer with about 20 feet thickness across the reservoir (Shimer, G, personal communication, 2012). The workflow used in the new geologic modeling is illustrated in Figure 9.

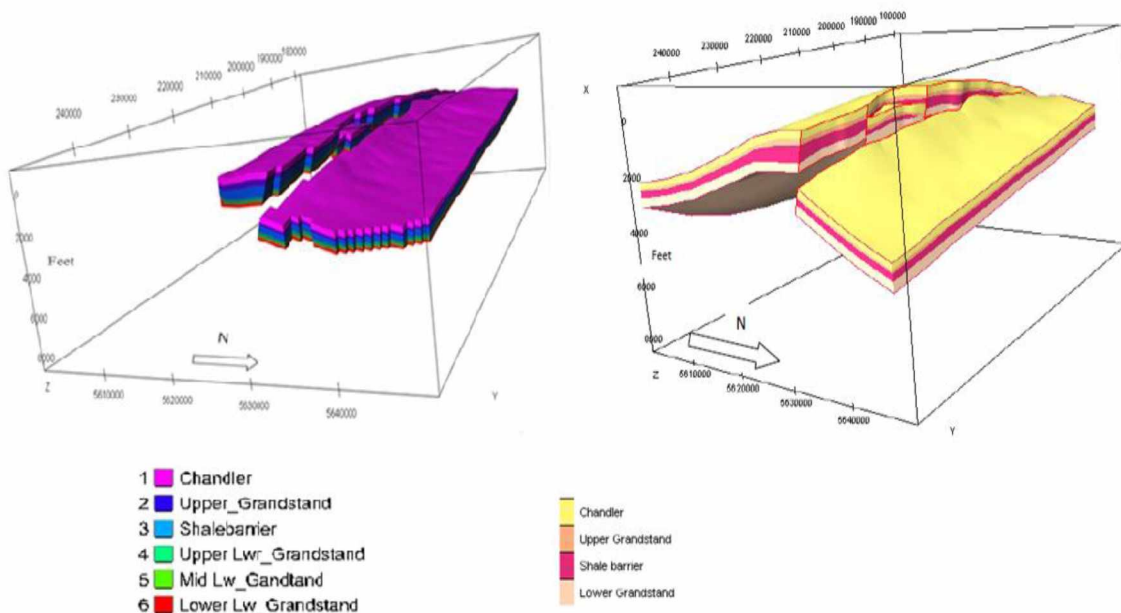


Figure 8. Horizon model of the previous Umiat geologic model (Levi-Johnson, 2010) and the updated horizon model with LGS divided into three sub-formations

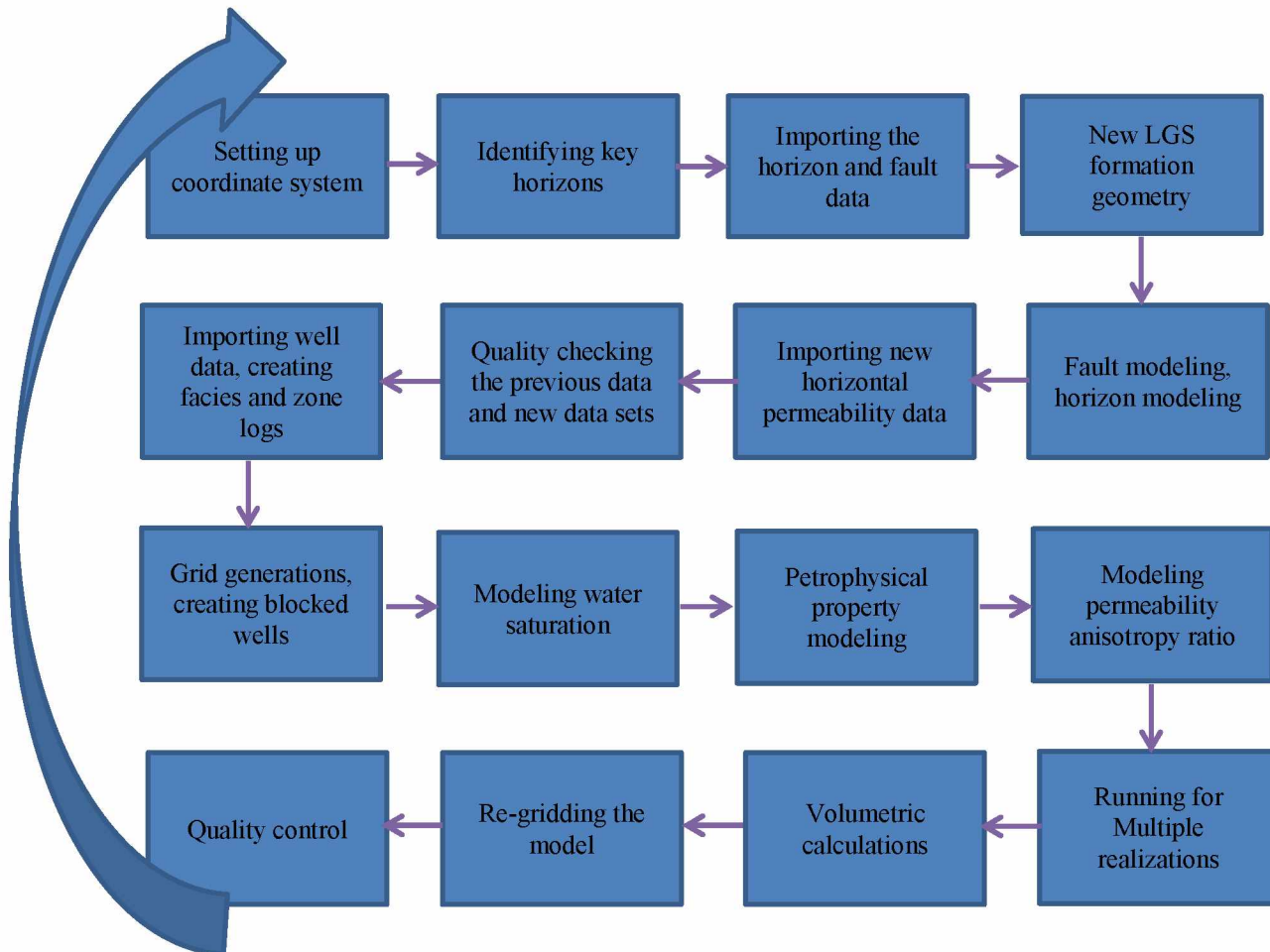


Figure 9. New workflow for the entire modeling procedure

Variogram Modeling: This involves defining the variability of the data based on geological knowledge and data analysis. The variogram is a statistical tool used to make approximations of data values in unsampled areas e.g. interwell areas (Krajewski and Gibbs, 2001). The similarity between two observations depends on the distance between them. Inconsistency between these observations increases with increasing separation distance (increment). The variogram value, according to Krajewski and Gibbs (2001) is the calculated variance of increment. Variograms are important because they provide information on the confidence with which the value of a cell can be predicted, based on

its distance from a cell with an identified value. Variogram terms used for the purpose of this work are:

Range: This is the distance within which no considerable variation is observed between samples (Table 4). It should have specified values for distance normal to azimuth (direction of sand progradation), parallel to azimuth and vertical (normal to dip) (Krajewski and Gibbs, 2001)

Table 4. Range values in the variogram for the sand bodies in the LGS formation

Range	Value (feet)
Parallel to azimuth	2,000
Normal to azimuth	500
Vertical (normal to dip)	15

The parameters presented in Table 4 along with an azimuth value of 45 degrees are the variogram input data that control the population of grid cells based on the petrophysical data observed in the blocked wells.

Sill: Although this is not frequently present, it represents the flat area of the variogram (Figures 10 and 11). The higher the sill, the higher is the variability and vice versa (Krajewski and Gibbs 2001).

Lag Distance: This is the distance in field units within which sample differences are compared (Krajewski and Gibbs, 2001) (Figures 9 and 10).

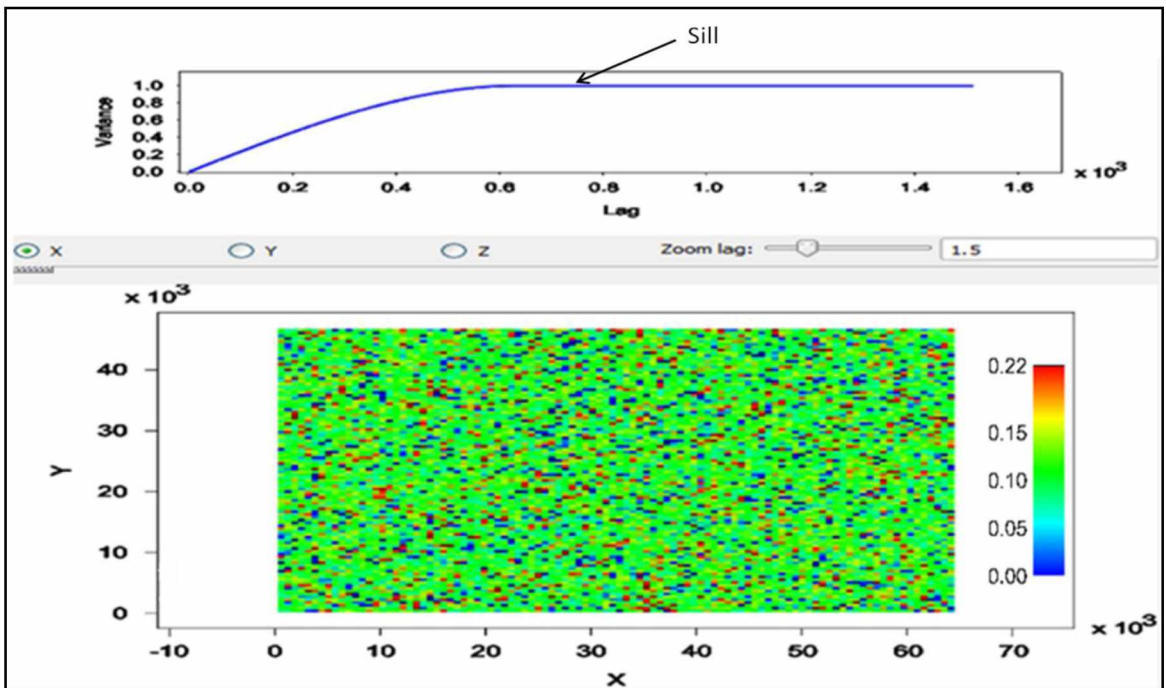


Figure 10. Porosity variogram result of sand in the LGS in the X-Y direction (Axes in feet)

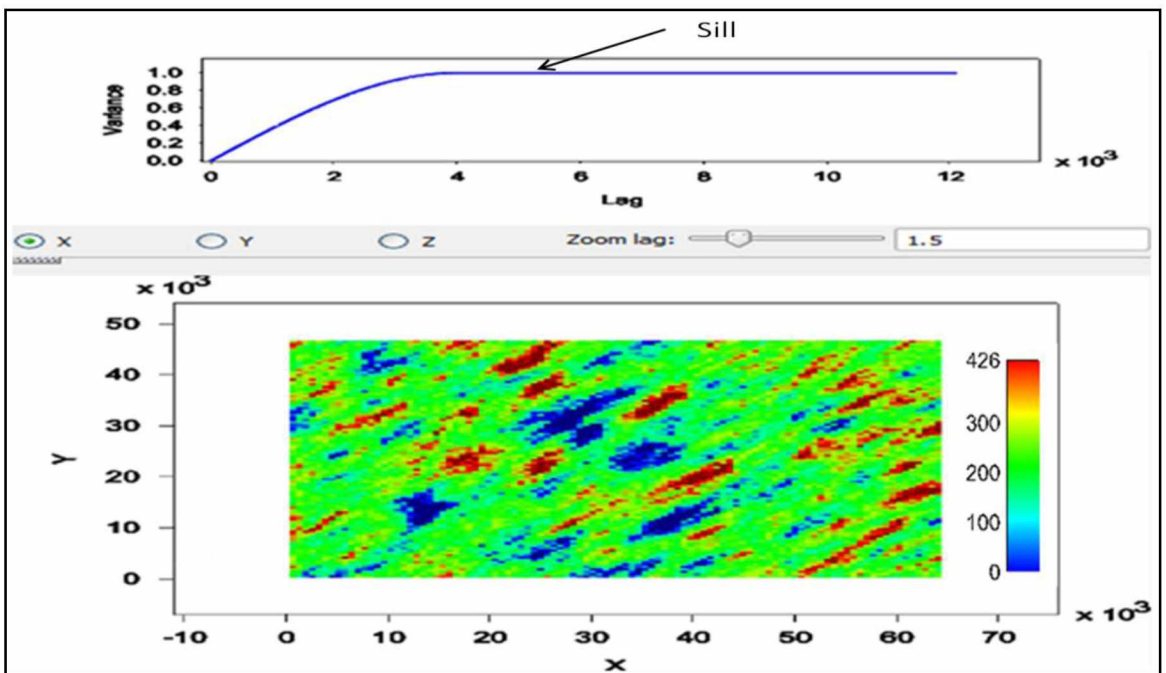


Figure 11. Permeability variogram result of sand in the LGS in the X-Y direction (Axes in feet)

The generated properties for the variogram were conditioned at the wells, meaning that at these locations, the grid cell properties are in good alignment with the well data. In the interwell areas the properties were distributed according to the statistical properties (such as standard deviation, mean and variance) of the well data. Figures 12 and 13 represent the porosity and permeability distribution in the X-Y direction in the LGS after the variogram analysis.

The histograms for the permeability and porosity in the LGS are presented in Figure 14 and Figure 15, respectively. As it can be seen, the mean value for permeability in the LGS is about 43 md and the mean value for porosity is 12 percent.

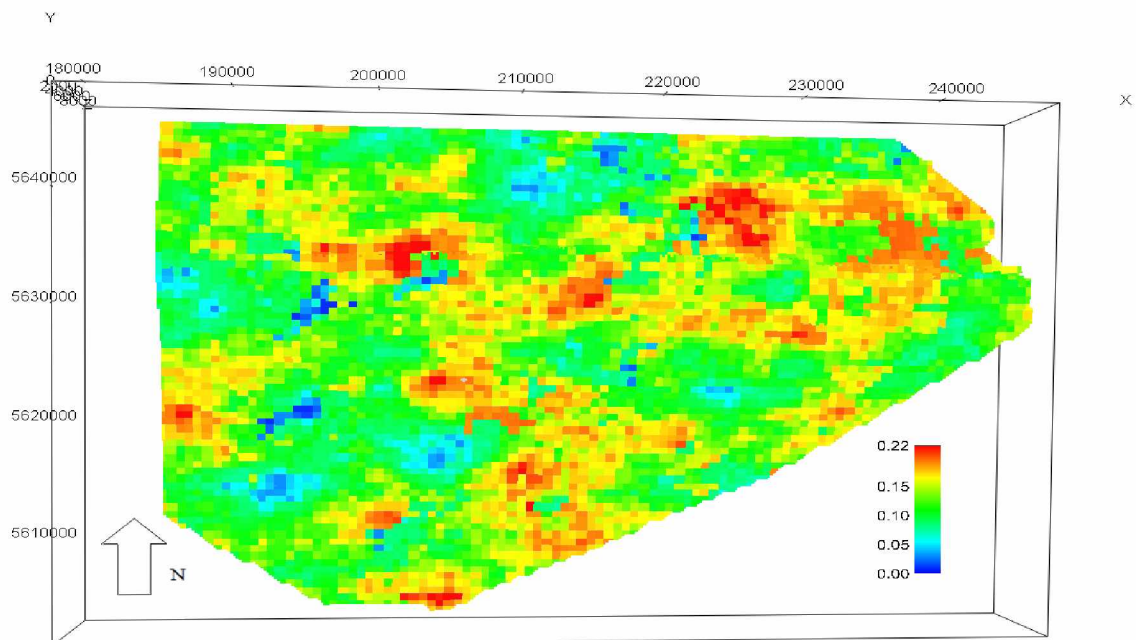


Figure 12. 2D distribution of porosity in uppermost layer of LGS for one realization

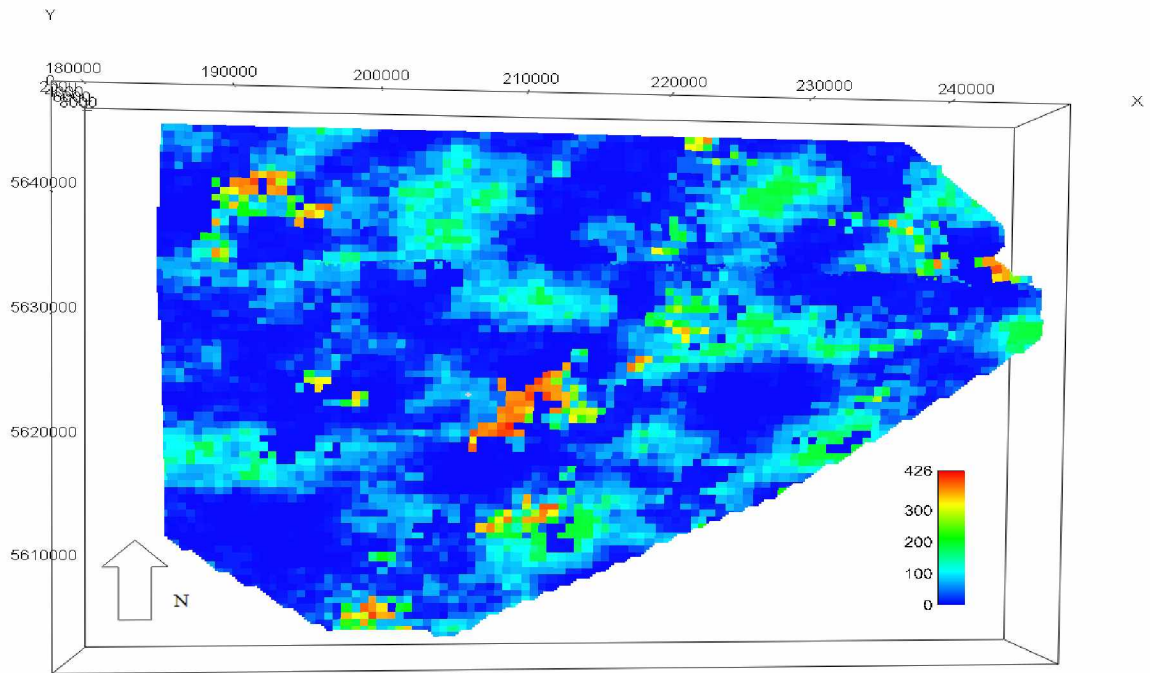


Figure 13. 2D distribution of horizontal permeability in uppermost layer of LGS for one realization

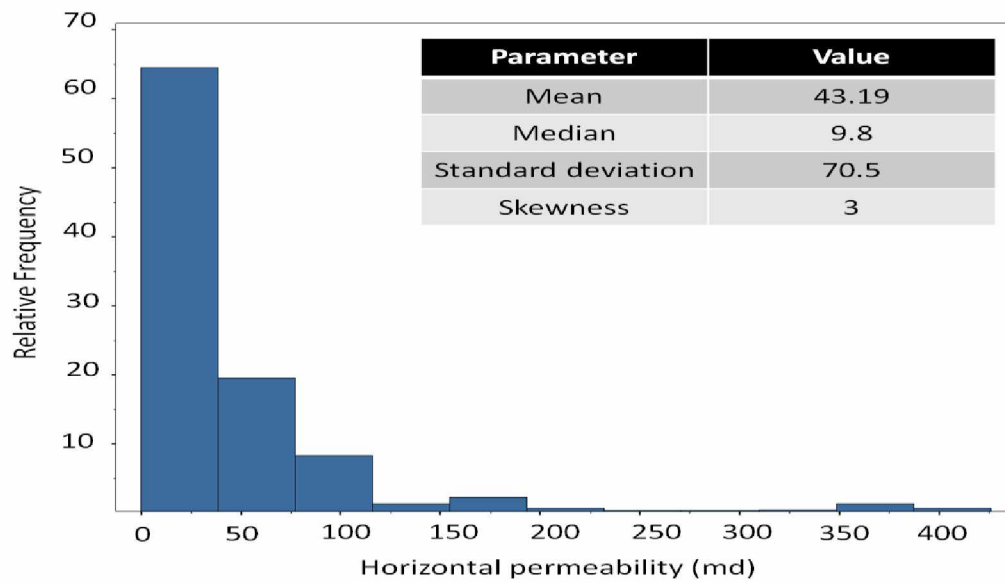


Figure 14. Histogram analysis for the permeability in the LGS formation

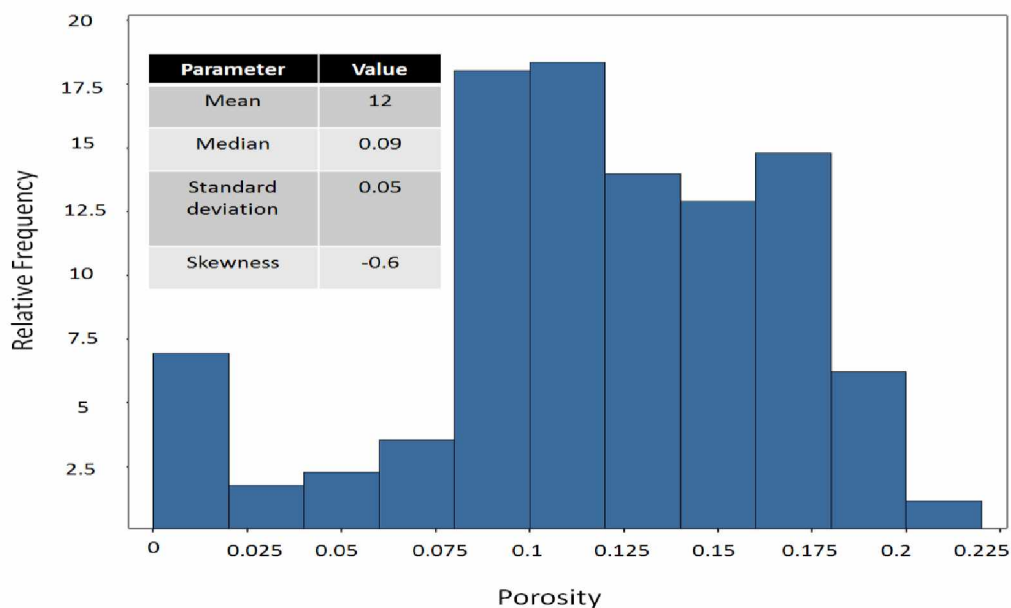


Figure 15. Histogram analysis for the porosity in the LGS formation

3.2 Permeability Anisotropy

The Levi-Johnson model had to be updated with new permeability measurements. A team of geologists and engineers traveled to Eagle River to measure absolute permeability and observe if there is any natural fractures in the core. The cores were cut into flat surfaces and their absolute permeabilities were measured. They were mostly from Wells #9 with a few exceptions from Well #11. Then the data were calibrated and examined to measure anisotropy ratio. For some cases, unreasonable permeability anisotropies were observed and assumed to be due to permeameter and human error. Horizontal permeabilities were more accurate than vertical permeabilities (Shimer, G, personal communication, 2012).

Figure 16 shows a graph of measured permeability anisotropy ratio versus depth in Umiat #9. The 2D distribution of modeled vertical permeability is shown in Figure 17. After

smoothing out the available data, an average value of 0.45 was chosen as the base case permeability anisotropy value. A set of higher and lower values was included in the sensitivity analysis in the reservoir simulation. Impact of the permeability anisotropy on reservoir simulation results are presented in the next chapter.

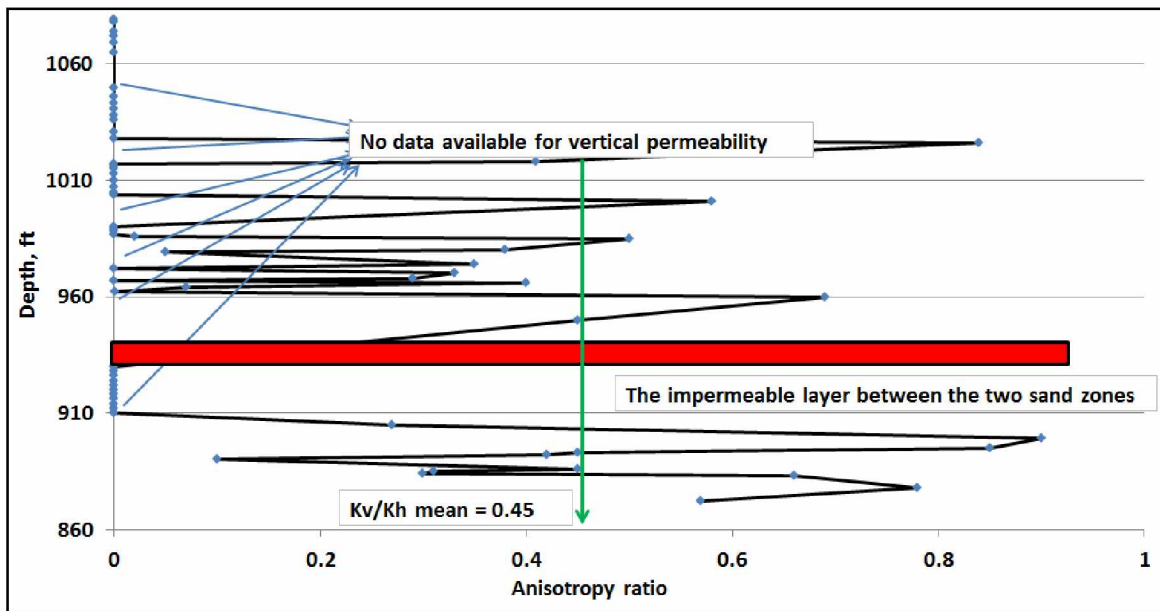


Figure 16. Permeability anisotropy ratio data versus depth for Well #9 (data collected from Shimer, G, personal communication, 2012)

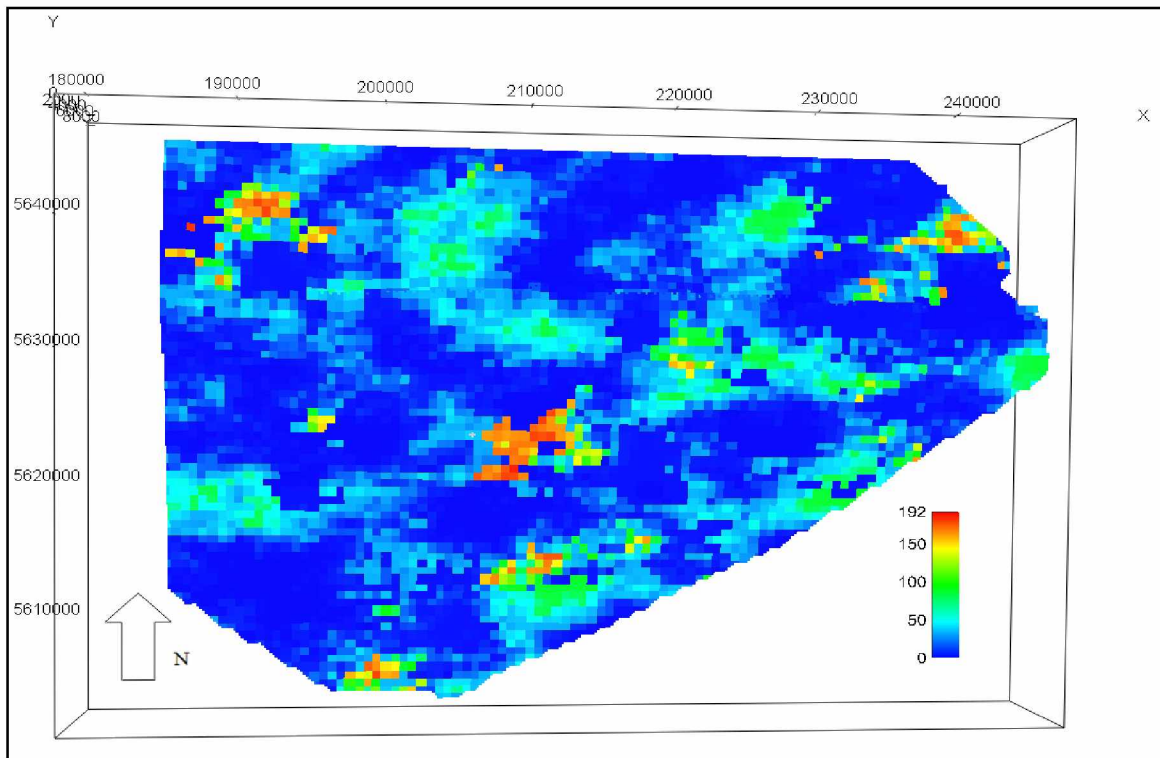


Figure 17. Permeability distribution in vertical direction, K_z (md) in layer #1 of LGS

3.3 Optimal Geologic Grid Design for Simulation

In the Levi-Johnson model, the grid resolution was not refined enough for simulation purposes. Therefore, in this study we decided to downscale the geologic model in all directions in order to decrease the x and y dimension size of grid cells and y dimension of grid layers. First in vertical direction, we wanted to see how much heterogeneity we would lose if we coarsened the layers. Based on porosity for which we had more data, an algorithm was written for layer coarsening (King et al. 2006). The algorithm can be found in Appendix A. As can be seen in Figure 18, the original number of layers corresponds to 100% heterogeneity. When the number of layers is reduced, the loss of heterogeneity will become totally unacceptable, which could eventually lead to unrealistic breakthrough

monitoring and history matching. Therefore, the original number of layers from Levi-Johnson's model in the LGS formation was kept unchanged.

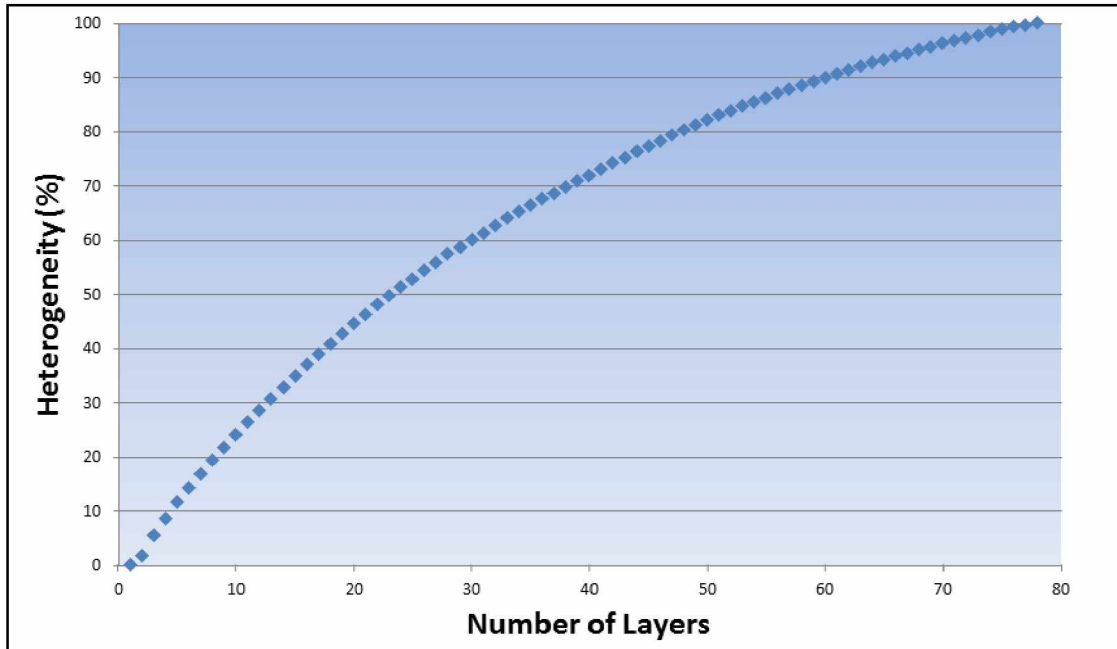


Figure 18. Relation between heterogeneity in the Umiat model and number of layers in z direction

Table 5 shows the number of grid layers per each zone in the LGS formation. Figure 19 presents the histogram for layer thickness in the geologic model. The layer thicknesses ranged from 1 foot in the sands to 45 feet in the shales.

Table 5. Layer information in the Umiat geologic model

Zone	Layer
Upper LGS	1 to 18
Middle LGS	19 to 20
Lower LGS	21 to 32

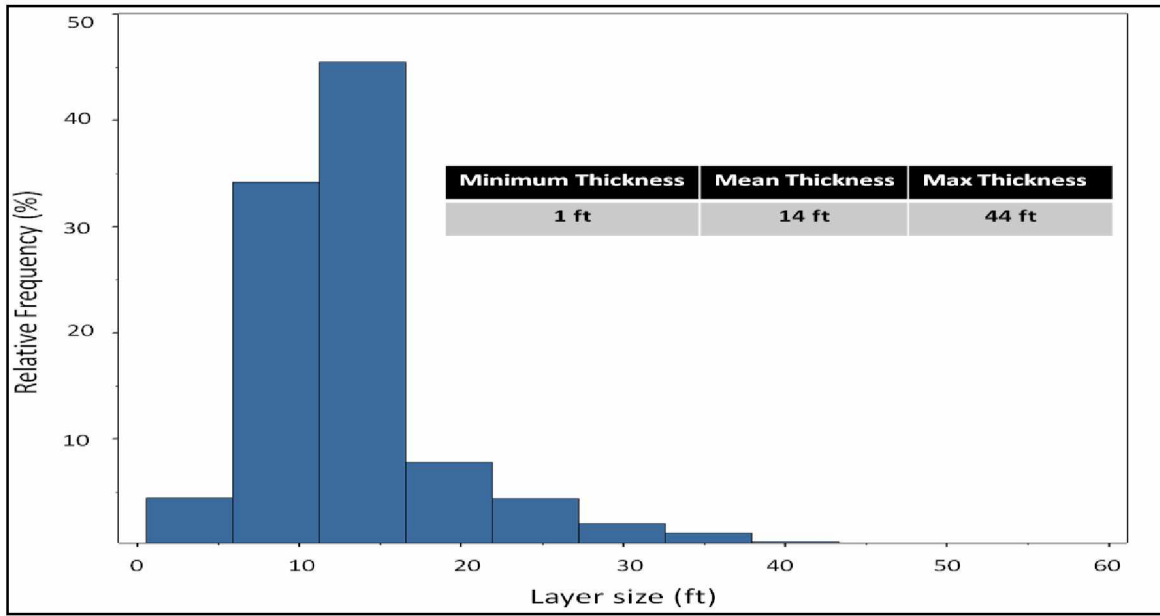


Figure 19. Histogram distribution for grid layer thickness in the LGS formations

In the x and y directions, we decreased grid dimensions up to the computer's computational capacity. The results are shown in Figures 20 through 22. Corresponding grid resolutions for the LGS formation is also shown in Table 6. Simulation grid optimization is presented in the next chapter.

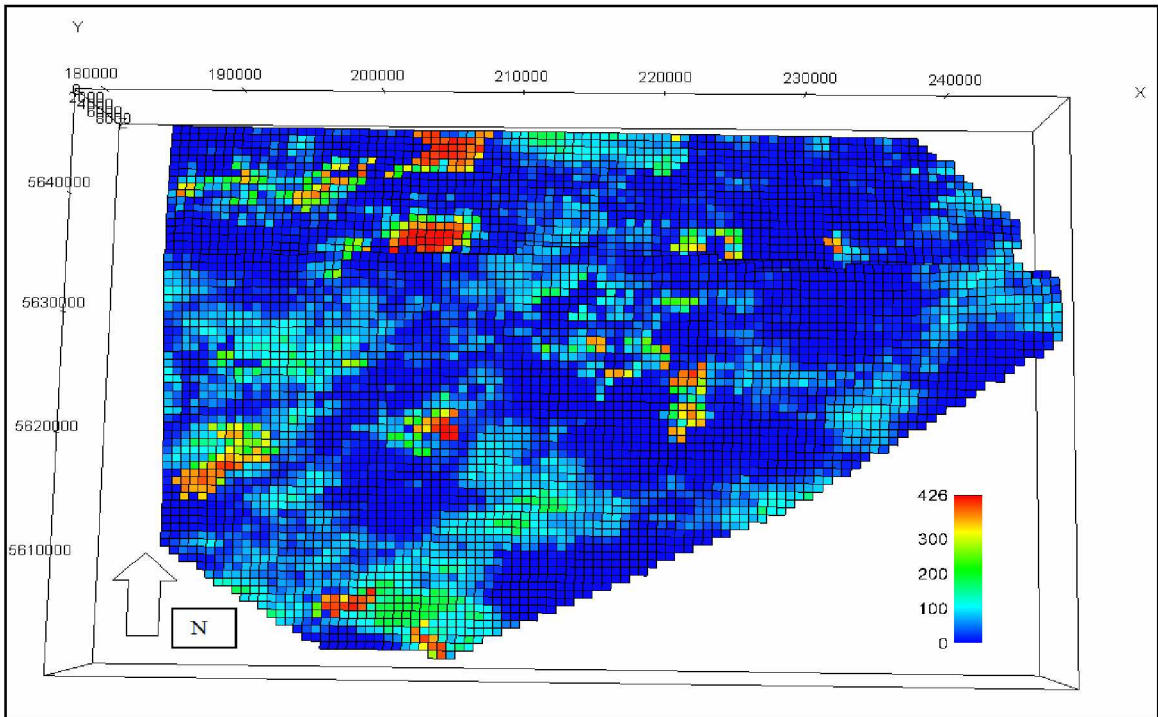


Figure 20. Grid view of permeability in x direction for layer #1 with grid dimensions of 600 ft * 600 ft

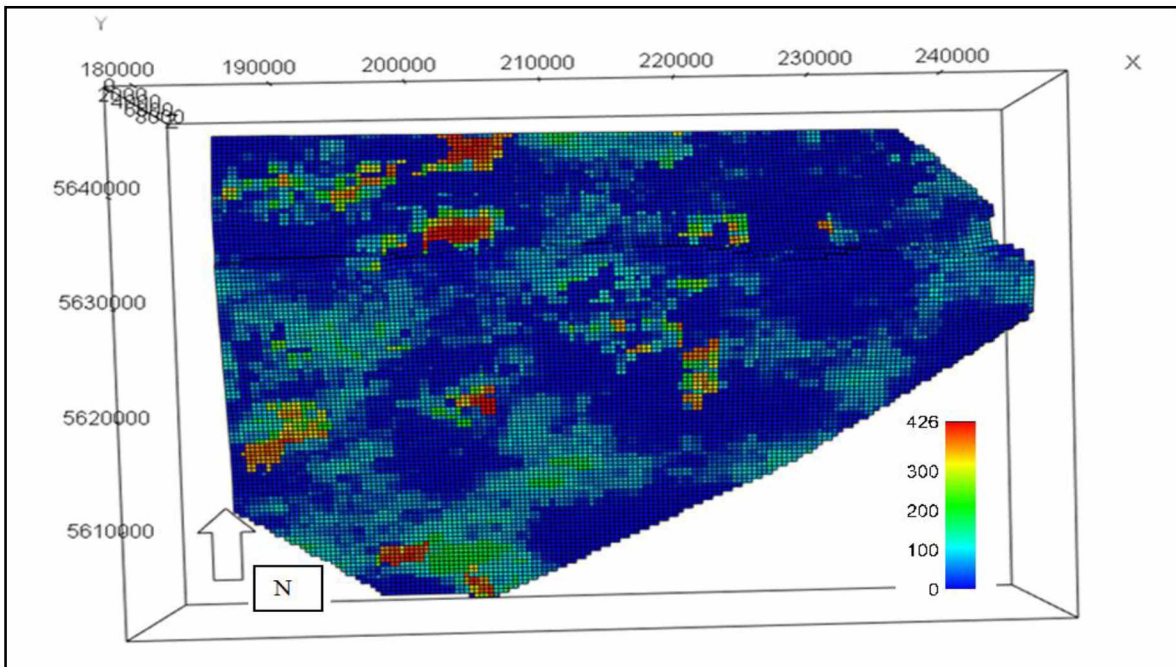


Figure 21. Grid view of permeability in x direction for layer #1 with grid dimensions of 400 ft * 400 ft

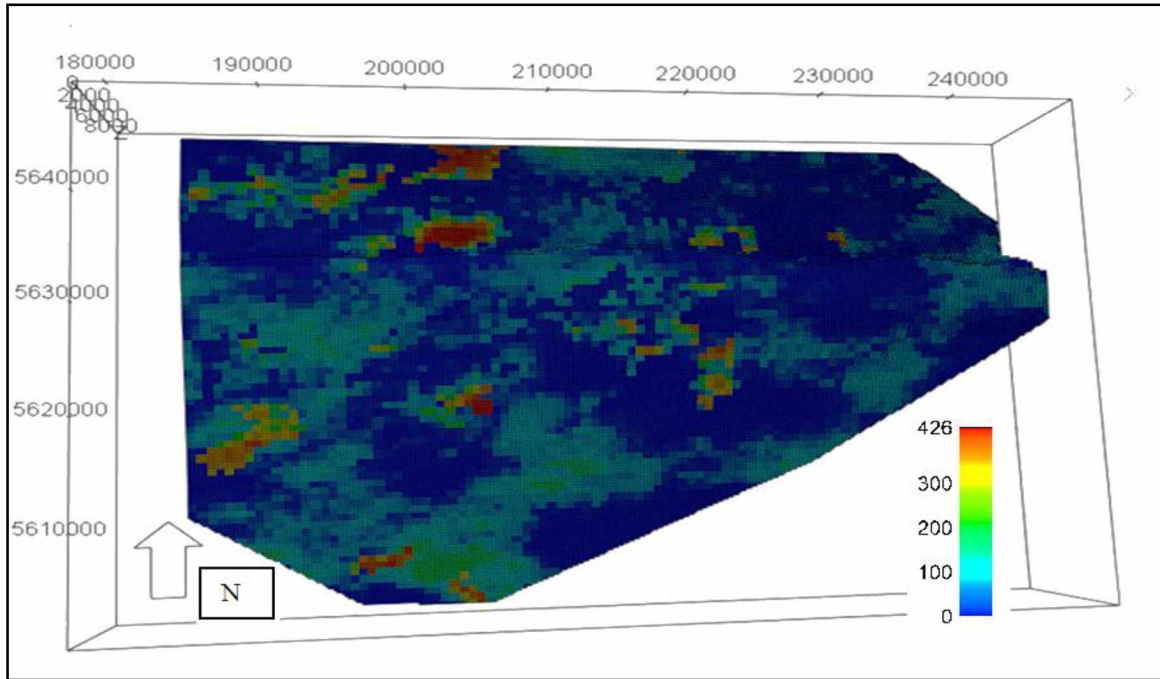


Figure 22. Grid view of permeability in x direction for layer #1 with grid dimensions of 200 ft * 200 ft

Table 6. Different grid resolutions of the geologic model

Grid Resolution	Number of Total Cells	Column * Rows * Layers
600 ft * 600 ft	260,224	107 * 76 * 32
400 ft * 400 ft	583,680	160 * 114 * 32
200 ft * 200 ft	2,344,960	320 * 229 * 32

3.4 Model Geometry

Shimer (Shimer, G, personal communication, 2012) provided new well data not in alignment with previous model descriptions. The data, in some cases, showed that each horizon intersects the existing wells at an upper or lower depth different from the Levi-Johnson model depending on the well locations. Table 7 shows this new well pick data. A value of X indicates no data available. A new workflow was conducted in order to

implement the new horizon modeling. When the horizon modeling was done, we observed inconsistencies in the new model in terms of structure uniformity (Figure 23.a). We believed they were caused by having new horizon layers on old geometry. An attempt was made to make both geometry and horizons consistent by changing the thickness of each formation in agreement with the new horizon design. It should be mentioned that in both the Levi-Johnson and the updated models, the confidence factor based on the Chandler formation was 95%. Other formation thicknesses depend on the true thickness of the Chandler formation. The problem was solved as shown in Figure 23.b.

Table 7. Well pick data from geologist

Well:	1	2	3	4	5	6	7	8	9	10	11
Top: Upper LG	1740	790	X	740	780	X	1200	1260	870	X	2800
Top: Impermeable layer	1790	880	X	830	860	X	X	X	950	X	2940
Top: Lower LG	1820	900	X	X	880	X	X	X	960	X	2960
Base: LG	1970	1050	X	X	1040	X	X	X	1080	X	3090

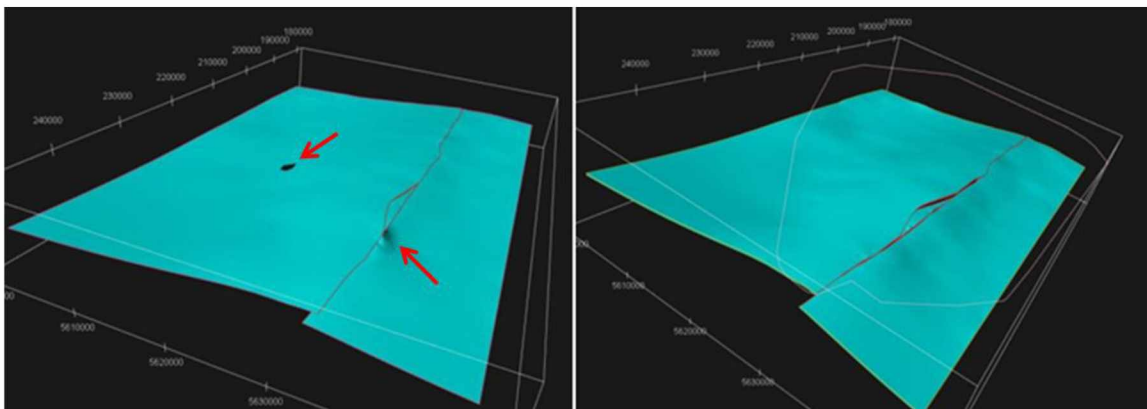


Figure 23.a (Left) and 23.b (Right). Inconsistencies in model caused by new data

Based on new well picks and other data interpretations (Figure 24) (Shimer, G, personal communication 2012), the model further needed to be structurally updated so that the Lower Grandstand could be divided into three sub-formations. The geologist believed that there is an impermeable layer of shale in the LGS formation that separates it into two different zones. In order to incorporate this geometry into the model, another workflow was constructed for new horizons and structural framework. Then the model was re-gridded again and populated with the petrophysical properties (Figure 25). A list of well pick data and their corresponding measured depth (Shimer, G, personal communication, 2012) used in the model geometry are provided in Appendix B.

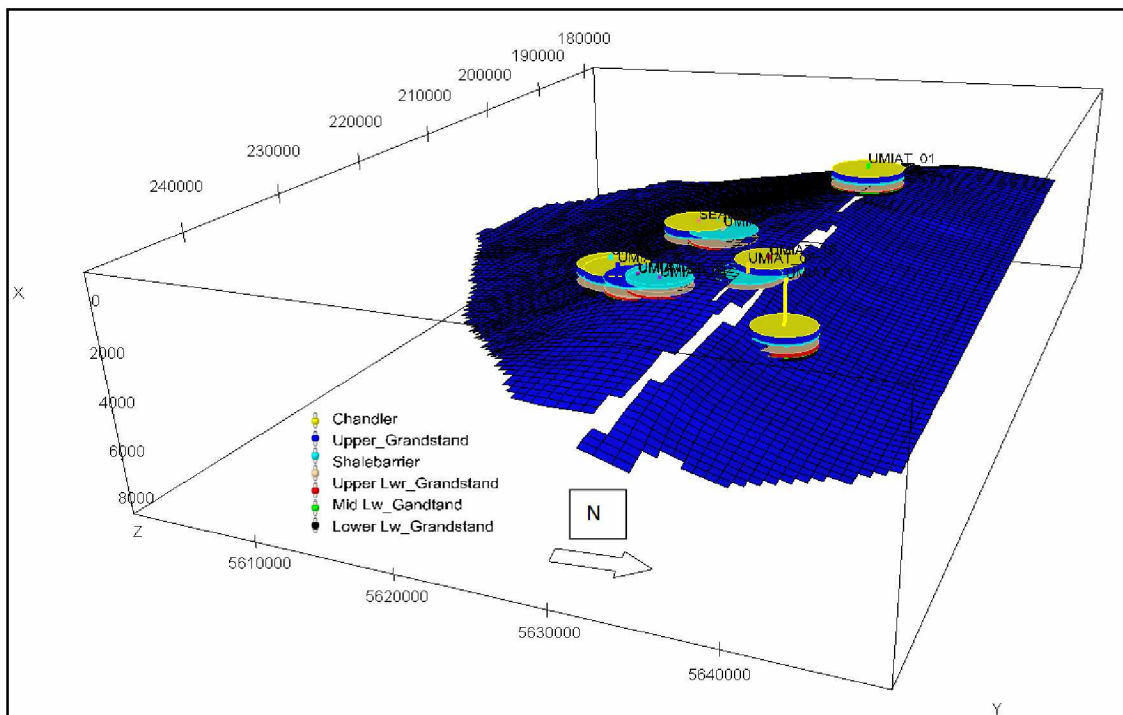


Figure 24. Design of structural framework incorporating new well pick data; note that the circles show the well pick data and the blue surface shows the uppermost layer of the Middle LGS formation which is layer #19

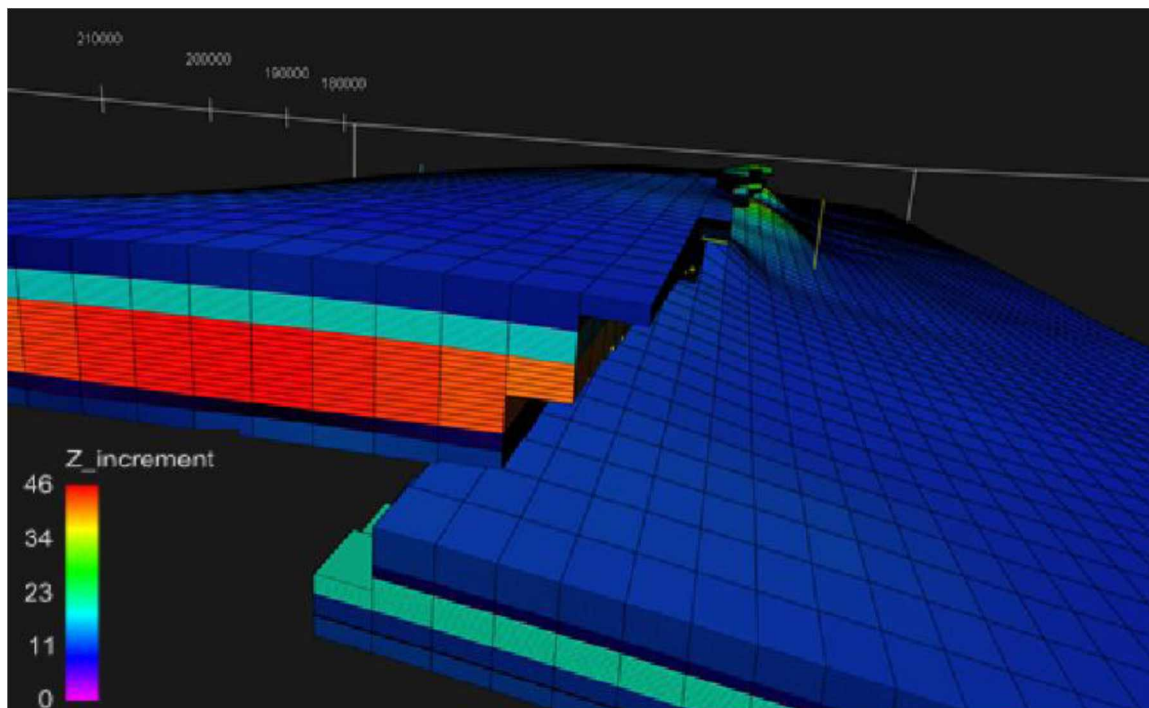


Figure 25. Grid view of the full field model with 500,000 active cells and 90*70*78 dimensions. The colors represent the grid cell thickness

3.5 Modeling of Water Saturation: Concepts and Challenges

Water saturation is the fraction of water in a given pore space. Three phases of gas, oil and water may exist in reservoir. These phases are separated due to density difference with a transition zone caused by capillary forces. The height of the transition zone depends on factors like permeability, porosity, and capillary pressure (Roxar manual guide, 1994-2008).

Accurate modeling of water saturation variation in the transition zone is important to reservoir simulation (Ghedan et al., 2006) and determination of original oil in place.

Water saturation in the reservoir is commonly determined by interpretation of electrical resistivity measurements using the Archie's law (Masoudi et al., 2011). Use of the Archie equation entails having adequate resistivity logs and S_w -log-derived data.

A semi-log plot of (K/Φ) vs. Φ for the LGS taken directly from Irap after the geologic modeling is shown in Figure 26. For any range of porosity there is a wide range of permeability which could be due to varying degree of clay in the reservoir. It could also be related to other textural features such as grain size and grain sorting. Based on the large variation in permeability (0-500 md) and a lack of a relationship between the sandstones grain sizes, composition, porosity, and permeability, the sands were classified into three sand groups (rock types) based on three ranges of permeability (Table 8). This will help in creating a more accurate distribution of water saturation in each sand group and obtaining capillary pressure data for use in reservoir simulation.

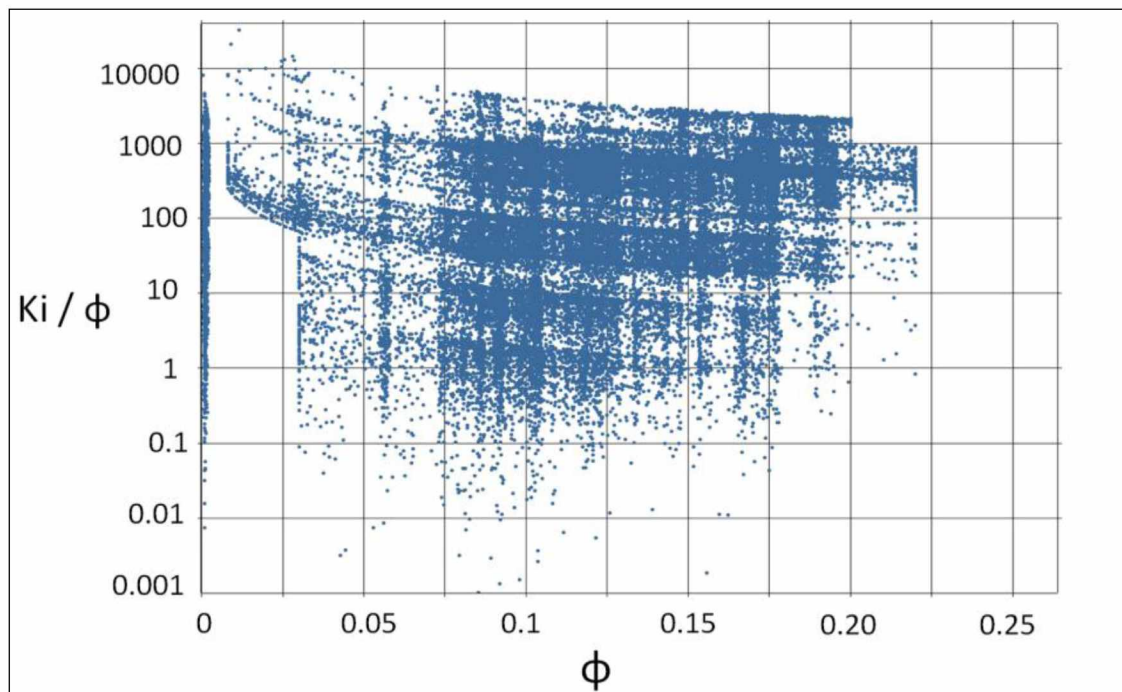


Figure 26. Semi-log plot of (K/Φ) vs. Φ in the LGS formation

With no available resistivity log, a methodology was developed to use the available air-kerosene capillary pressure data (Godabrelidze, 2010) to derive the saturation-height functions for each sand group (rock type) in the model. The fact that the capillary pressure-saturation curves of nearly all naturally porous materials have many features in common has led to attempts to devise some general equation describing all such curves (Ahmed, 2001). Since the P_c data was available for the sand group #1 (rock type #1) from the core #60, the Leverett J-function (Amyx et al., 1960) was used to correlate capillary pressure data for other rock types based on the average values of their permeability. The Leverett J-function in consistent units is defined as:

$$J = \frac{P_c * \text{Sqrt} \left(\frac{K}{\Phi} \right)}{\sigma * \text{Cos} \theta} \quad (1)$$

Where:

K = permeability (sq cm)

Φ = fractional porosity

σ = interfacial tension (dynes/cm)

P_c = capillary pressure (dynes/ sq cm)

θ = contact angle

If we assume that the porosity range is the same in each sand group, by neglecting the interfacial tension forces, the capillary pressure is inversely proportional to square root of permeability (Equation 2).

$$P_c = P_{c_{60}} * \text{Sqrt} \left(\frac{K_{60}}{K} \right) \quad (2)$$

Where:

$P_{c_{60}}$ = capillary pressure for core #60

K_{60} = absolute permeability for core #60

K = absolute permeability average for other sand groups

Table 8. Different rock types in the Umiat reservoir

Sand group	Permeability range (md)	Representative K for Pc class (md)	P_c categorization
1	$K < 1$	0.408	Pc-1
2	$1 < K < 50$	22.5	Pc-2
3	$K > 50$	100	Pc-3

The water-kerosene capillary pressure data were mathematically converted to oil/brine system at the reservoir condition (350 psi, 26°F). Typical interfacial-tensions ($\sigma_{\text{air-mercury}}=487$ dynes/cm, $\sigma_{\text{water-kerosene}}=48$ dynes/cm) were used while possible difference in the contact angles were ignored as input to the simulator. Figure 27 shows the capillary pressure versus the water saturation. The transition zone for the core plug #60 (Pc-1) with the low permeability data is the highest among three sand groups. It should be noted that the P_c data are only shown for oil and water. The capillary pressure between oil and gas is generally ignored because of large density differences between them and there is no initial gas cap in the reservoir.

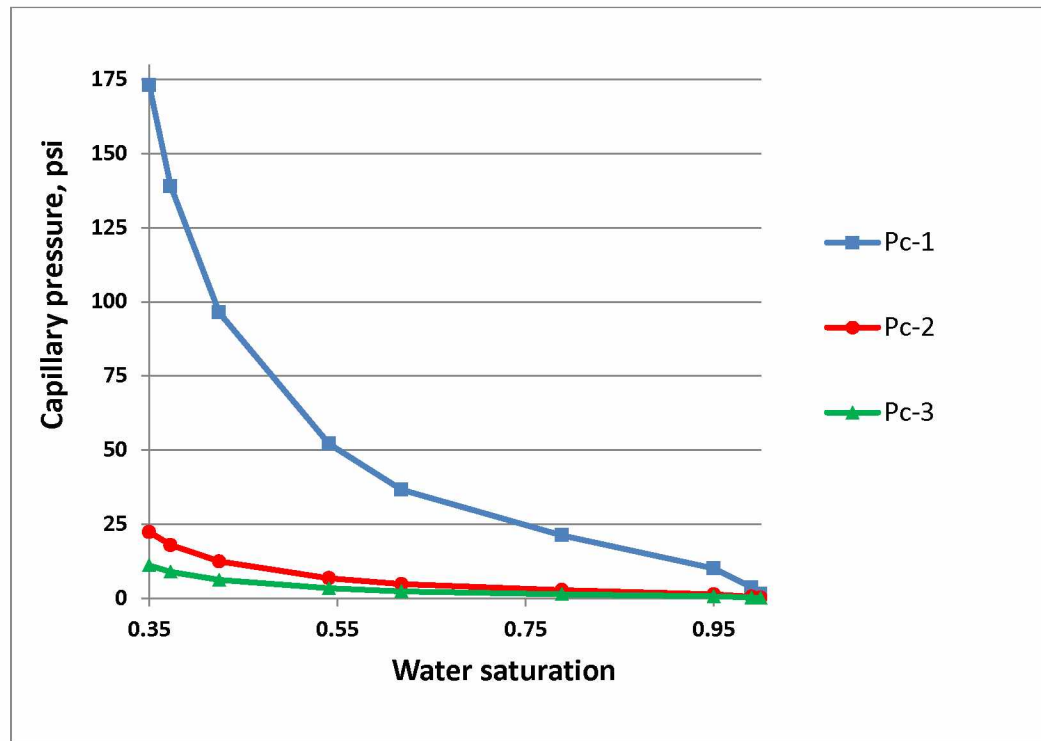


Figure. 27. Oil-water capillary pressure data based on absolute permeability

Then by using Equation 3 and oil and pure water densities at reservoir conditions (Table 9), the obtained capillary pressure data were transformed to the respective capillary heights in the reservoir and a look-up function for each sand group was built in IRAP to account for different trends of S_w versus depth (Figure 28).

Table 9. Oil and water density at reservoir conditions

Water density (lbm/ft ³)	Oil density (lbm/ft ³)
62.4	52.6

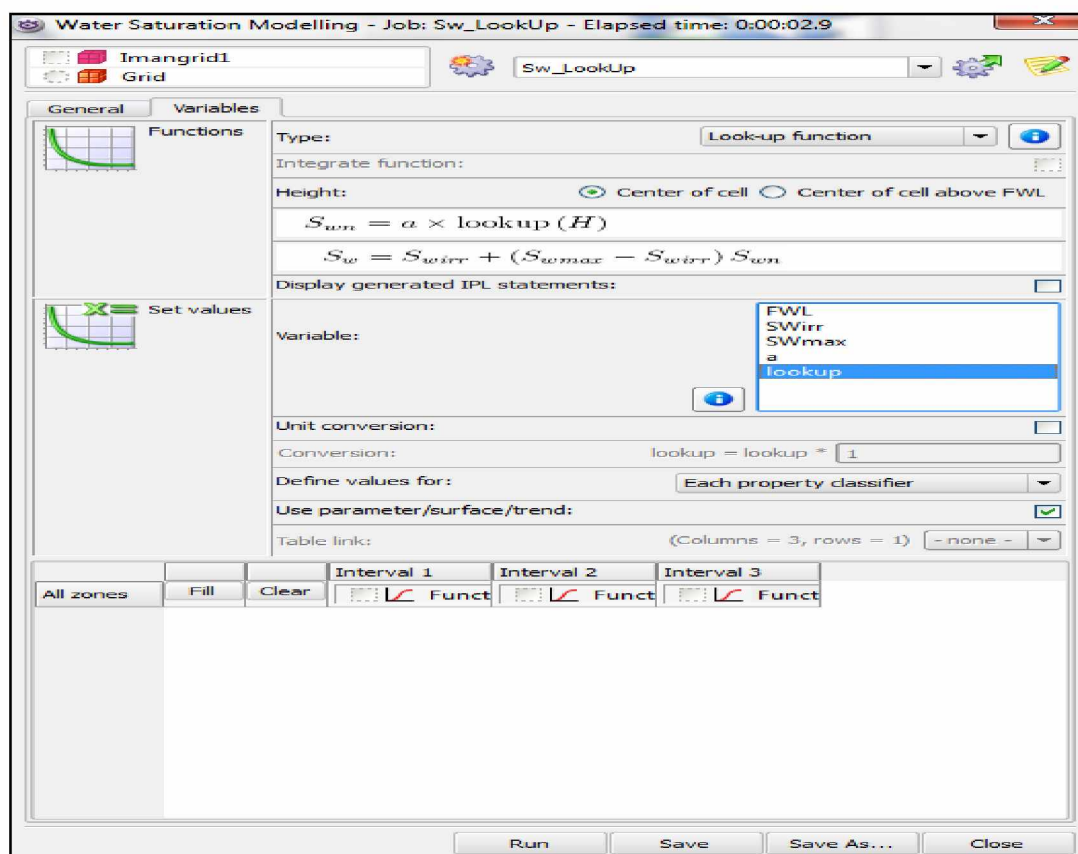


Figure 28. Using a simplified look-up function to incorporate Sw height relationships

The generated saturations were plotted against the height above the free water level (Figure 29). As it can be seen in the Figure 28, water saturation data changes with respect to depth for different sand groups. As expected, sand group# 1 has the lowest permeability range and consequently has the highest transition zone height compared to other sand groups in the reservoir. At the end, the petrophysical modeling was run to distribute the water saturation in the model. Figure 30 shows the 2D distribution of the water saturation in the model after executing the workflow.

$$h = (144 * Pc) / (\rho_w - \rho_o) \quad (3)$$

Where:

H= height above free water level (ft)

Pc= capillary pressure (psi)

ρ_w = water density (lbm/ft³)

ρ_o = oil density (lbm/ft³)

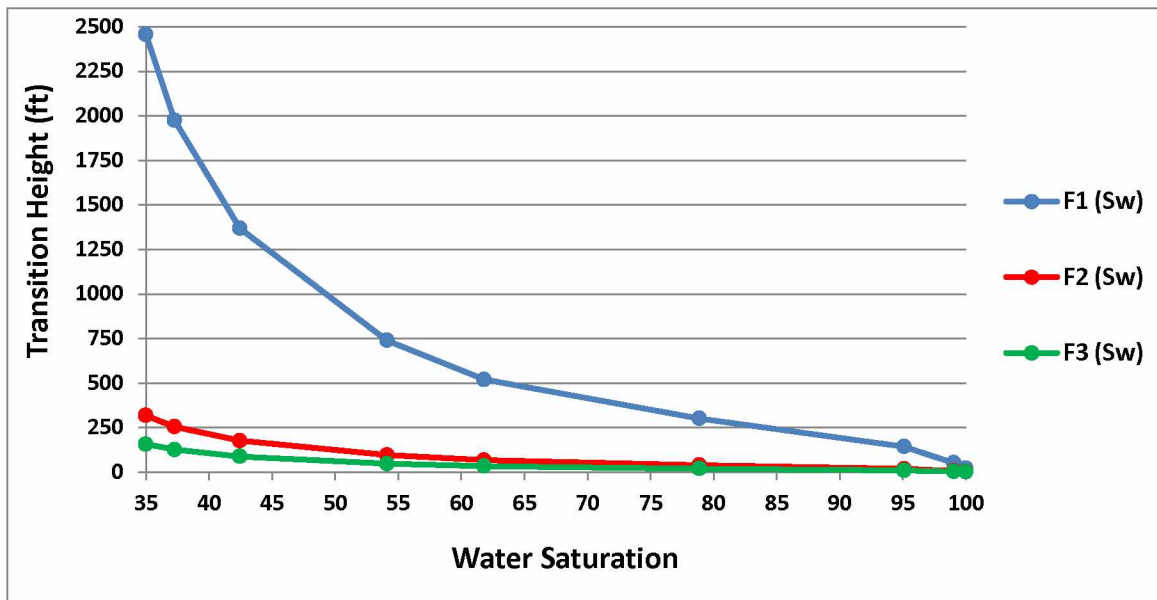


Figure 29. Water saturation height functions for different sand groups

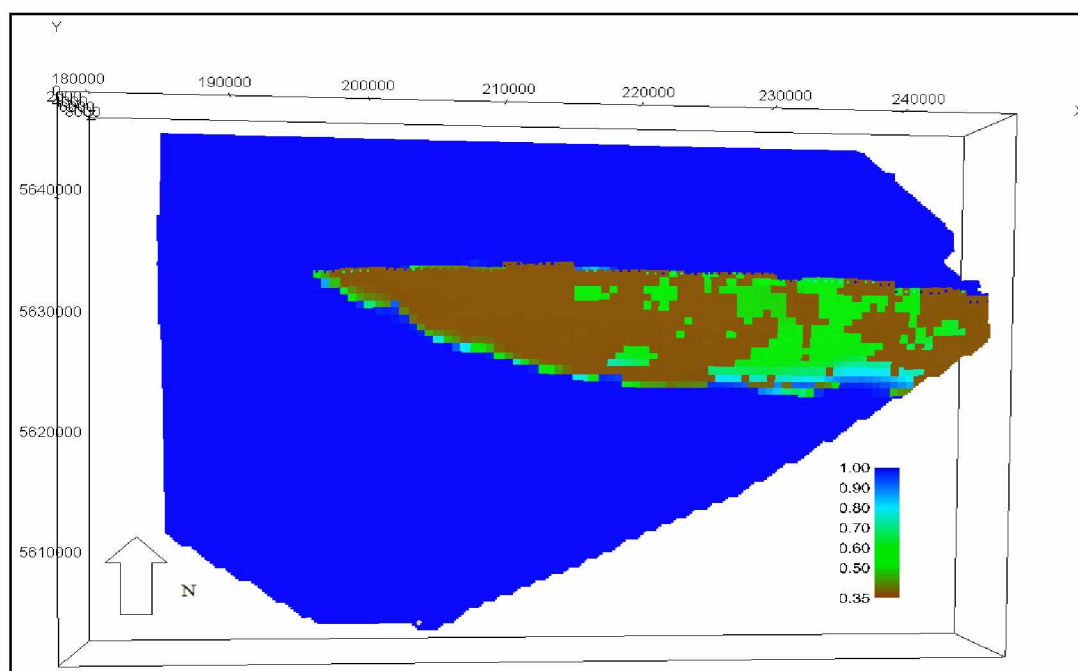


Figure 30. Modeling of water saturation in the Umiat reservoir by use of capillary height functions in upper part of LGS.

3.6 Application of Petrophysical Cut-offs

“Cut-off” refers to a joint effort by geoscientists and engineers to define a value to discriminate non-reservoir rock (shale) from reservoir rock (Dachang and Myra, 1997). Particularly in the Umiat reservoir, due to its relatively large area, a high number of grid cells in the geologic model, and computational concerns for the reservoir simulator, a sensitivity study was implemented on the application of petrophysical cut-offs (porosity, and water saturation) and the results were re-examined.

Since the aquifer is not considered active, all cells having S_w equal to 1 were considered to be undefined cells. The sensitivity analysis included running different volumetric scenarios based on simultaneous application of porosity and permeability cut-offs to optimize the number of grid cells and to reduce the impact of the cut-offs on the original

oil in place calculations. Two impact ratios (Equations 4 and 5) was defined for the effect of applying cut-offs on the active cells (Actnum) and the original OOIP. In this particular situation, the approach helped to distinguish the non-pay rock from reservoir rock.

$$\text{Resource Impact Ratio (RIR)} = (R - R_c) / R \quad (4)$$

$$\text{Cell Impact Ratio (CIR)} = (C - C_c) / C \quad (5)$$

Where:

R: The OOIP without application of cut-off

R_c: The OOIP after cut-off

C: The Original Actnum

C_c: The Actnum after cut-off

As can be seen in Figures 31 through 33, the optimum porosity cut-off was determined to be 5%, in such a way that the cut-off application will have the lowest impact on the OOIP value and the highest effect on the number of inactive cells. In other words, the optimum cut-off is when we have the lowest values for both resource impact ratio and cell impact ratio. By applying this methodology, we were able to exclude about 500,000 cells, which translates into saving about 900 MB in the RAM space and an equivalent computation time of about 5 hours.

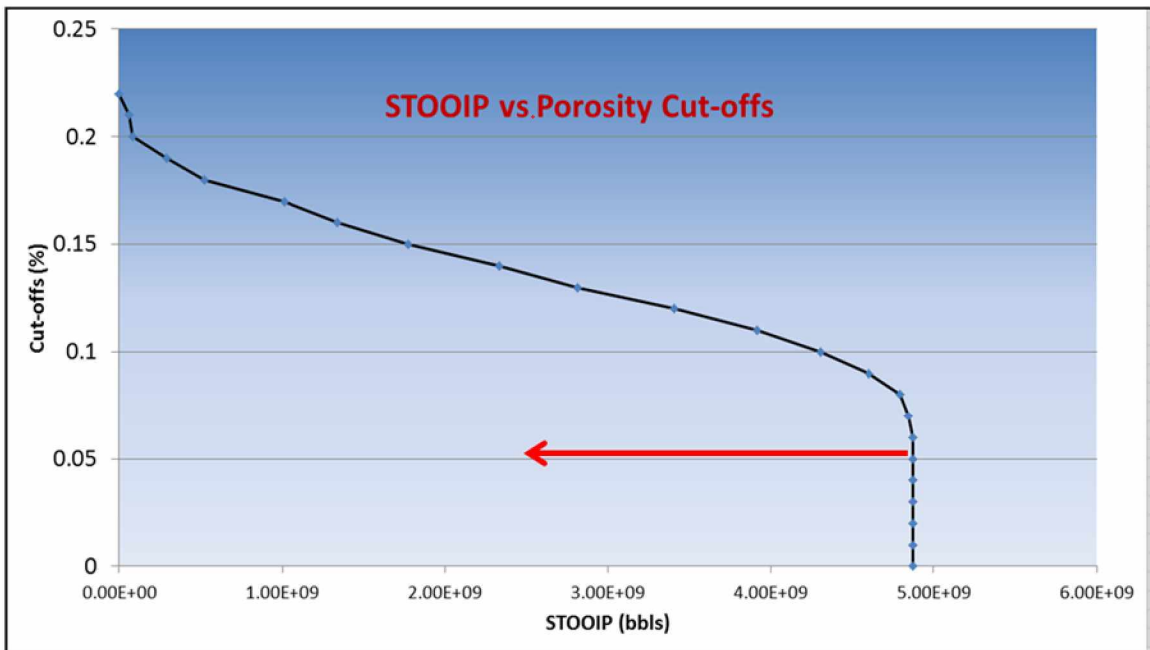


Figure 31. Application of porosity cut-off and its effect on the oil in place

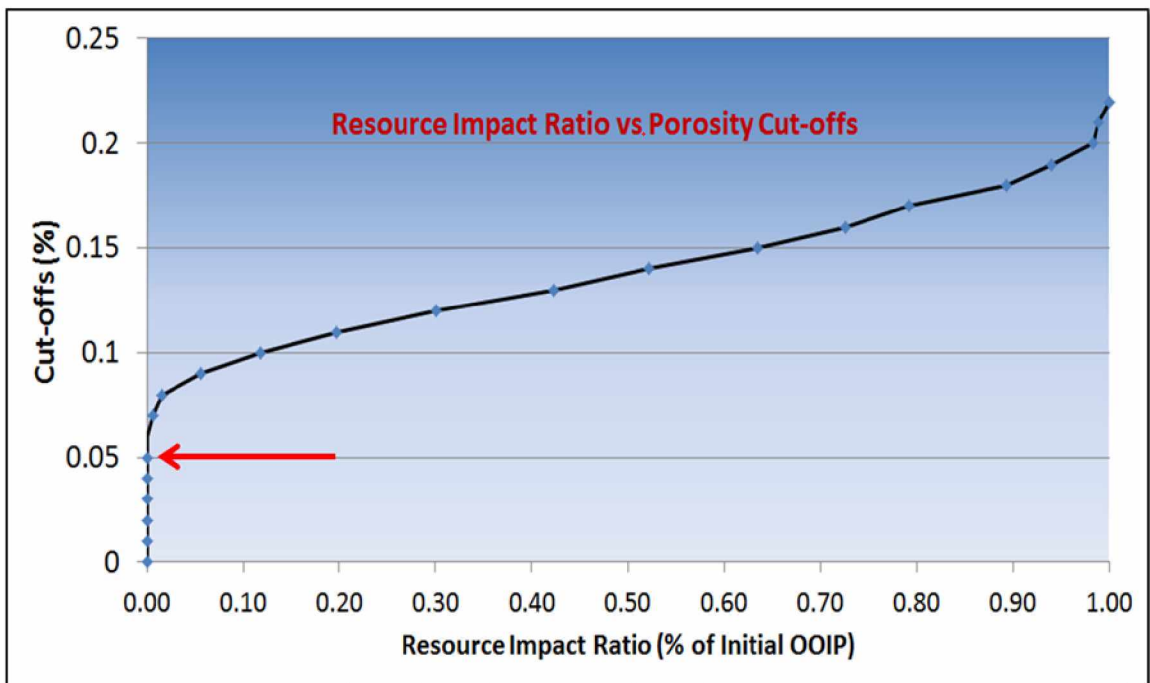


Figure 32. Application of porosity cut-off and its effect on OOIP by use of RIR parameter

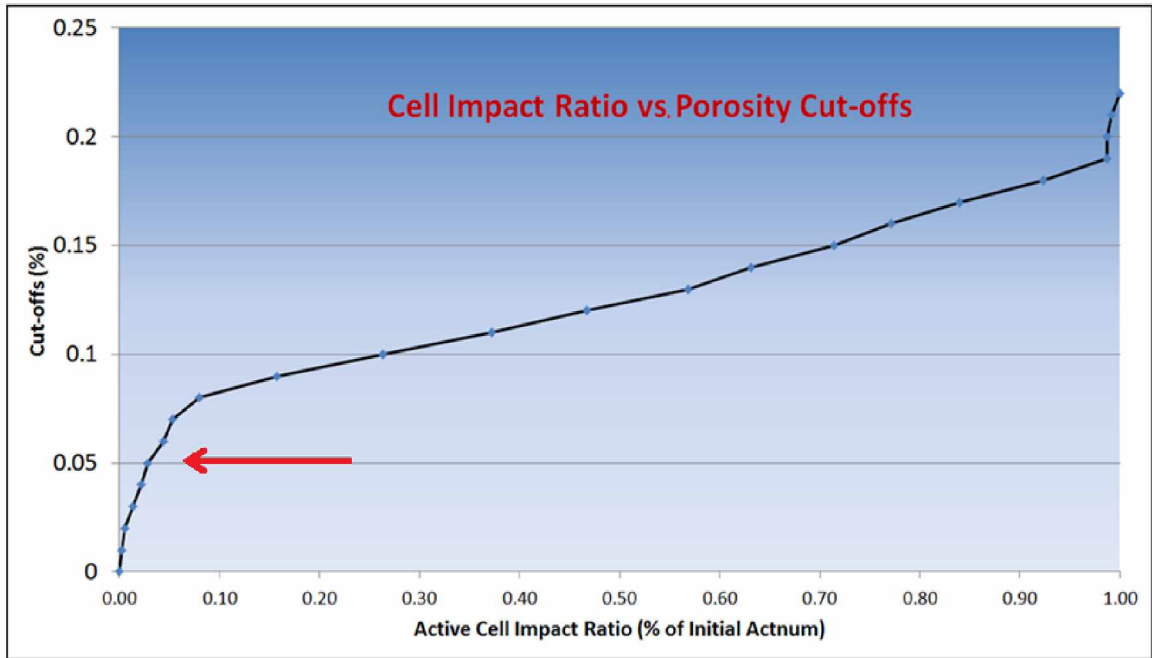


Figure 33. Application of porosity cut-off and its effect on Actnum by use of CIR parameter

As discussed earlier, one reason for applying cut-offs is to differentiate between non-reservoir rock and reservoir rock. In this particular situation, by applying the cut-off procedure for porosity and permeability, the non-reservoir rocks were distinguished from the reservoir rocks and excluded from the model. Figure 34 shows the exclusion of non-pay rocks.

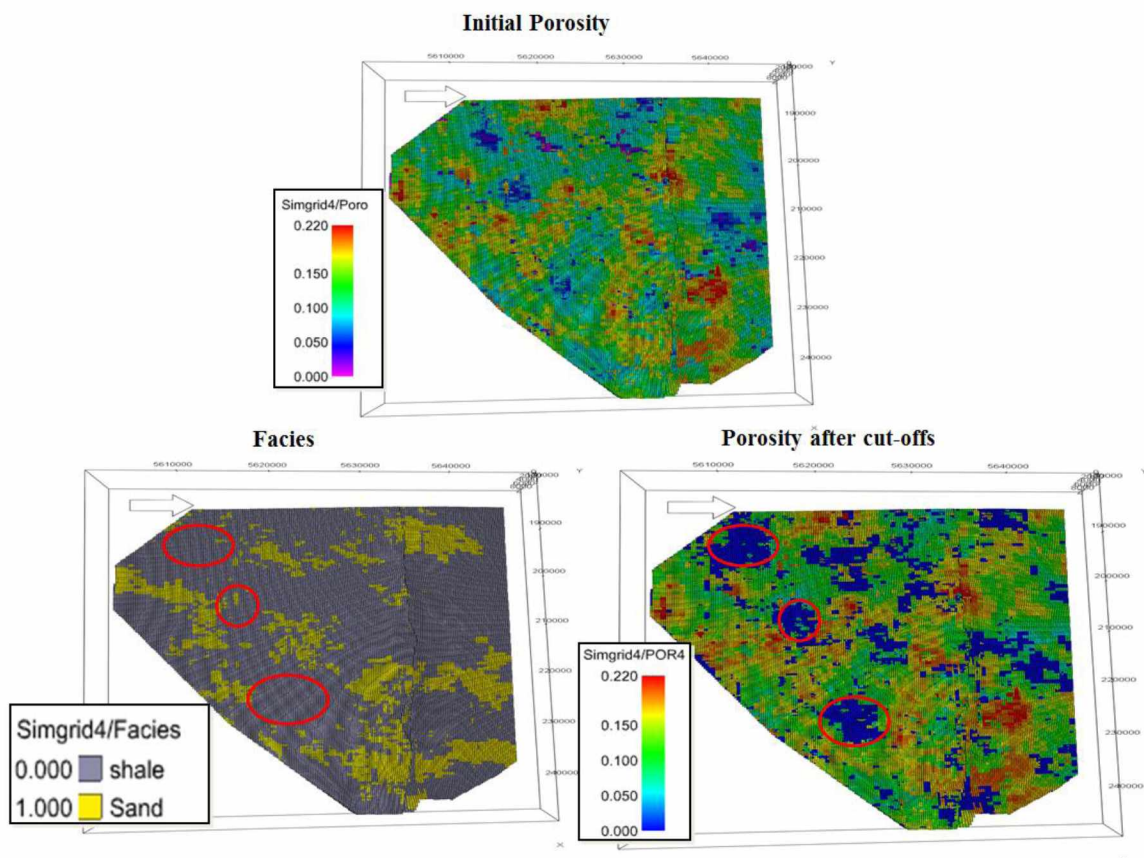


Figure 34. Maximizing the exclusion of non-reservoir rocks from the model, the circles show the area hit by application of cut-offs

3.7 Monte Carlo estimation of OOIP

The estimated original hydrocarbon in place is one of the most important factors when considering an accumulation for development. The estimates provided in previous reports (Watt et al., 2010; Levi-Johnson, 2010) were based on a single realization of the geological model that honored the average values of data reported from limited number of wells. Having different realizations for combinations of different volumetric factors helps one understand this element better and make better decisions. A Monte Carlo (MC) simulation was conducted by considering different ranges of 5 input variables in 10,000

runs. The range of input variables used in the MC simulation and the results are provided in Tables 10 and Table 11 for three sub-formations in the LGS.

Targeting specific quantiles such as P10, P50, and P90 realizations is a challenge. There are statistical methods to establish P10, P50, and P90 figures. Approaches to estimate resource are divided into deterministic and probabilistic methods. In the deterministic approach, a single value is used for each parameter. The probabilistic approach however, uses a full range of input parameters in the resource estimation. The probabilistic method was utilized in IRAP and the P quantiles are provided in Table 12. The result of this simulation yielded STOOIP estimations ranging from P90 of 750 million to a P10 of 2474 million bbl. The P50 value for STOOIP estimate was 1550 million bbl (Figure 35).

Table 10. Different variable ranges used as input into the Monte Carlo simulation

Input	Range
Initial water saturation	0.35–0.45
Net to gross ratio	0.1–0.7
Bulk volume (E+9 ft ³)	36–56
Porosity (%)	5.00–22.00
WOC depth (ft)	700–1500

Table 11. STOOIP estimations for each zone in the LGS formations

Zone	STOOIP (MM barrel)
Upper LGS	791
Middle LGS	7.80
Lower LGS	704
Total	1502

Table 12. P quantiles for resource estimations

Probability	Value (MMM STB)
P10	2474
P50	1550
P90	790

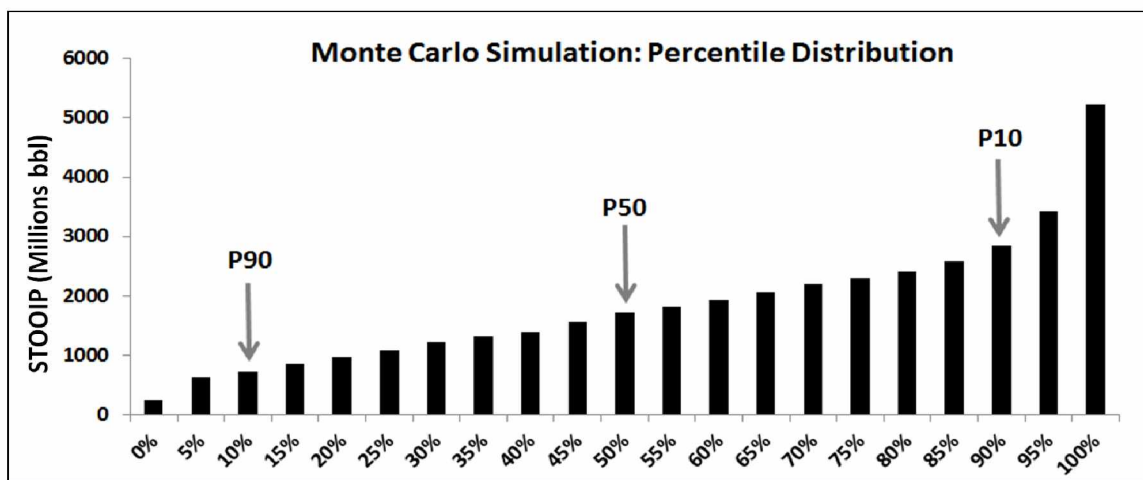


Figure 35. Graphical representation of Monte Carlo simulation for 10,000 runs for LGS

3.8 Uncertainty Parameter Ranking by Multiple Realizations

Because large investments have to be made early in the life of the fields, the uncertainty in the hydrocarbon in-place volumes and production profiles may have a direct impact on important economic decisions (Meisingset, 1999). There is significant risk involved with reservoir management. One of the main reasons for the risk is uncertainty in reservoir models. Uncertainty is everywhere and one cannot escape from it (Lindley, 2006). The uncertainty can range from the core data to uncertainty in well configuration and optimal production plan. The uncertainties associated with a geologic model are many and have such varying impact that is necessary to know what to look for (Roxar manual guide, 1994-2008).

The structural uncertainty can be caused by processing and interpretation of seismic data, and subsequent uncertainty in fault and data resolution (Figure 36). In geologic uncertainty, parameters such as facies and rock type, isochore variation and reservoir distribution (channel, pinchout, etc...) are involved. Fluid contacts are another source of uncertainty in geologic modeling that can hugely impact the reserve estimates (Figure 37). Misinterpretation of well test data and fluid measurements such as B_o , B_g , and GOR causes fluid uncertainties that also could potentially affect the dynamic behavior of the flow.

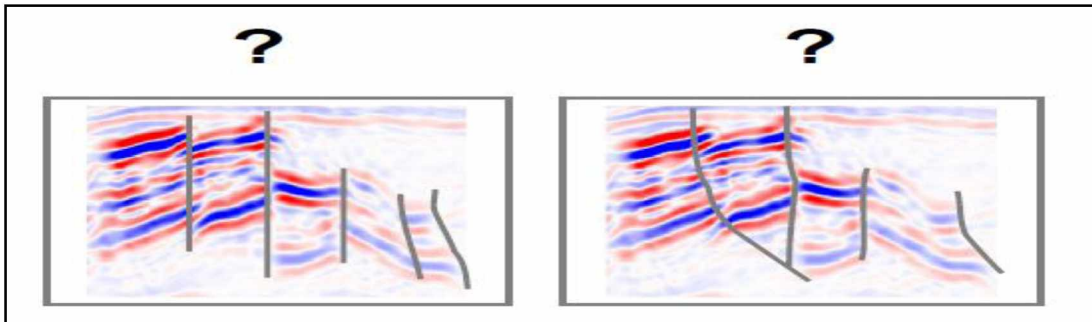


Figure 36. Uncertainty in fault interpretation (Poete, 2012)

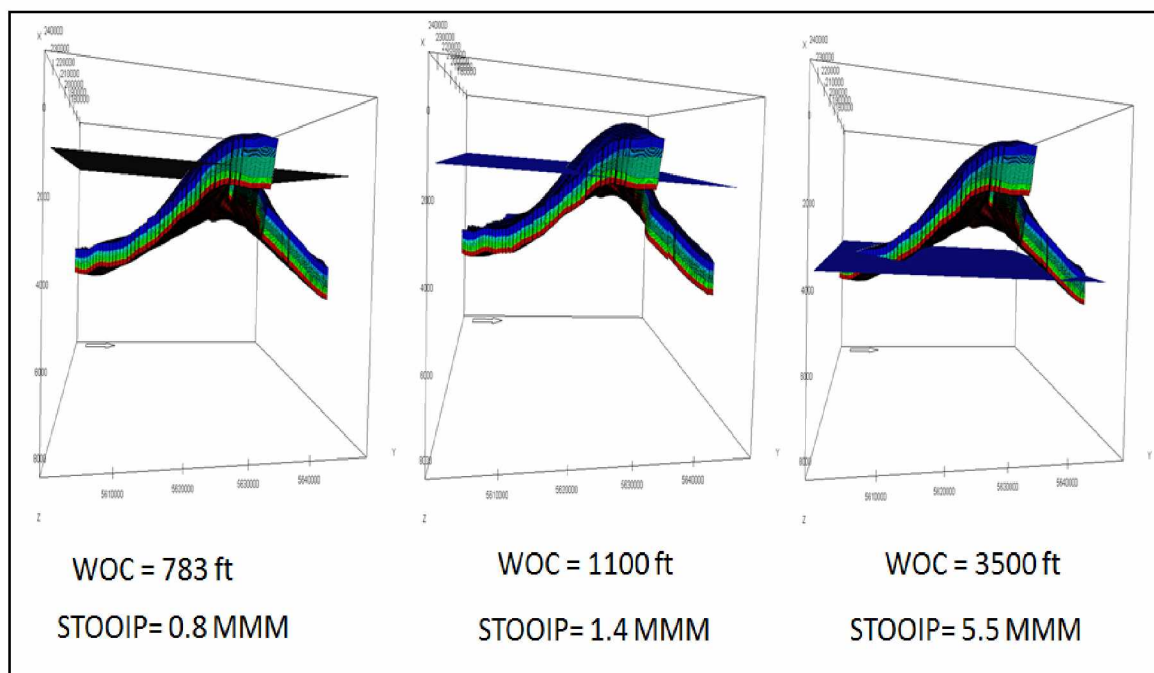


Figure 37. Uncertainty to oil water contact in Umiat reservoir

Uncertainties in petrophysical properties are widely accepted, but rarely applied in formation evaluation and reservoir characterization (Zeybek et al., 2009). Petrophysical uncertainty in porosity, permeability and saturation is fundamentally different from other mapping-related uncertainty and causes the relative importance of petrophysical uncertainty to increase throughout a field's life cycle until it will become the most important source of HCPV (Hydrocarbon Pore Volume) uncertainty (Fylling, 2002).

Without proper consideration of these uncertainties, estimation of the STOPIP can be in error (Cronquist, 2001). This is particularly important for reservoirs such as the Umiat oil field with unique characteristics. This uncertainty analysis can be used in the field development when evaluating the formation characteristics.

Available data in the Umiat oil field were generally not enough to minimize the level of uncertainty for one perfect geologic model and to capture all sources of uncertainties. In this study, focus was placed into the available data sources that were available and a sensitivity uncertainty parameter ranking was conducted to see which parameters contribute more to the resource estimation.

This section presents a methodology to simulate multiple realizations of key uncertainty parameters associated with geological complexity and the petrophysical property models in the range of global uncertainty. The proposed workflow was developed in IRAP RMS and includes construction of the geologic model and population of the geologic model with petrophysical parameters and uncertainty analysis. The uncertainty parameters were defined and used, and all combinations of parameters were tested. Uncertainties related to choice of parameters such as variogram characteristics (type, range, and sill) were also included in the analysis.

Multiple realizations allow for a better decision-making process in risk analysis, reservoir forecasting, and management. In this study, 100 realizations were run and reservoir uncertainties were ranked based on their impact on STOOIP. Input data to the uncertainty realization runs are summarized in Table 13.

Table 13 The input uncertainty parameters for multiple realizations workflow

Input data	Range of values
Structural uncertainty	30 ft
Water oil contact depth (ft)	783 to 1500
Water saturation	3D modeled Sw
Porosity	3D modeled porosity
Net to Gross	3D modeled NTG
B _o (rb/stb)	0.9 to 1.05
Variogram range normal to azimuth (ft)	1000 to 10,000
Variogram range parallel to azimuth (ft)	1000 to 10,000

Since each parameter is considered as an input to the volumetric calculations, its effect on the results can vary depending on how many times it is utilized in a base case STOOIP. A base case was chosen to serve as the basis of comparison between different outcomes. A Tornado-style plot was used to rank each parameter in terms of its contribution to the initial oil in place. Results are shown in Figure 38. The highest-ranked contributor to the volumetric estimates was found to be depth of the oil water contact. Variogram ranges in both normal and parallel range was ranked next. This implies a large degree of uncertainty in the special distribution of the data. Water saturation, porosity, and net to gross ratio were found to be the next most important parameters. B_o was the lowest-ranked uncertainty parameter in the presence of other input data.

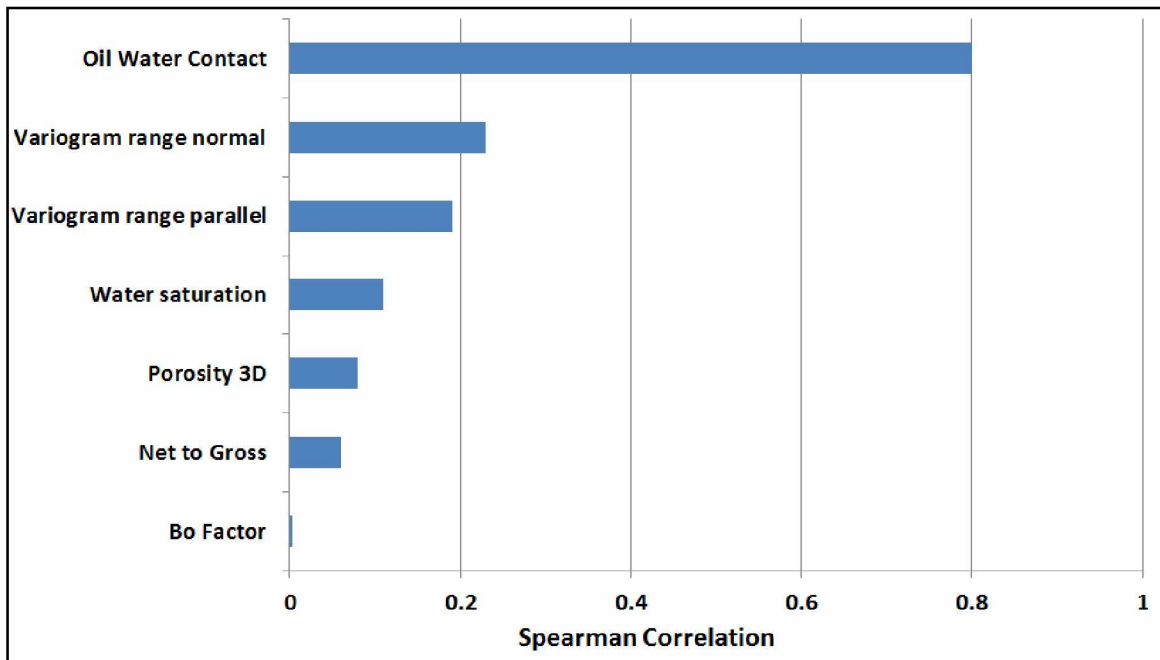


Figure 38. Uncertainty parameter ranking in terms of contribution to STOOIP

Chapter 4 Preparation of Input Data for Simulation Model

A set of input data required to build a simulation model are presented. In order for a reservoir model to behave like the reservoir it must be conceptually and dynamically similar to the reservoir. Thus it is important that dynamic input data accurately represent reservoir rock and fluid properties.

Ensuring long-term well integrity and optimum production and injection performance is important for the economic development of any field. To address these challenges and considering the environmental conditions in Umiat, a program used for designing well profiles at the Umiat LGS reservoir is presented at the end of this chapter.

4.1 Rock and Fluid Data

Rock and fluid data required to construct a simulation model must be reviewed and reorganized once they have been collected because they might have been obtained for different reasons and normally have not been screened to be of immediate use in reservoir simulations. In several cases, there were not enough data; however, many objectives could be met even with insufficient data by evaluation of sensitivity of reservoir performance to reservoir description or other parameters over a range of values believed to encompass the actual values. Review of the available rock data revealed several inconsistencies that needed to be resolved.

4.1.1 Relative Permeabilities to Oil and Gas

Permeabilities to oil and gas in presence of ice were measured in laboratory by unsteady state method (Godabrelidze, 2010) for 6 Umiat core plugs. There was only one core

(Core #60) from the LGS formation. The original data for Core #60 are shown in Figures 39 and 40.

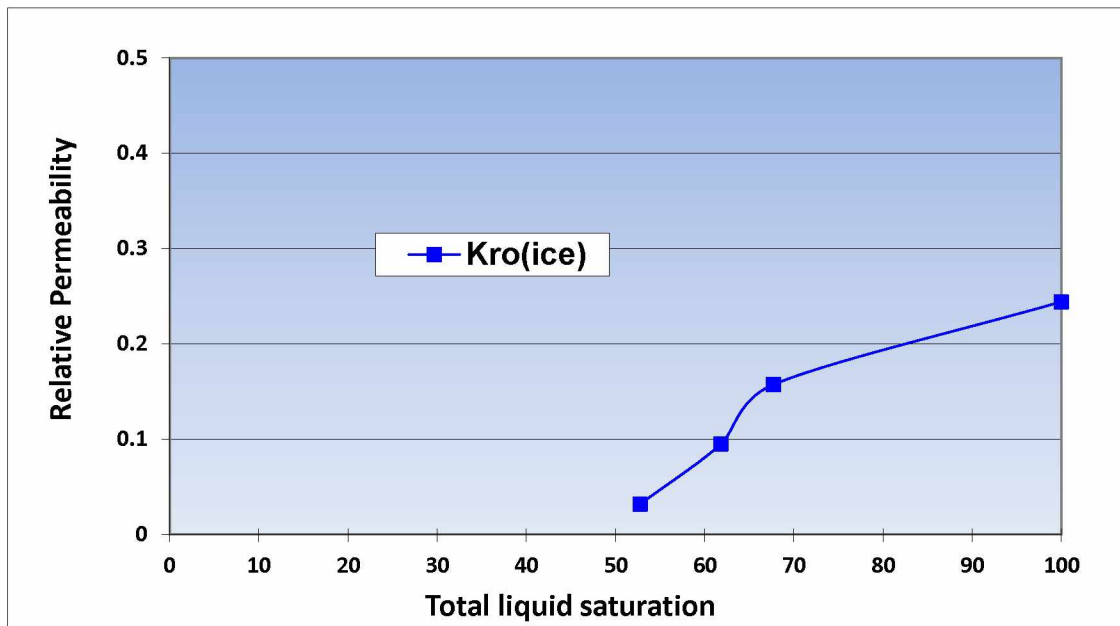


Figure 39. Relative permeability to oil in presence of ice for core 60

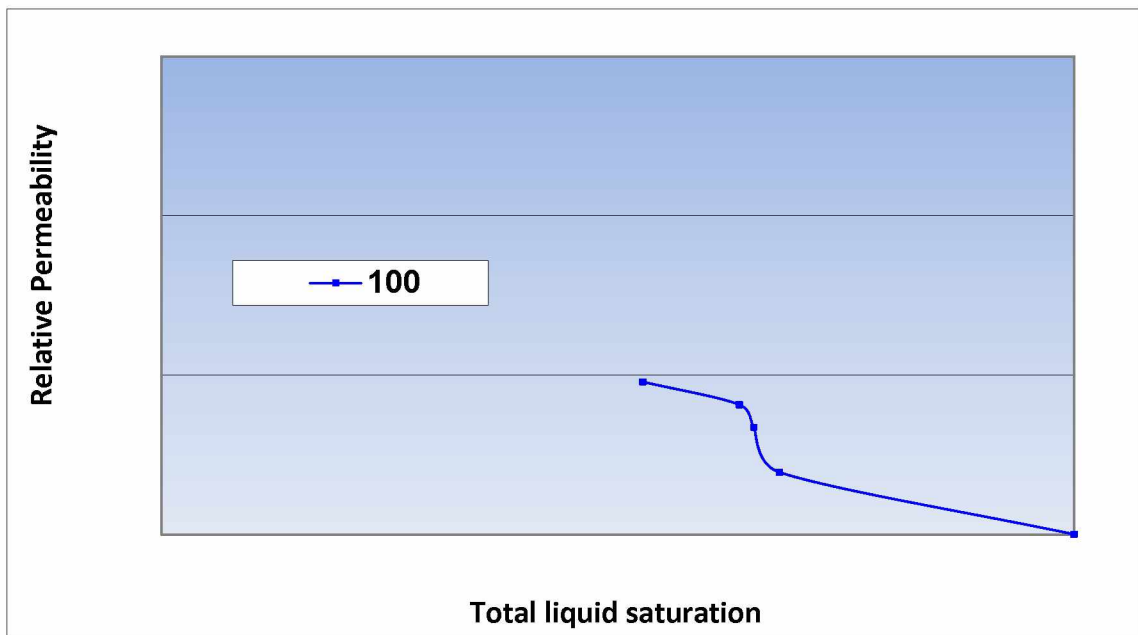


Figure 40. Relative permeability to gas in presence of ice for core 60

Effect of Non-Darcy on Gas Injection Core Experiment: The injection of gas into a core plug would cause some end effects on the end point relative permeability to gas if the gas velocity was beyond the linear flow assumptions for the applicability of Darcy law. Geerstma (1974) defined an inertial coefficient ratio to account for the non-linear flow that resembles the Reynolds number in fluid flow through porous media. Applying the core dimensions along with other core properties and unit conversions, the turbulence pressure drop was found to be 0.2249 psi which is negligible compared to the pressure draw-down in the reservoir. However, the end point relative permeability to gas was found to be higher ($K_{r_{go}} = 0.02855$) than the case without considering the non-Darcy effect (Figure 41). The calculation is provided in Appendix E.

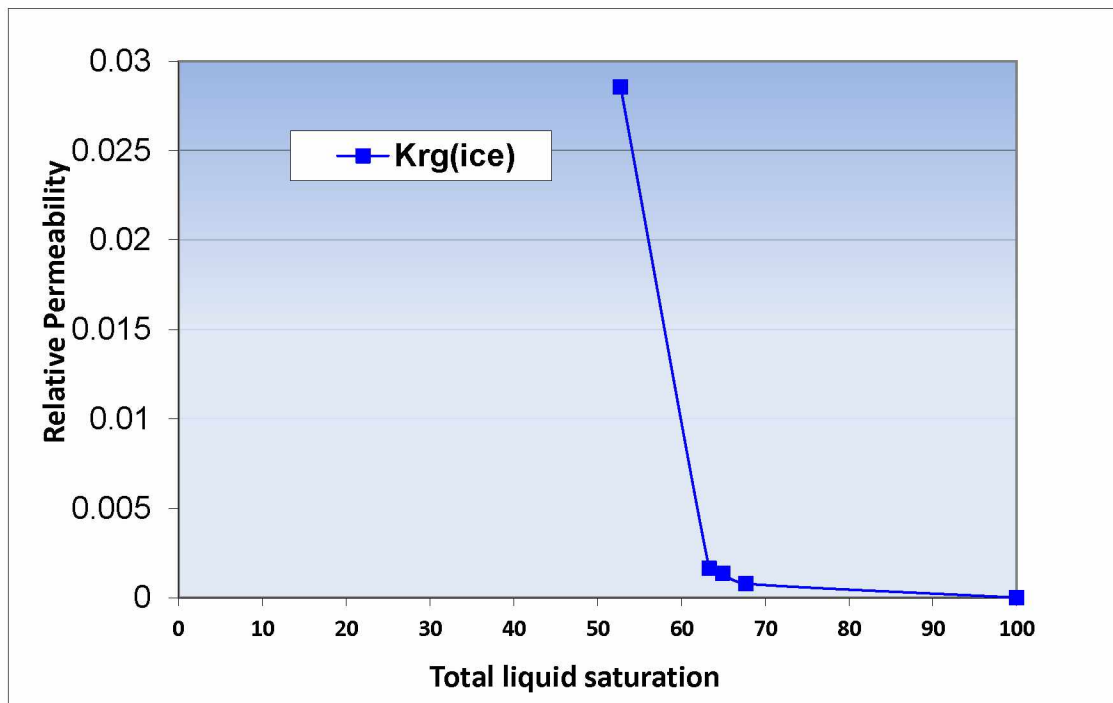


Figure 41. Relative permeability to gas in presence of ice for core 60 after including the non-Darcy effect

As it can be observed, the values of the measured relative permeability to gas for the core plug #60 is extremely small compared to the conventional values. The reason for this phenomenon might be the pore size distribution in the Umiat formation. If the ice is located at the center of the pore, there is an additional pressure drop for the fluid to pass the pore, but if the ice is instead attached to the pore walls, there would not be such pressure drop (Venepalli, 2011). In order to see both K_{ro} and K_{rg} in the same graph, K_r values are log-scaled and both of the relative permeability data can be seen in Figure 42.

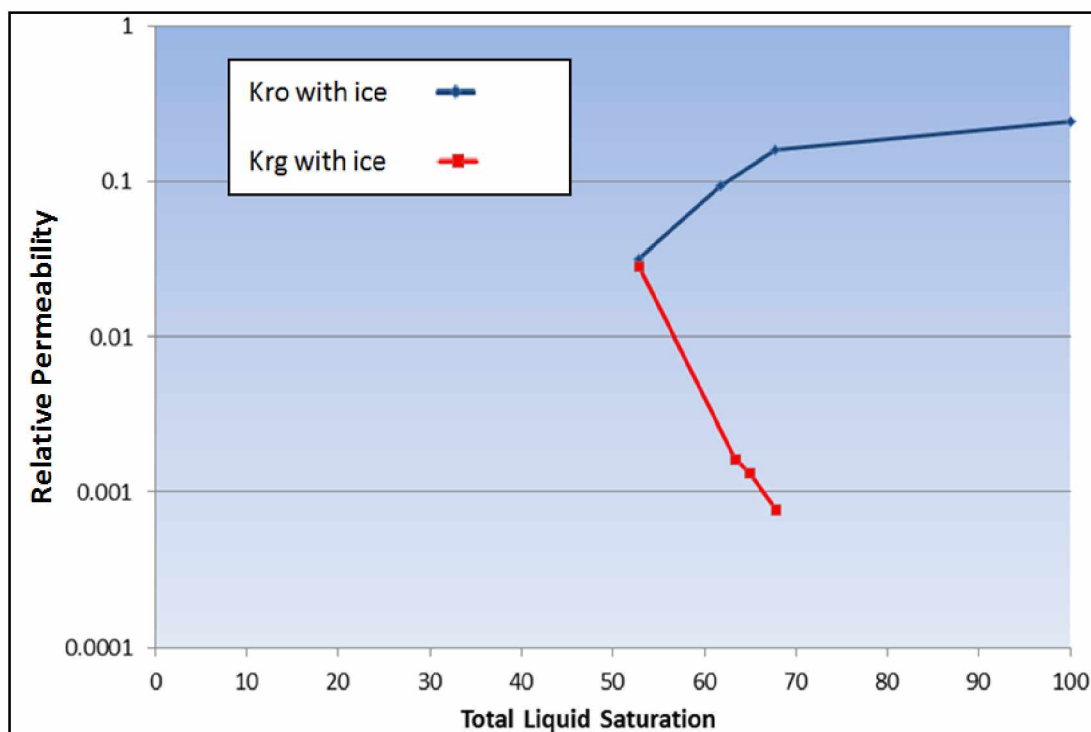


Figure 42. Relative permeability to oil & gas in presence of ice after including the non-Darcy effect

Since three rock types are defined in the model, there has to be three gas-oil relative permeability curves. Figure 40 is only valid for the rock type for which the core plug #60 is representative. With the lack of experimental data, a capillary pressure-based correlation (Schneider, 2003) was utilized based on the pore size distribution for each class of

capillary pressure. Brooks and Corey observed that a log-log plot of S_w^* vs. P_c results in a straight line with a slope $-\lambda$ which is characteristics of the pore structure (Brooks and Corey 1964). They proposed the following relationship (Equation 6) between the drainage capillary pressure and the wetting phase saturation:

$$P_c = P_{ce} \times (S_w^*)^{-1/\lambda} \quad (6)$$

Where P_{ce} is the capillary entry pressure (or in other words this is the minimum pressure required for mercury to invade the large pores) S_w^* is the normalized wetting phase saturation defined as (Equation 7):

$$S_w^* = \frac{S_w - S_{wi}}{1 - S_{wi}} \quad (7)$$

Where S_{wi} denotes irreducible wetting phase saturation.

The gas-oil relationship can be defined with the following equations (Equations 8 and 9):

$$K_{ro} = (S_{wo}^*)^{(2+3\lambda)/\lambda} \quad (8)$$

and

$$K_{rg} = (1 - S_{wg}^*)^2 * (1 - S_{wg}^*)^{(2+\lambda)/\lambda} \quad (9)$$

Where:

$$S_{wo}^* = \frac{(S_L - S_{or} - S_{wr})}{(1 - S_{or} - S_{wr})}$$

$$S_{wg}^* = \frac{(S_L - S_{wr})}{(1 - S_{wr} - S_{gc})}$$

K_{rg} = gas phase relative permeability

K_{ro} = oil phase relative permeability

S_o = oil saturation

S_{or} = residual oil saturation

S_{wr} = irreducible water saturation

$S_L = S_{wr} + S_o$

S_{gc} = critical gas saturation

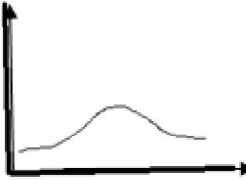
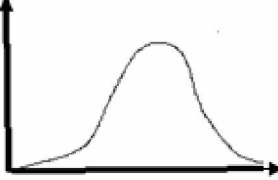
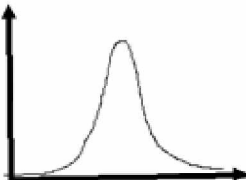
λ = Lithology factor obtained from capillary pressure curve

We have assumed the S_{wi} in all three rock types is constant at 0.35 and immobile. Three lithology factors were obtained by calculating the slope of the capillary pressure curves for each rock type and they are presented in Table 14. A small λ indicates a very large distribution of pore size, while larger λ value indicates uniformity of pore size (Van Golf-Racht, 1981). Since water freezes in higher percentages in larger pores than small pores and the water-to-ice ratio is higher in smaller pores than larger pores (Godabrelidze, 2010), the critical gas saturation which conventionally occupies the largest pores in a medium due to lowest capillary pressure, is influenced by distribution of ice in each rock type. Depending on the position of larger pore size associated with respect to the total reservoir pore structure, the percentage of ice varies in each rock type.

The presence of ice and where it is located in the pore can significantly impact the quality of the oil flow (Venepalli, 2011). It is recommended that NMR (Nuclear Magnetic Resonance) experiments be conducted on Umiat cores in order to examine the

relationship between the pore size distribution and unfrozen water content at different temperatures in order to accurately model the distribution of ice within the pore structure.

Table 14 Different rock types and their corresponding lithology factor. It also shows how the pore size frequencies are relatively different from each other.

Rock type	1	2	3
λ	0.62	0.84	1.23
Pore size frequency			

The data for relative permeabilities to oil and gas for different rock types versus gas saturations are included in Figure 43 through 45.

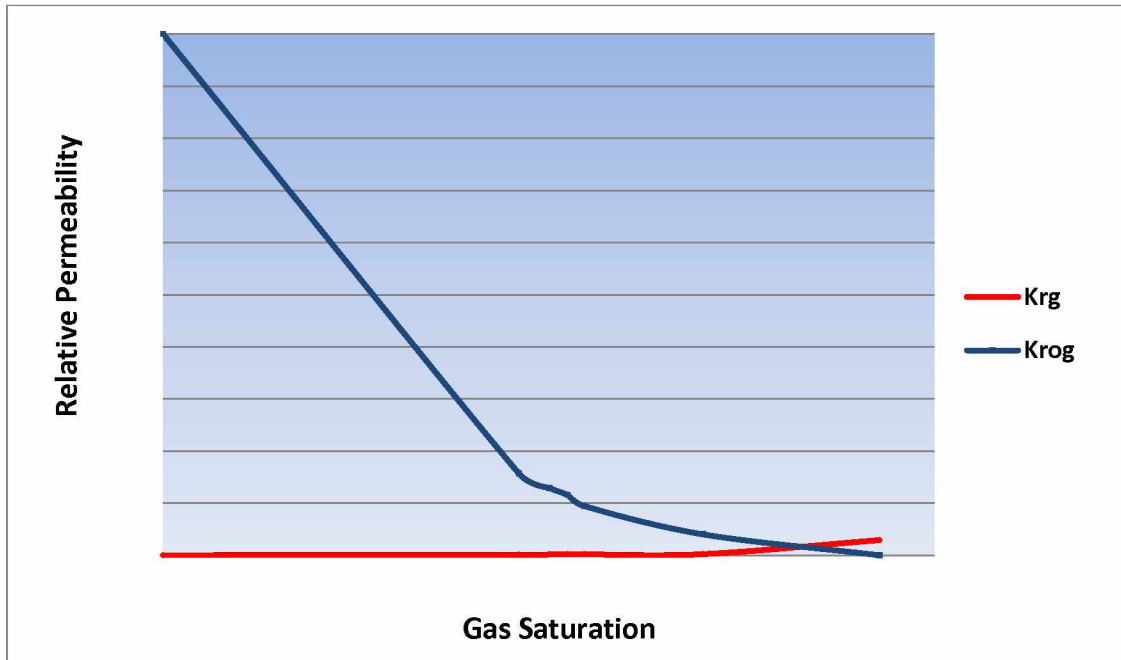


Figure 43. Relative permeability to oil and gas for rock type #1 as input to the simulator

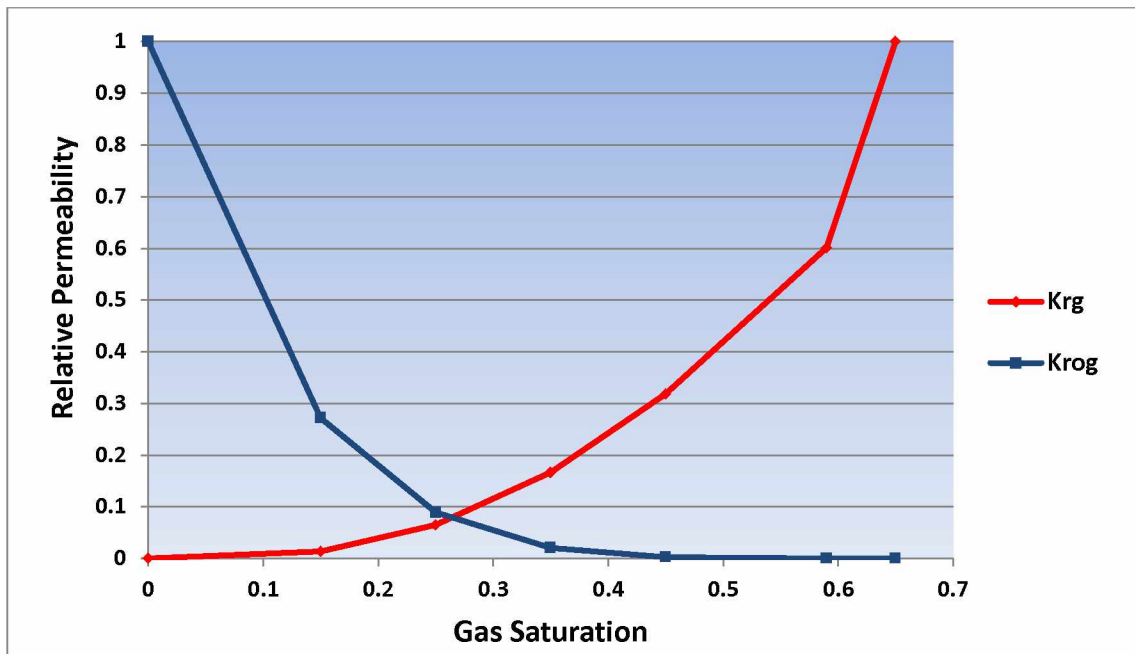


Figure 44. Relative permeability to oil and gas for rock type #2 as input to the simulator

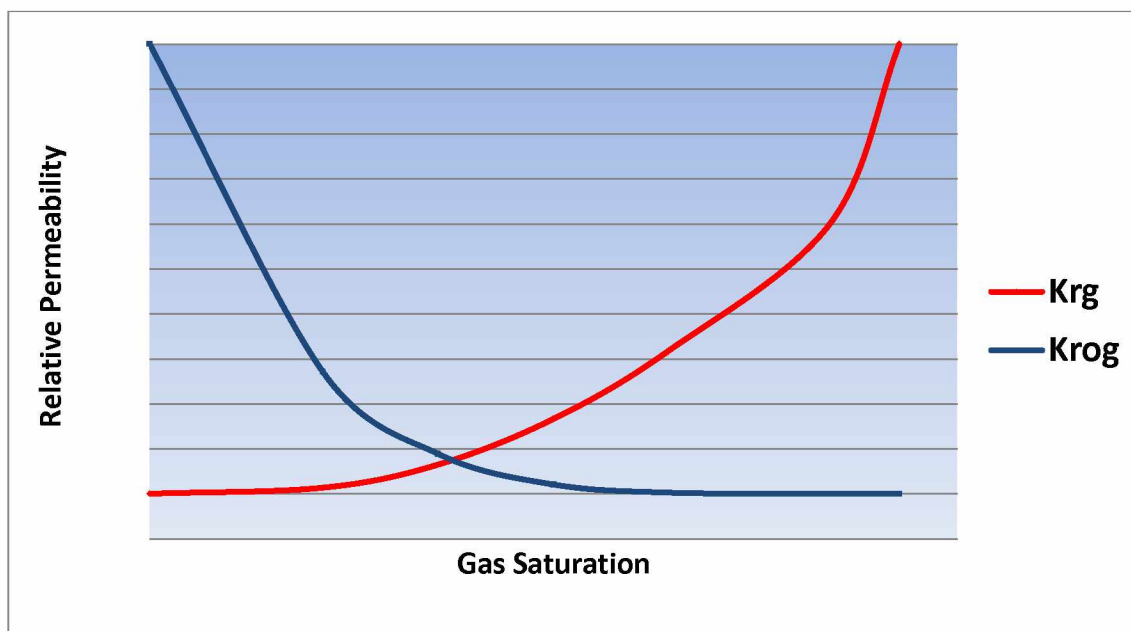


Figure 45. Relative permeability to oil and gas for rock type #3 as input to the simulator

4.1.2 Relative Permeabilities to Oil and Water

Due to flooding issues at water-freezing temperatures, there was no water-oil relative permeability data available for input into the simulator. The only available information was the end point to oil relative permeability ($K_{r_{ow}}$) at the reservoir temperature of 26 °F (Venepalli, 2011). Therefore, an existing correlation (Corey, 1954) was adapted and modified to account for the presence of ice in the pore throats. A constant multiplier was used to customize the K_r data to the freezing temperature. Since there is no active aquifer considered in the model, we assume that the relative permeability to water will have no significant role in the recovery calculations and the irreducible water saturation is the same for all the three rock types.

The oil-water relative permeability data that was used for all the three rock types is presented in Figure 46.

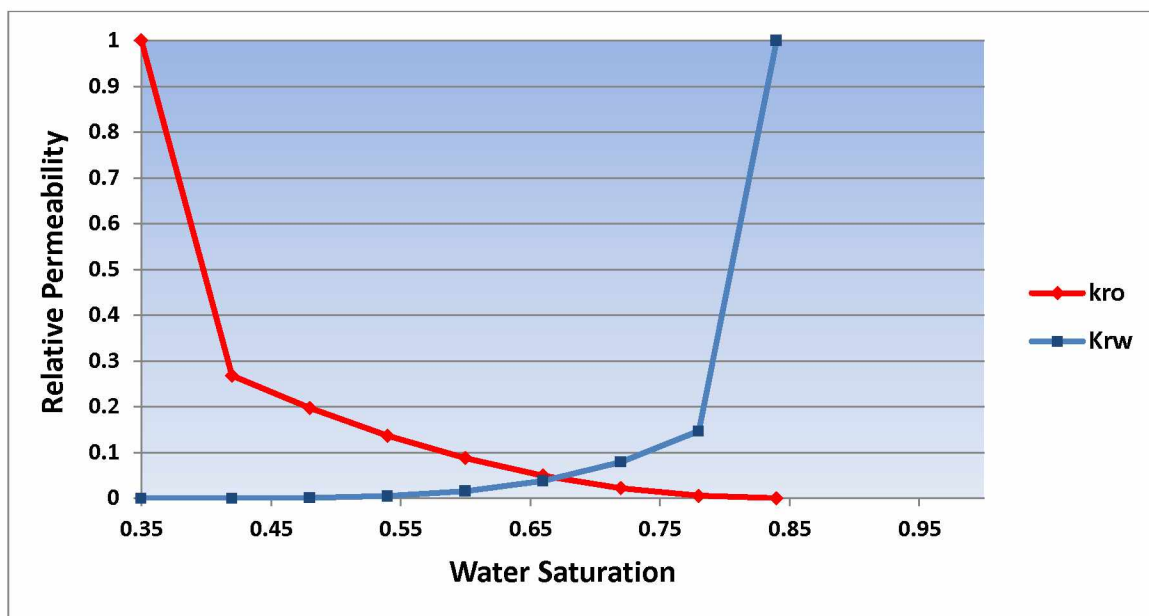


Figure 46. Oil-water relative permeability curve as input to simulator for all three rock types

4.1.3 Capillary Pressure

The capillary pressure data obtained in Section 3.5 were used as input into the simulator. In our case, there were only three core plugs with known capillary pressure obtained by mercury injection method, but only one core plug #60 was available for measurement from the LGS formation. Other two core samples (#56 and #59) were broken before the experiment (Godabrelidze, 2010).

4.1.4 Fluid Properties

Fluid properties required for the black-oil reservoir simulator include oil, water, and gas reservoir volume factors, viscosity, density, compressibility, and gas in solution. Some of these parameters have been obtained by laboratory measurements; others had to be calculated using suitable correlations (Table 15).

Table 15. General fluid properties for reservoir simulation at surface conditions

Parameter	Value	Source	Source name
Oil density	52.1873 lb/ft ³	Given	Shukla, 2011
bubble point pressure	345 psi	Given	Shukla, 2011
Gas density	0.04539 lb/ft ³	Given	Shukla, 2011
Water phase density	62.4 lb/ft ³	Reference	http://www.simetric.co.uk
Water FVF	1.002	Correlation	McCain, 1990
Water compressibility	3.06e ⁻⁶ 1/psi	Reference	https://www.fekete.com
Water viscosity	1.78 cp	Reference	Beal, 1964

The most reliable way of obtaining reservoir oil properties and gas-oil relationships is by analysis of bottom-hole or reconstituted fluid samples. However, the small amount of available Umiat oil was severely weathered and limited traditional PVT and phase behavior analysis. Shukla (2011) developed a method to physically recreate a pseudo-live reservoir oil sample by comparing the composition of the weathered Umiat fluid with a theoretical Umiat composition derived using the Pedersen method (Pedersen et al., 1989). Given the conspicuous lack of complete fluid characterization and phase behavior data on Umiat oils when the wells were originally drilled, and the unavailability of “live” oil samples from Umiat, an experimental study was undertaken to characterize the available small volume of dead Umiat oil collected in 1940’s and to subsequently quantify phase behavior. A PVT model which was generated by PVT simulator (Shukla, 2011) was directly entered into the simulator as tables, with properties defined as function of pressure (Table 16). It should be mentioned that only one PVT region has been defined in the model assuming that the oil API gravity is the same across the reservoir.

Table 16. Fluid properties input data to the simulator

P (psi)	Rs (scf/bbl)	Bo (rsbbl/STB)	Bg (bbl/ft³)	Viso (cp)	Visg (cp)
14.7	0.4362	0.9913	0.16587	8.3314	0.01022
50	7.8321	0.994	0.04842	7.7841	0.01029
100	18.2051	0.9977	0.02397	7.1047	0.01036
150	28.5321	1.0014	0.01582	6.5106	0.01043
200	38.853	1.005	0.01174	5.9876	0.0105
250	49.1819	1.0087	0.0093	5.5253	0.01058
300	59.5227	1.0124	0.00767	5.1151	0.01065
350	68.8393	1.0157	0.00661	4.7848	0.01073

4.2 Initializing the Model Based on Initial Reservoir Conditions

A simulation model is initialized (i.e., pressure and saturation values are assigned to each grid block) assuming static pressure equilibrium. Under this equilibrium condition, the modeling of fluid saturation can be done using capillary pressure (P_c) data, the static pressure at the WOC depth, and a correct water-oil contact (WOC) where water saturation is 100%.

In order to initialize the Umiat reservoir model, several reservoir parameters were needed (Table 17) to calculate the equilibrium conditions for each phase in the model. Since there was no initial gas in the reservoir, the equilibrium was based on the capillary and gravity forces between the oil and water phases. In this procedure, the pressure and saturation variables for each grid cell are averaged and assigned to each cell based on reference pressure and reference depth. The pressures for each phase are calculated from the reference depth upwards by using the fluid densities. Then, the capillary pressure at each depth is obtained by subtracting the pressures from each phase. The average saturation is finally calculated for each cell by using the capillary height functions.

Table 17. Reservoir parameters for initializing the simulation model

Parameter	Value	Source	Source name
Reservoir temperature	26°F	Given	Baptist 1960
Reservoir pressure	350 psi	Given	Baptist 1960
Reference depth	900 ft	Given	Arbitrary
WOC depth	1500 ft	Given	Geologic model

4.3 Design of Production and Injection Wells

Dramatic improvements in drilling technology over the past thirty years have encouraged more and more field operators to develop their field with multilateral wells. Ensuring optimum well placement is a key for the economic development of any field. This becomes even more important for Umiat because of its unique, technically challenging environment and remoteness.

Interpretation of data from well Umiat #2 suggested multiple zones within the LGS reservoir interval in the Umiat field that are separated by barriers consisting of shale (Middle LGS).

A wagon-wheel pattern is the most efficient means of accessing the maximum amount of the Lower Grandstand reservoir intervals (Upper LGS and Lower LGS) while minimizing the surface footprint (Figure 47).

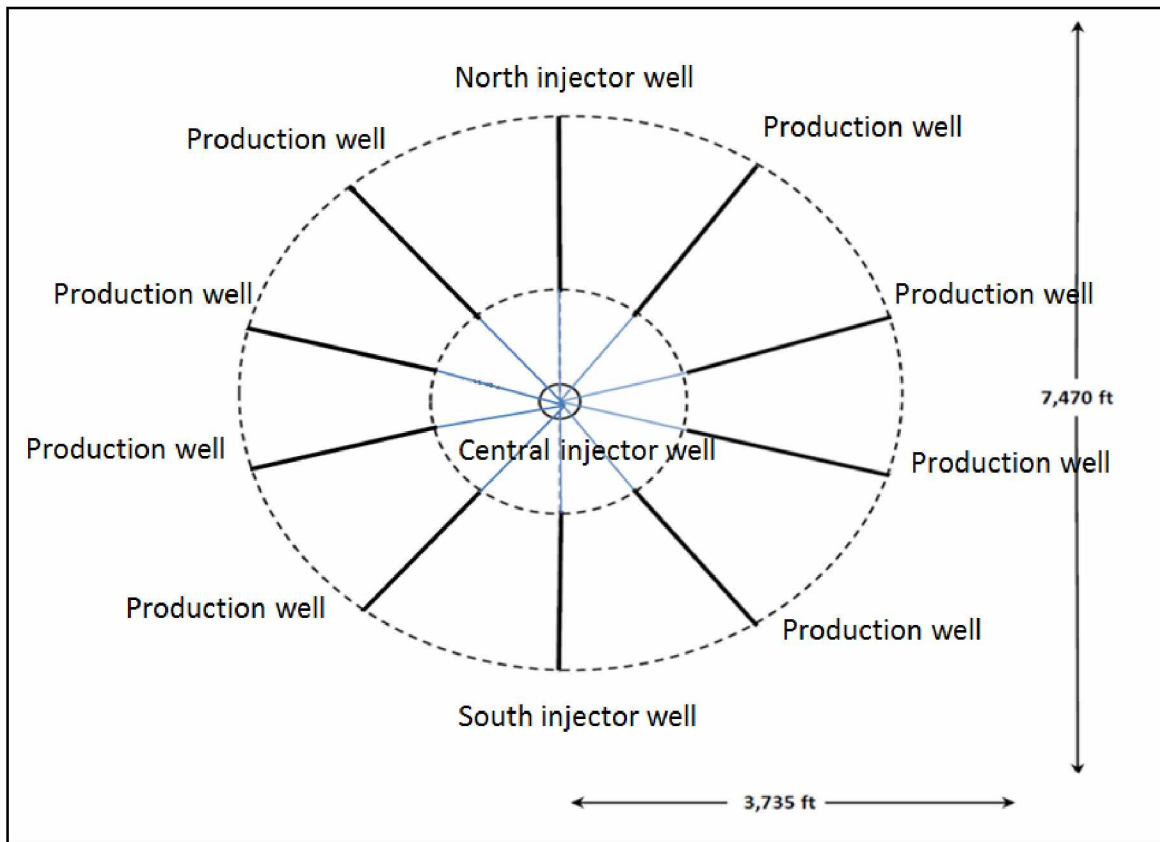


Figure 47. The proposed well pattern for the Umiat drilling program (Modified from Linc Energy, 2012).

The proposed well scenario consists of:

- Injection well #1 is a vertical well from the surface all the way to bottom
- The North/South injection wells (#2 & #3) are dual lateral completions in the top of the Lower Grandstand with:
 - The injector “Heel” at a radius of 1,235 ft from the pad
 - The injector “Toe” at a radius of 3,235 ft from the pad
 - 1500 ft slotted liner completion
- The Production wells (#4 through #7) are dual lateral completions in the Lower Grandstand with:

- The lateral “Heel” at a radius of 1,235 ft from the pad
- The lateral “Toe” at a radius of 3,235 ft from the pad
- 1500 ft slotted liner completion
- 36 degree angle between wellbores

In the proposed pattern provided by Linc Energy, one vertical well in the center along with two dual lateral injectors in the north and south at the top of the Lower Grandstand sand supports pressure for a combination of four dual lateral producers at the bottom of the interval, each one angled at 36 degree in a square mile spike configuration (Figure 48). The wells have about 1500 ft length of 4.5” wide open hole completion across the productive area with a total well length of 3000 ft.

To reduce surface impact and the cost of infrastructure, only 5 pad locations are being considered. The limited number of pad locations is a result of: 1) tundra and social considerations, 2) topography, 3) logistics (gravel, roads, facilities, etc.), and 4) cost of infrastructure.

A practical workflow was designed to create the well profile as input to the simulator by utilizing RMS Well Planning and IPL programming. Some basic definitions of the independent concepts used in this workflow are (Roxar manual guide, 1994-2008):

Target: A location in a reservoir where a well will be placed. A target can be representative of a single target or part of a target group.

Target Axis: A line defining where a target should be eventually completed.

Planned trajectory: The planned path of a well.

Drilled Trajectory: The actual path of a well which consists a set of survey data gathered when drilling a well.

Tie-in depth: A connection point for a Well directory and a target, from which a connection to surface facilities exists. A tie-in point can be at any point of an existing well, or a single wellhead, or a Slot.

Slot: A hole in a pad from which a Well can be accessed. A slot may be empty, or have one or more wells assigned to it.

Side-track: A curve representing an inclined well starting from another well right from the surface or geologically side-tracked from another well beneath the surface..

The proposed single pad well pattern was repeated across the reservoir 5 times. The 5 pad locations were assigned in grid cells located in the upper structure of the reservoir to allow access to the deeper oil-bearing layers in the LGS formations by horizontal producers and injectors and away from the WOC depth. In order to ease the plan the well directory through different grid cells in the grid structure, first, a horizontal target was defined so that the well drilling path could be snapped to a specific layer in the formations (Figure 48).

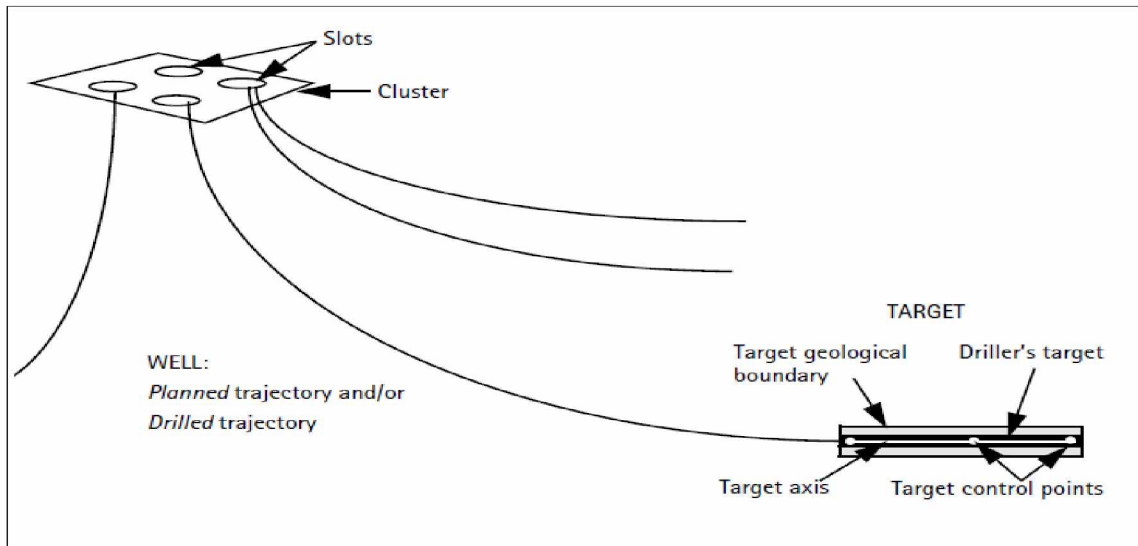


Figure 48. Well targeting and trajectory design in RMS Irap™ (Courtesy of Roxar manual guide)

Each pad was designed at optimum distance with respect to each other to allow for future well length sensitivity analysis. Each pad consisted of one production slot and one injection slot. To simplify the procedure, only two vertical wells have been designed at each well pad and have been geologically side tracked to account for the horizontal dual lateral producers and injectors and to obtain the optimum design as quickly and efficiently as possible (Figure 49).

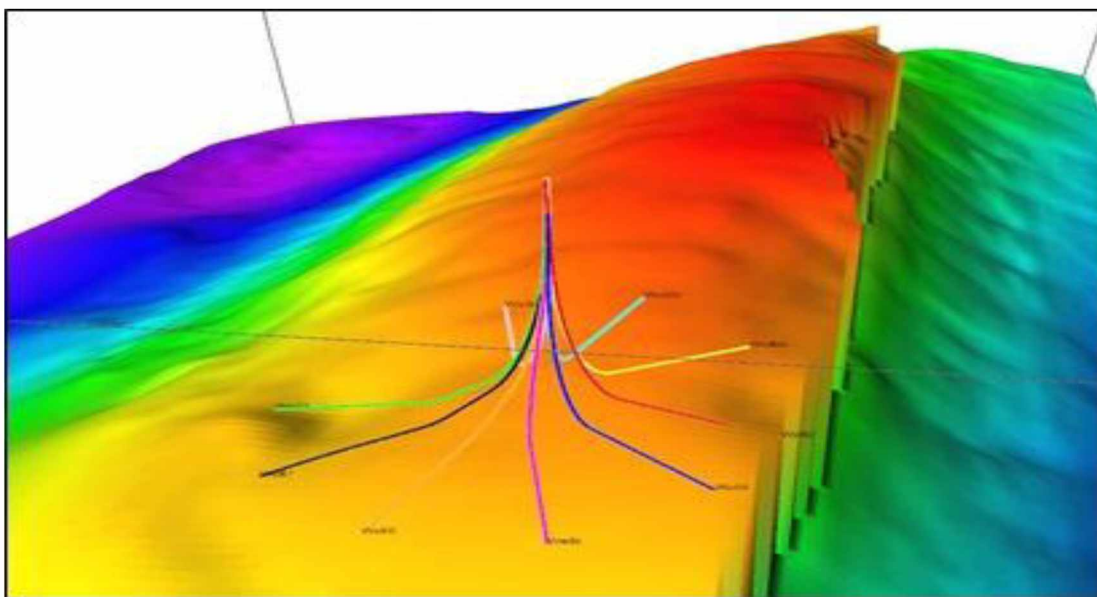


Figure 49. The design of the well model

An IPL program was written to implement the proposed well diagram in a radial pattern in the model. It included target point controls and target axis to each grid cell in the planned trajectory based on the Cartesian coordinates of the grid structure. Dogleg severity (DGS) was kept below 5 degree per 100 feet to prevent excessive friction pressure and allow easier installation of bottom-hole assembly later in the actual well drilling program. When the IPL program was run, survey drilling trajectories were drawn based on the Kelly Bushing depths settings and the well target. Because of the high number of wells, it was necessary to name the wells based on their type if they are injection or production. Since the simulation scenario consisted of gas injection, the upper laterals were selected as injection wells and the lower legs were considered as production wells. Figure 50 shows the final well design for the simulation model. A list of Kelly Bushing depths and tie-in well depths are presented at Appendix C.

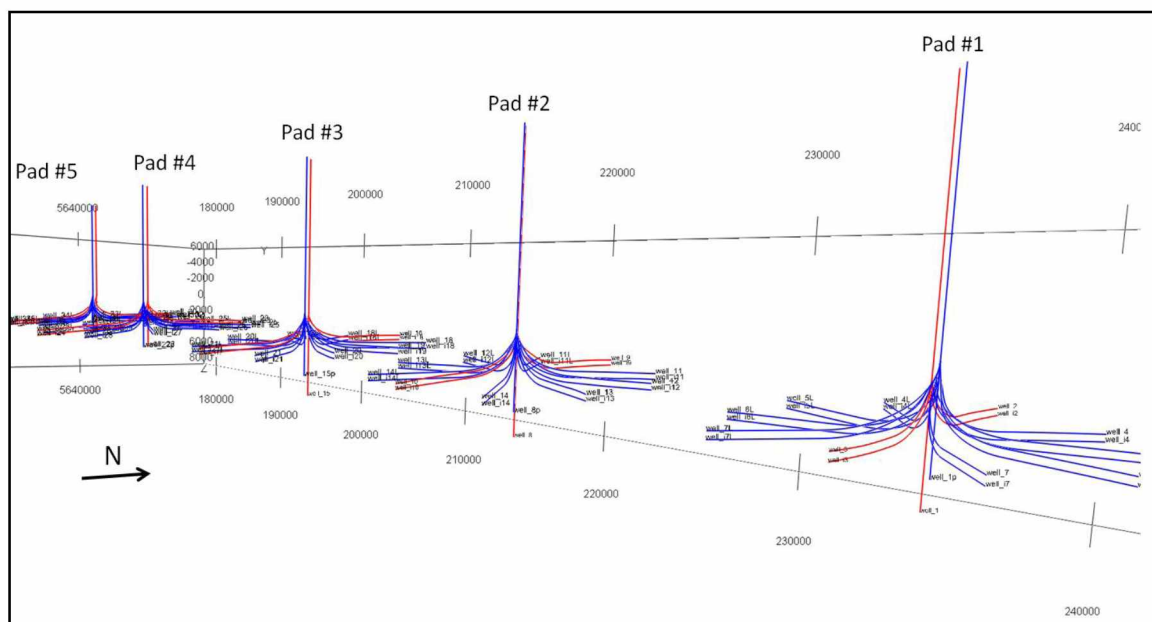


Figure 50. The final well profile used in the reservoir simulation. The well lines have been magnified for better visualizations. Note the blue line show the production wells and the red line shows the injection wells

Each pad has 4 producers (8 legs) on the east side and 4 producers (8 legs) on the west side, totally 16 production legs on each pad which basically are sidetracked from one single production well.

For the injectors, each pad has one injector well in its center, one injector (2 legs) to the north, and 1 injector (2 legs) to the south, totally 5 injecting legs on each pad which basically are sidetracked from one single injection well.

Flowing and injecting bottom-hole pressures of 80 and 400 psi were set for the base simulation case. These bottom-hole pressures came from Schlumberger's report to Linc Energy (Linc Energy Report, 2012). A sensitivity analysis was done to investigate the impact of these parameters on the ultimate oil recovery.

Table 18 shows the summary of well parameters in the LGS formation used in the simulation model. It's important to note that we have assumed that 100% of the drilled horizontal length in the intersecting layer is a producing length. A total combination of 80 producers and 25 injectors, controlled by flowing bottom hole pressures were used in the simulation model.

Table 18. Well model parameters used in the simulation model

Well Parameter	Producer	Injector
Total depth (ft)	3000	3000
Length of lateral (ft)	1500	1500
Wellbore radius (inch)	4	4
Completion type	Open-hole	Open-hole
Minimum Flowing Bottom-hole Pressure (psi)	80	-
Bottom-hole Gas-injection pressure (psi)	-	400
Skin Factor	0	0

Chapter 5 Modeling Results

5.1 Oil Recovery by Gas Injection (base case)

A base case model was defined to observe the performance of the reservoir under gas injection. Table 19 defines the base case parameters that were used in the simulation model. The model was run with all the wells producing and injecting against pressure limitations only. The injection started from the first day of production with 100% methane (CH₄) as the injecting gas. The producers were assigned a minimum flowing bottom-hole pressure 80 psi and the injectors were assigned a constant pressure 50 psi more than the initial reservoir pressure.

Table 19. Simulation parameters used in the base case model

Parameter	Description
Upper production wells	Completed open hole at layer 18
Lower production wells	Completed open hole at layer 32
Upper injection wells	Completed open hole at layer 1
Lower injection wells	Completed open hole at layer 21
Simulation dates	01/01/2013 to 01/01/2063
Economic limit for each well	5 STBD
Permeability anisotropy ratio	0.45
Horizontal well length	1500 ft
Grid size dimensions	200 ft * 200 ft
Flowing bottom-hole pressure (FBHP)	80 psi
Bottom-hole injection pressure (BHIP)	400 psi

5.2 Grid Size Optimization

The base case scenario was used to optimize the simulation grid dimensions.

The grid cell thickness was discussed in Chapter 3 where the porosity was considered as a descriptive parameter to quantify the level of heterogeneity in the vertical extent of the reservoir. Variations in grid cell sizes in horizontal directions are also important in keeping the flow zones counted in displacement efficiency and avoiding numerical dispersion in the model. To be an effective tool, the reservoir model must simulate future reservoir behavior under production or injection strategies. These behaviors include well productivity and producing GOR.

Below is the workflow used for grid size optimization:

- 1) Run the base case using the finest grid that your computer can handle. This may take several days to run.
- 2) Run the base case with a larger grid size
- 3) The model with biggest grid size which also can mimic the fine grid size in the geologic model within the engineering accuracy is chosen as optimum grid size.

A 100 feet by 100 feet grid system was designed and run in a simulation run for 20 years with gas injection (2013 to 2033). The results were compared with the 200 feet by 200 feet case and are shown in Figures 51 and 52 for one of the production wells (Well # 11). The run time for each case as well as the number of their simulation grid cells are presented in Table 20. Although the finer grid system gives more accurate results in terms of reservoir behavior and geology, there is no significant difference when compared to the coarser grid. To save computational time, the 200 feet by 200 feet dimensions were selected as the optimal grid sizes for the simulation study.

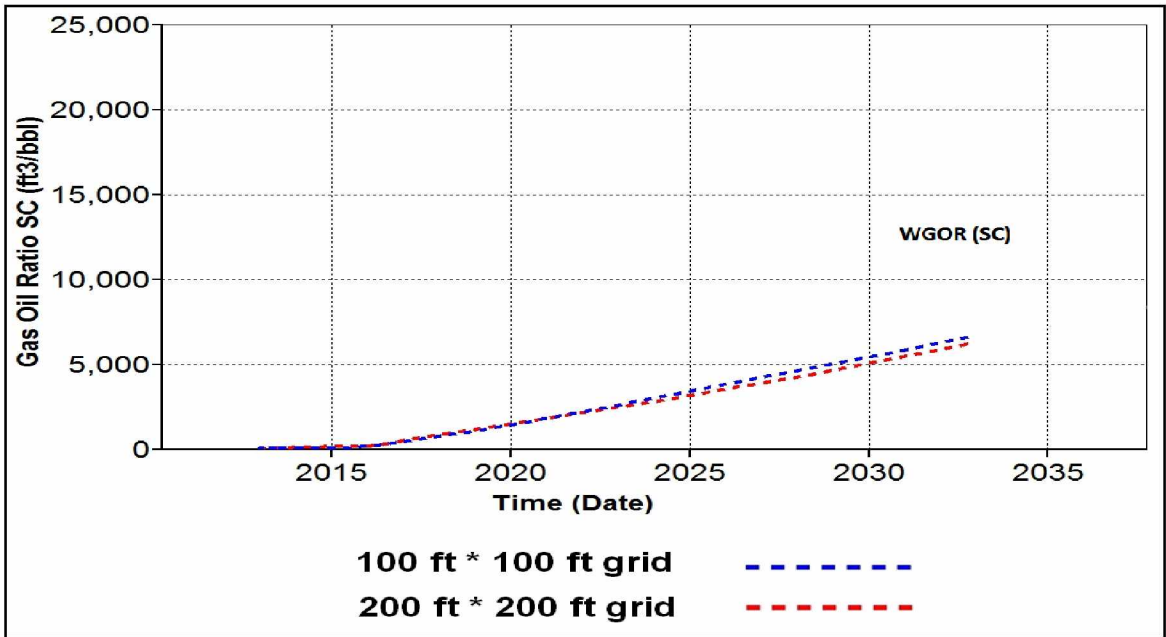


Figure 51. Producing GOR for two grid systems with different dimensions

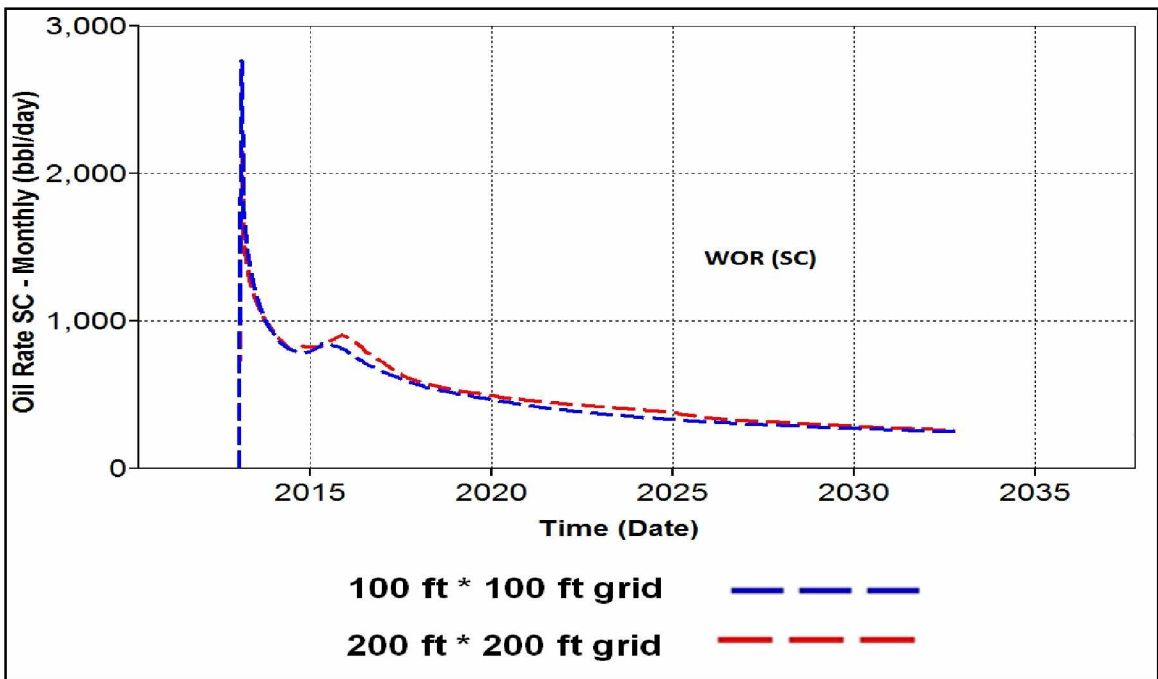


Figure 52. Well oil rate for two grid systems with different dimensions

Table 20. Run time and grid dimensions for two grid resolutions

Grid resolution	Number of active cells	Run time
200 ft * 200 ft	500,000	3 hrs
100 ft * 100 ft	1,100,000	12 hrs

5.3 Parameter Optimization

As in all engineering investigations, pertinent parameters should be defined and studied. The consideration of important parameters in development plan of an oil field affects the decision making process; the quantification of such impacts allows the operator to invest in design and implementation of relevant oilfield operations and not waste capital on processes that would give high risk and low revenue. In this study, two parameters have been selected for optimization purposes: injection pressure and horizontal well length.

5.3.1 Horizontal Well Length

In addition to the 1500 ft horizontal well length proposed by the field operator, a case with a horizontal length of 3000 ft was also designed and used as the well model in the simulator. The ability to drill horizontally further into the reservoir is of critical concern due to weight on bit and raises questions of economic consequences of the project. However, if the well performance with longer length is significantly higher than the smaller length, the project can be considered practical.

The results for field cumulative oil recovery for the two different horizontal well lengths are shown in Figure 53. As it can be seen, the cumulative oil recovery in the model with the shorter well length is not significantly different from the model with the longer horizontal well length. This could be due to drainage area of the well models and its relation to the vertical fluid flow in the vicinity of the wellbore. This would suggest that there is no advantage to drilling the longer well length in terms of additional oil recovery.

It is important to note that the pressure drops due to friction forces in multiple phase flow have not been included in this study. Based on the literature (Novy, 1995), if the loss of oil rate is less than 10%, then the pressure loss should be ignored. That means if we design our horizontal well in a way that pressure drops are high in such a way that it causes our production to drop more than 10%, we should consider a new design. Such well length corresponding to this critical pressure drop is called the Length of Significant Pressure Drop (L_{sf}). It can be mathematically shown that when friction reduced flow rate (q) by at least 10%, the wellbore pressure drop is more than 15% of drawdown.

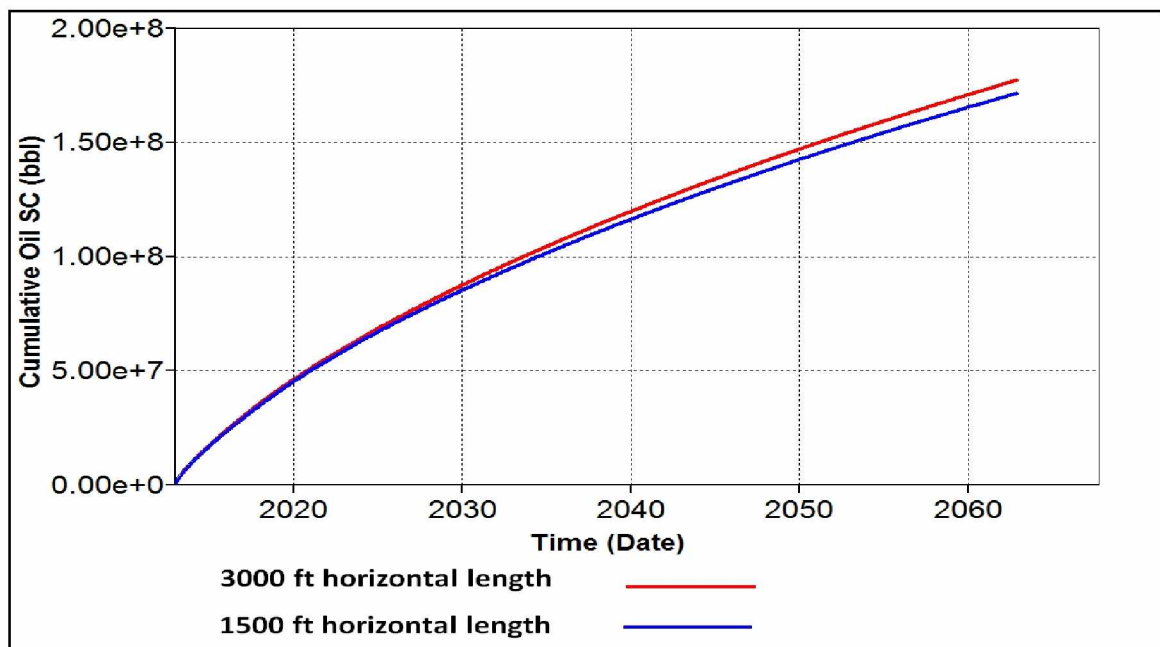


Figure 53. Field cumulative oil production and field oil rates for two different horizontal well lengths

In this study, friction losses for different well lengths and flow regimes were investigated by use of Hagedorn and Brown correlation (1964) for a constant borehole size of 4 inch and are presented in Figure 54. As it can be seen in the graph, as the production rate increases, the friction losses in the horizontal wellbore increases more significantly in the case of length 3000 ft than the case of 1500 ft. At the rate of 10,000 bpd, the estimated friction loss in the wellbore is about 400 psi. This amount of pressure loss is unacceptable comparing to the low reservoir pressure at Umiat.

Given the low reservoir pressure in Umiat, we concluded that 1500 ft of horizontal well length is the best case scenario applicable to Umiat reservoir conditions.

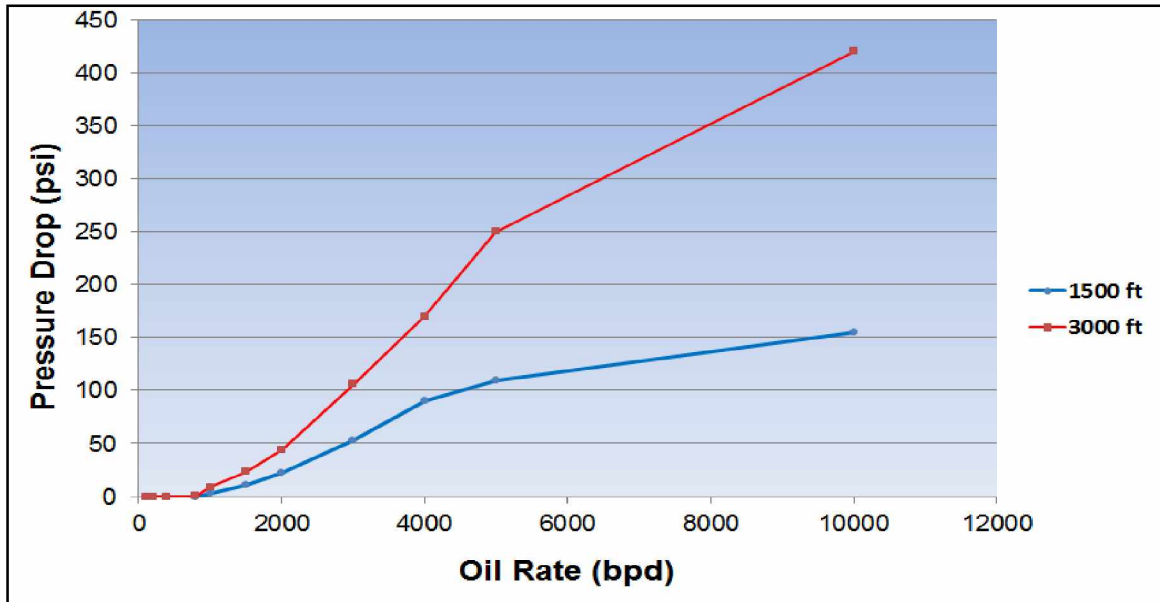


Figure 54. Pressure drop versus oil rates for two different horizontal well lengths

5.3.2 Injection Pressure

The more gas is injected, the more oil can be displaced. A good gas injection operation can result in increased oil recovery and optimizing reservoir production characteristics such as decreasing depletion time and increasing well productivity (Roebuck, 1987).

Three models with gas injection pressures of 400 psi and 600 psi were designed and run. Figures 55 and 56 show the simulation results. The case with no gas injection gives the lowest total oil recovery. The oil rates start to increase at about the same rate but after a few months, the case with highest injection pressure (600 psi) declines very quickly down to about 30,000 bpd and it maintains the same oil rate for a couple of months and then starts to decrease, initially at a higher rate and then at a slower rate. The case with no injection continues to decline further down and then it repeats the same decline rate as the case of 600 psi but at lower production rates. The case with gas injection pressure 600 psi gives the highest producing GOR compared to other two cases. As more oil is produced, more gas is moving with oil and is produced. The rate of producing GOR in the case with injection pressure 600 psi is almost two times higher than the base case (injection pressure 400 psi) at any given point. The case with no gas injection gives insignificant amount of producing GOR (less than 1000 ft³/bbl).

In terms of average reservoir pressure, as expected, the case with higher gas injection which is BHIP 600 psi maintains a higher reservoir pressure compared to the other cases. Although the case with BHIP 600 psi gives the highest oil recovery, since there was no information about the fracture gradient, the BHIP 400 psi is probably the safest option. Exceeding the fracture gradient could have catastrophic consequences on well integrity; consequently the actual fracture gradient will need to be determined prior to design of the injection plan.

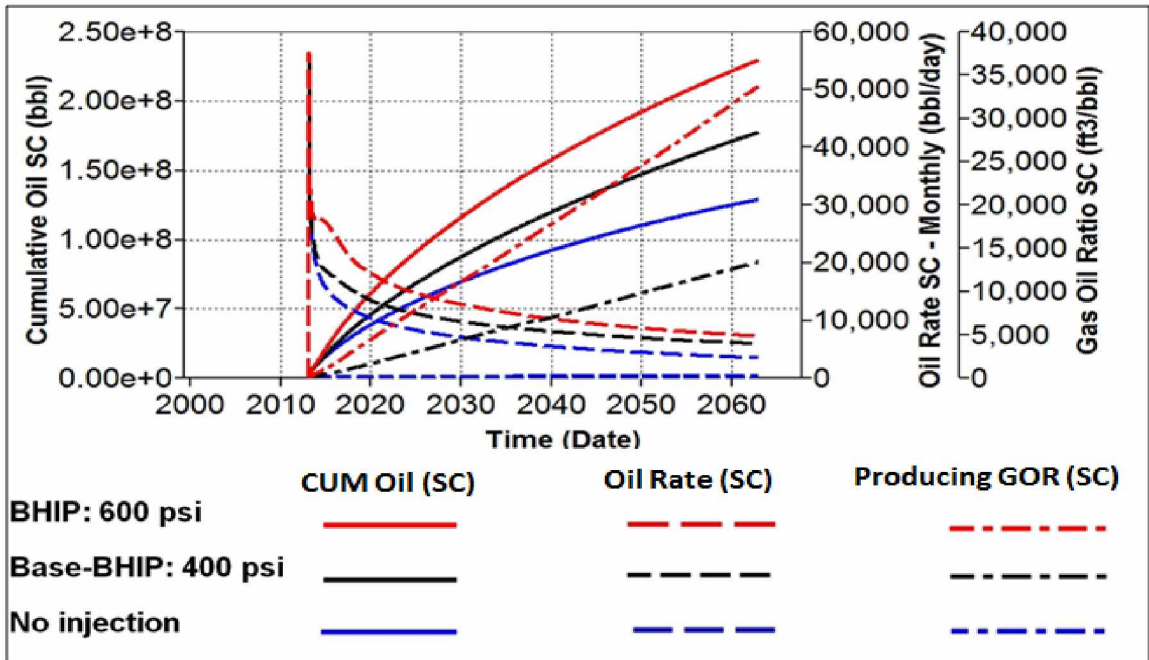


Figure 55. Field cumulative oil production, field oil rate, and producing GOR for different gas injection pressures

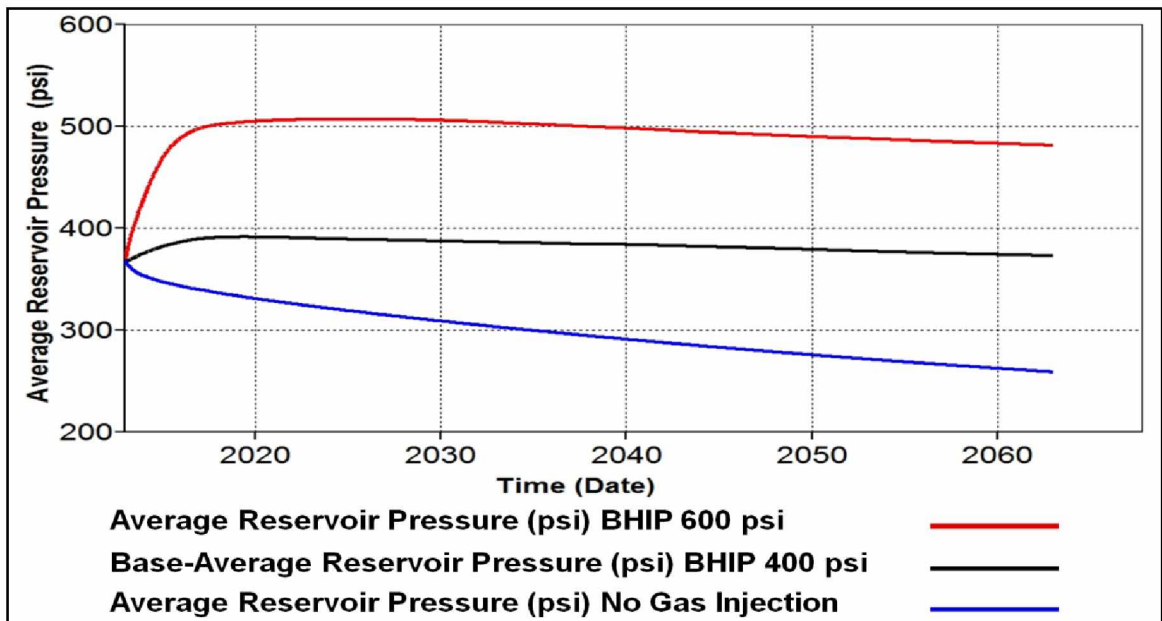


Figure 56. Average reservoir pressure for different gas injection pressures

5.4 Sensitivity Analysis

Since several input data such as relative permeability and permeability anisotropy have been estimated based on limited data, sensitivity analysis is a helpful tool in defining the impact of their variation on the oil recovery. Sensitivity to producing GOR, some end point relative permeabilities to oil and gas as well as different ranges of permeability anisotropy ratios are presented here.

5.4.1 Permeability Anisotropy

Permeability anisotropy is one of the most difficult parameters to measure (Ayan et al. 1994). The anisotropic nature of permeability can affect any process in which a density difference exists between fluids such as oil and gas (Ayan et al., 1994). The ratio of vertical permeability (K_v) to horizontal permeability (K_h) is often used to quantify the permeability anisotropy. K_v/K_h for a homogenous reservoir equals to one. Figure 57 shows different cases of permeability anisotropy with respect to well drainage area.

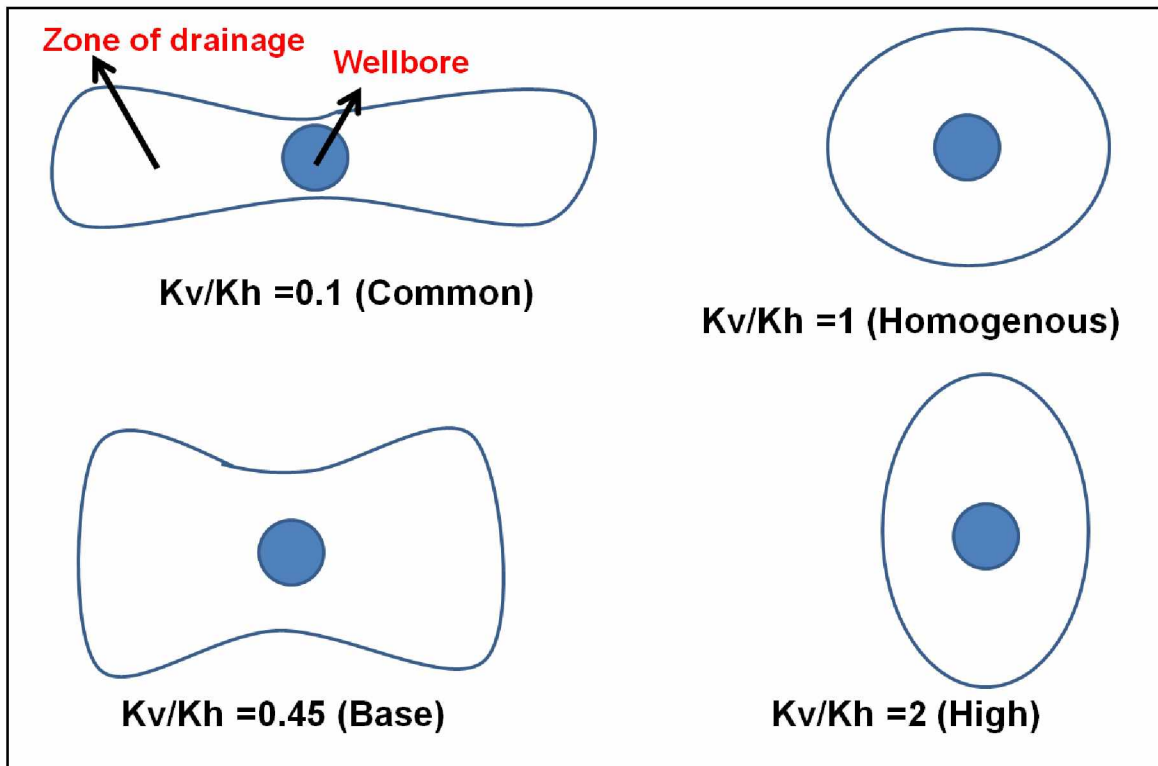


Figure 57. A vertical view with a horizontal well and different configurations of well drainage area with respect to permeability anisotropy (GEKEngineering.com)

The Umiat reservoir consists of shoreface and deltaic Cretaceous sandstones deformed by a thrust-related anticline (Hanks et al., 2012). New data indicated the reservoir has six facies associations with distinctive permeability trends. Both regional and local observations suggested that three sets of natural fractures may occur at Umiat (Hanks et al., 2012). These trends combined with diagenetic effects could impart a strong vertical and horizontal permeability anisotropy to the reservoir. Presence of natural fractures and their orientation with respect to horizontal well plane (Figure 58) can enhance the flow if open or can block flow if filled with ice or cement.

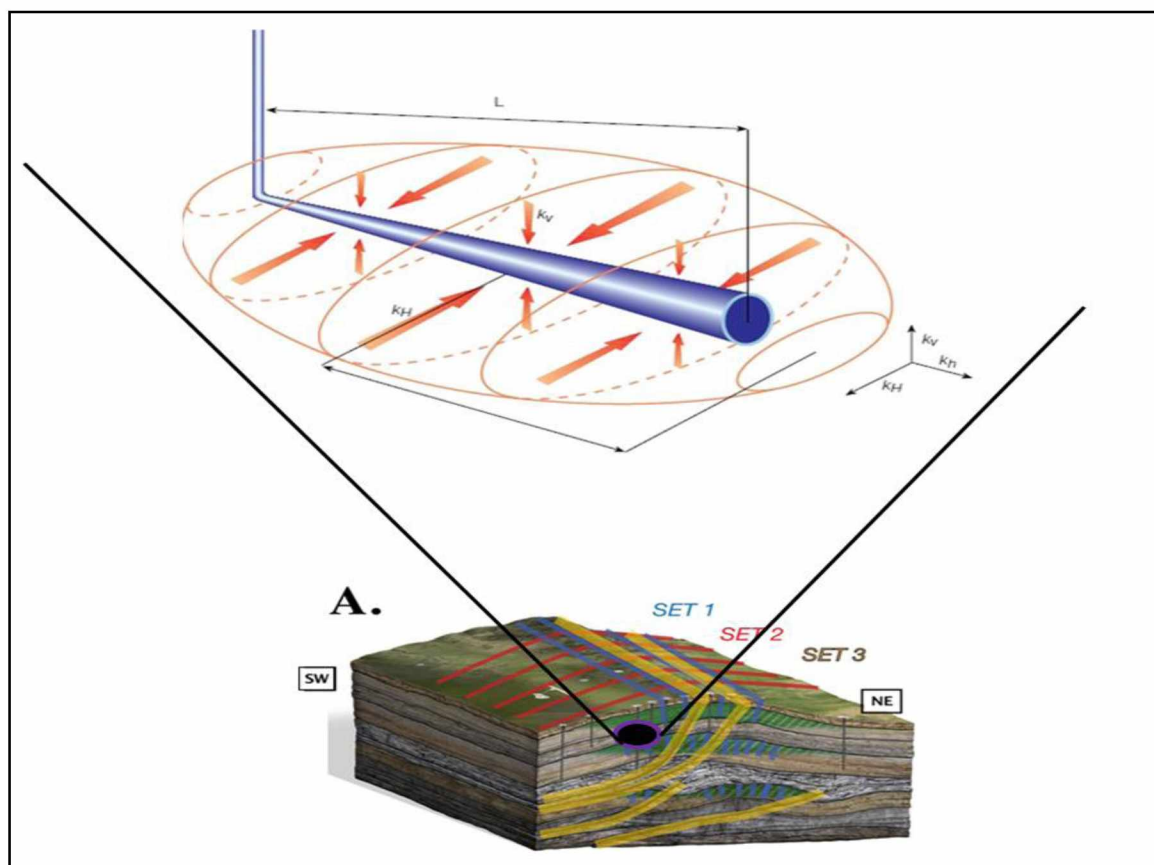


Figure 58. Natural fractures and their orientation with respect to permeability anisotropy in horizontal wells (Modified after Hanks et al., 2012; Ayan et al., 1994)

Since there was no data on flow characteristics of these fractures such as their effective permeability, spacing, shape factor, etc., we assumed that permeability anisotropy ratios could mimic the potential combined effect of the sedimentologic variation and the fractures. A set of seven permeability anisotropy ratios were selected and incorporated into the geologic model. The grid system for each case was populated and imported to the simulator. All the other parameters were kept similar to the base case model.

Figures 59 and 60 show the effect of changing anisotropy ratio. As the anisotropy ratio decreases from 0.75 to 0.05, the cumulative oil recovery decreases. When the anisotropy ratio decreases from 0.25 to 0.1, there is an unusual reduction in the production oil rates.

The oil rates then start to decline rapidly. As anisotropy ratio decreases, the oil rate decreases in the same trend as the case with $K_v/K_h=0.75$. The change in the oil rates between the cases of $K_v/K_h=0.25$ and 0.1 can be clearly seen. This might be due to sensitivity of the system to interconnectivity of fracture networks that are available for flow. Similar to previous cases, there is an abrupt increase in oil production rates when the system is opened to production.

In Figure 60, the average reservoir pressure and the producing GOR are plotted for the five cases of anisotropy ratios. The producing GOR for all the cases start to increase from early simulation time and increase gradually as more fluid is displaced. The higher the anisotropy ratio, the higher the GOR with one exception. The case with anisotropy ratio 0.25 starts with the smallest GOR values and then passes the other smaller anisotropy ratio GORs. For the case with smallest anisotropy ratio, the producing gas is restricted by limited vertical flow of gas towards the horizontal producers. The average reservoir pressure for the two smallest anisotropy ratios (0.05 and 0.1) tend to stay at higher values for a longer period of time compared to other cases. There difference between the case 0.25 and 0.1 which was observed in terms of oil rates and cumulative production is also detectable in the average reservoir pressure. The results in figure 60 can be interpreted to indicate that although higher anisotropy ratios maintain less average reservoir pressure, they have higher oil production. Smaller anisotropy ratios, on the other hand, have increased average reservoir pressure, but their gas injection performance is limited by ability of gas to move and displace the oil, resulting in lower overall oil production.

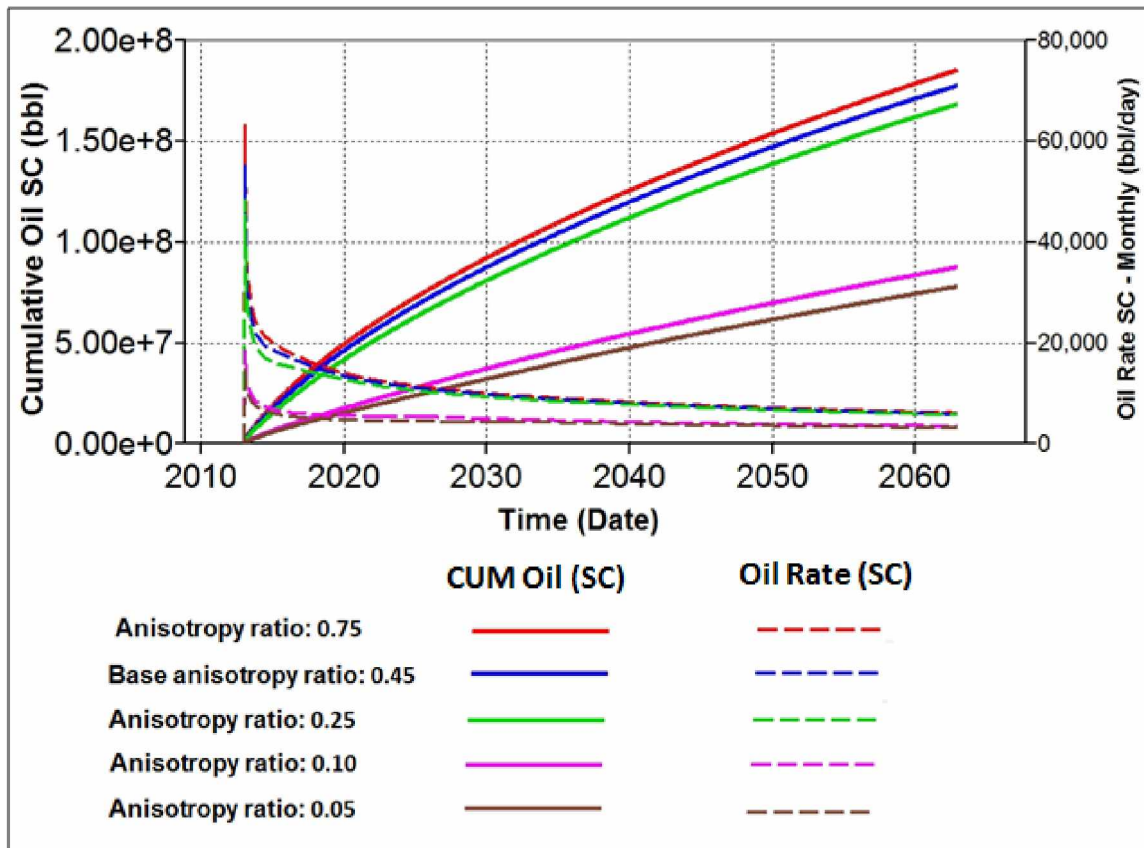


Figure 59. Field cumulative oil production and field oil rate for different permeability anisotropy ratio

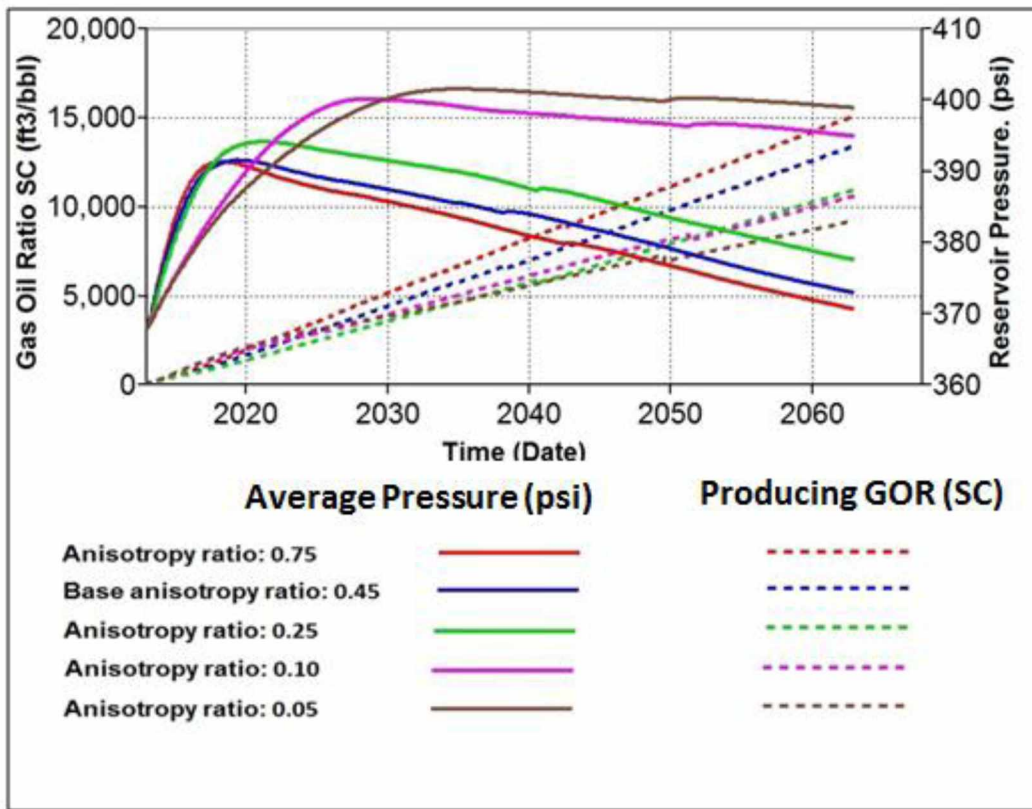


Figure 60. Average reservoir pressure and field producing gas oil ratio for different permeability anisotropy ratios

5.4.2 Relative Permeability and End Point Saturations

For a given simulator and known reservoir geology, endpoint saturations and relative permeabilities affect the performance among the various input modeling parameters. Inaccurate consideration of relative permeability data can result in underestimation or overestimation of oil recovery. This is particularly important in Umiat because given the remote location of the field, the decision to invest in implementation of technology and building infrastructure for the production is critical and has to be in alignment with the oil in place and recoverable oil. If the OOIP estimates were not accurate, the project would not get developed or cause unnecessary drilling costs.

The available relative permeability to gas at the residual oil saturation for the Umiat reservoir rock type #1 was significantly low. Thus, sensitivity to the K_{rg} values at the residual oil saturation was evaluated. Because only relative permeabilities to oil and gas was available for rock type #1, the Brooks and Corey (1964) correlation was used to estimate the relative permeabilities to oil and gas for rock types #2 and #3. Table 21 gives the data for the end points used in the base case simulation model. Residual oil saturation, critical gas saturation, and end point relative permeability to gas at residual oil saturations were considered for sensitivity analysis. The residual oil saturation is important to evaluate what percentage of the oil is mobile. Usually, the rock type with smaller pore size has higher residual oil saturation (Brooks and Corey, 1964). The critical gas saturation and the end point relative permeability to gas at the residual oil saturation also play an important role in the ability of the gas to flow and displace the oil.

Table 21. Relative permeability and saturation end points in the base case simulation

Rock type	S_{or}	S_{gc}	K_{rg}
1	0.16	0.32	0.0028
2	0.25	0.15	0.56
3	0.20	0.02	0.60

Table 22 presents the parameters used in the sensitivity analysis. Because the relative permeability data was not enough, these particular values were chosen to represent a change in the shape of the relative permeability curves and show variability of these numbers on the scale reservoir simulation results. The following cases were considered:

- Case 1: Change in S_{or} for all the rock types
- Case 2: Change in S_{gc} for rock types #2 and #3
- Case 3: Change in K_{rg} for rock type #1
- Case 4: Change in K_{rg} for rock type #2 and #3

Each case was run separately and compared with the base case model. The results are shown in a series of graphs as shown in Figure 61 through 68.

Table 22. Relative permeability and saturation end points used in sensitivity runs

Rock type	S_{or} (case #1)	S_{gc} (case #2)	K_{rg} (case #3)	K_{rg} (case #4)
1	0.24	0.32	0.03	0.0028
2	0.20	0.10	0.56	0.7
3	0.16	0.05	0.60	0.8

Figure 61 shows the cumulative oil and oil rates for the field. As it can be seen in the graphs, applying the S_{or} values in case #1 results in lower oil recovery and oil production rates. The oil recovery changes by about 10 MM STB difference in oil production or 7% change in the recovery factor when the residual oil saturations are changed by 20% in the model for rock types #2 and #3 only. There is no major change in the producing GOR, but the average reservoir pressure is also influenced by change in the residual oil saturation. The case #1 maintains a higher average reservoir pressure (5-15 psi) than the base case (Figure 62). This pressure difference corresponds to the oil recovery differences seen in the Figure 61.

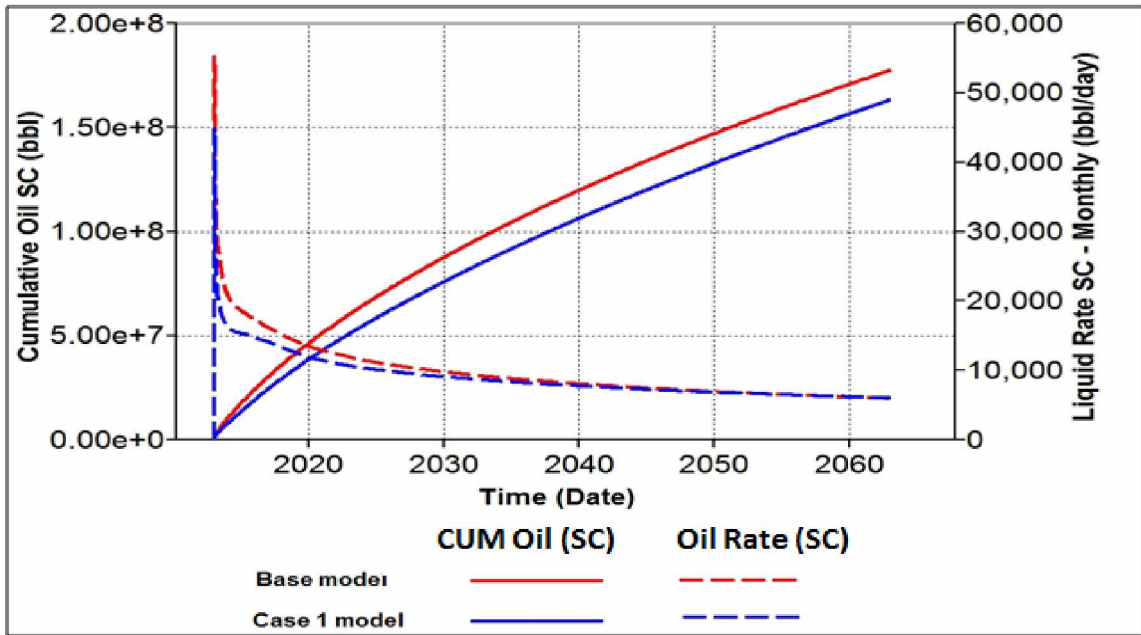


Figure 61. Field cumulative oil production and field oil rate for case #1: change in S_{or} for all the rock types

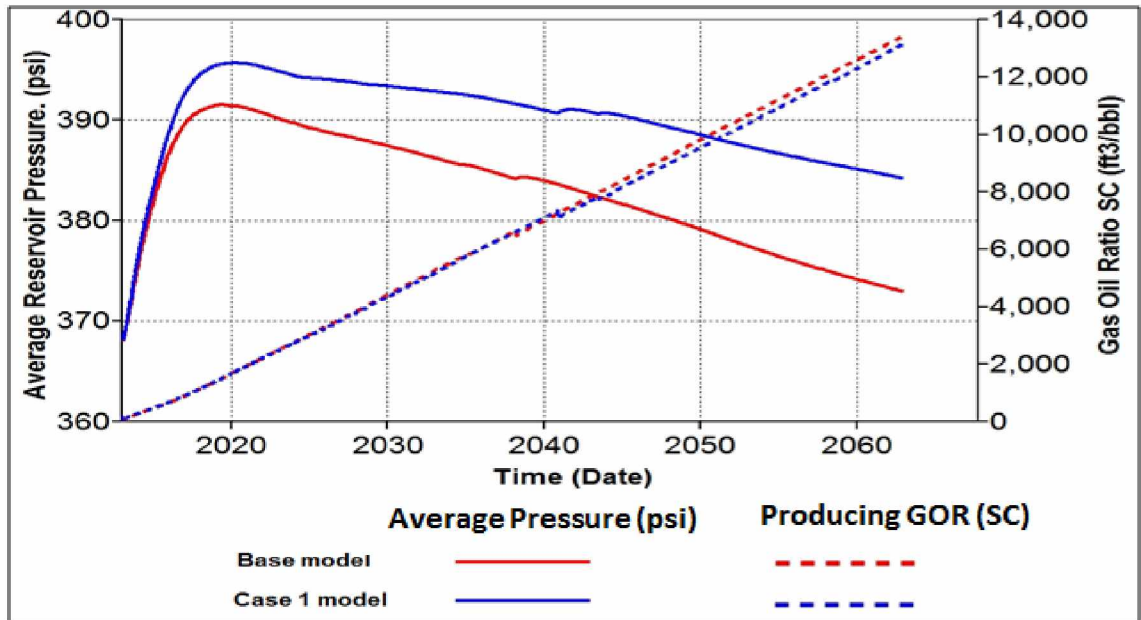


Figure 62. Average reservoir pressure and field producing gas oil ratio for case #1: change in S_{or} for all the rock types

Figures 63 and 64 present the results for case #2 when the critical gas saturation was subject to sensitivity analysis for rock types #2 and #3. These rock types were selected because their relative permeability data were correlation-based whereas the rock type #1 data was experimentally measured and was more reliable. There is about 5 MM STB difference between the cumulative oil for the base case and the S_{gc} sensitivity case and it shows that the oil recovery is also sensitive to changes in critical gas saturations.

The oil production rates except for some short amount of time follow the same trend (Figure 63). The difference between the GOR values is very small for the two cases. This shows that the amount of gas produced with the oil is not influenced by the onset of gas bubble growth when applied by changes in Table 22. The average reservoir pressure is higher in case #2 than the base case by about 1-2 psi during the simulation time (Figure 64).

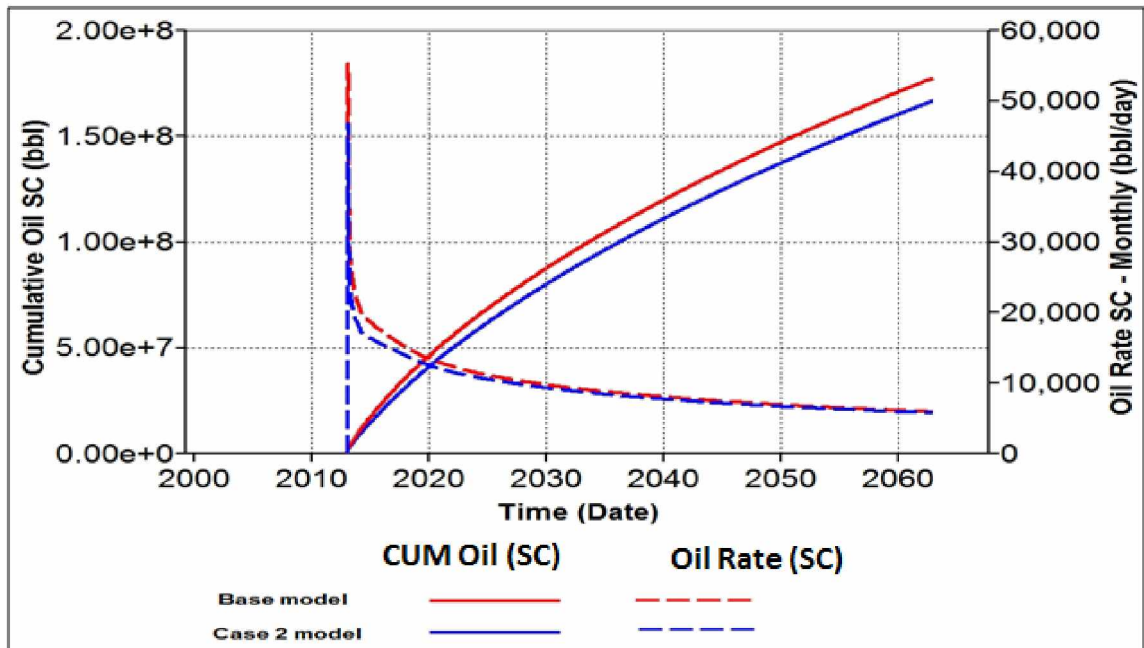


Figure 63. Field cumulative oil production and field oil rate for case #2: change in S_{gc} for the rock types #2 and #3

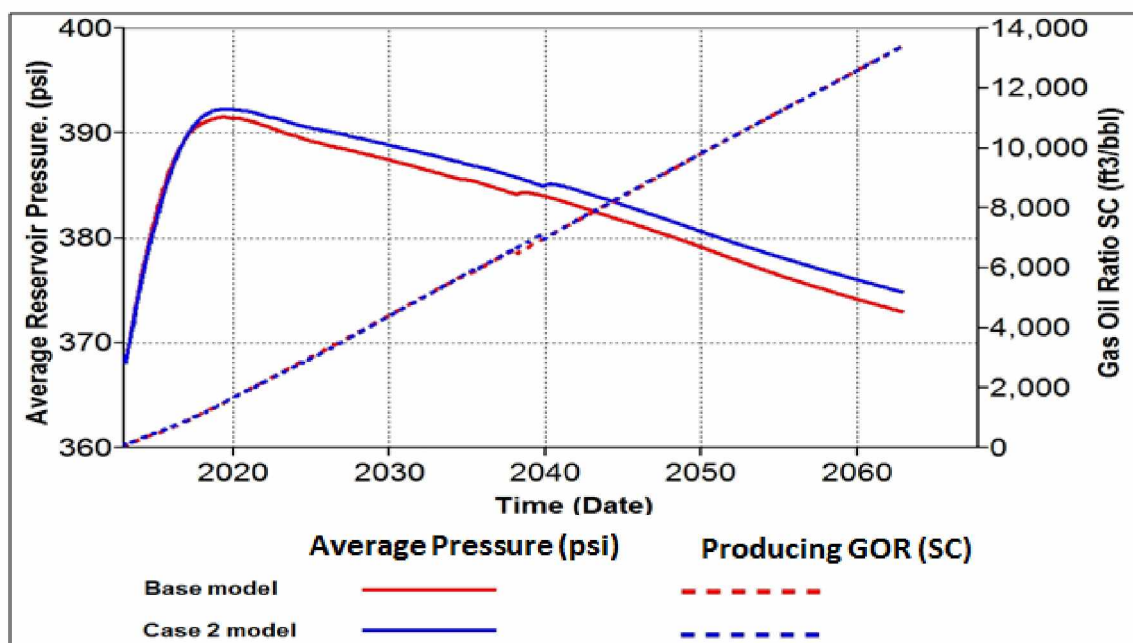


Figure 64. Average reservoir pressure and field producing gas oil ratio for case #2: change in S_{gc} for the rock types #2 and #3

Figures 65 and 66 show the results for field cumulative oil and oil production rates. The results demonstrates that the increase in relative permeability to gas at the residual oil saturation in rock type #1 with no changes in rock type #2 and #3 does not have any significant changes in oil recovery, average reservoir pressure, and the producing GOR. This might be due to extremely low permeability of rock type #1. It could be also due to heterogeneities in the reservoir. However, when the relative permeabilities to gas at the residual oil saturation in rock types #2 and #3 are increased by 25% and 33% respectively, there is a significant increase in the oil recovery and a sensible reduction in the average reservoir pressure. The ultimate oil recovery decreases by 9% (Figure 67) and the final average reservoir pressure decreases by 3% (about 8 psi) (Figure 68).

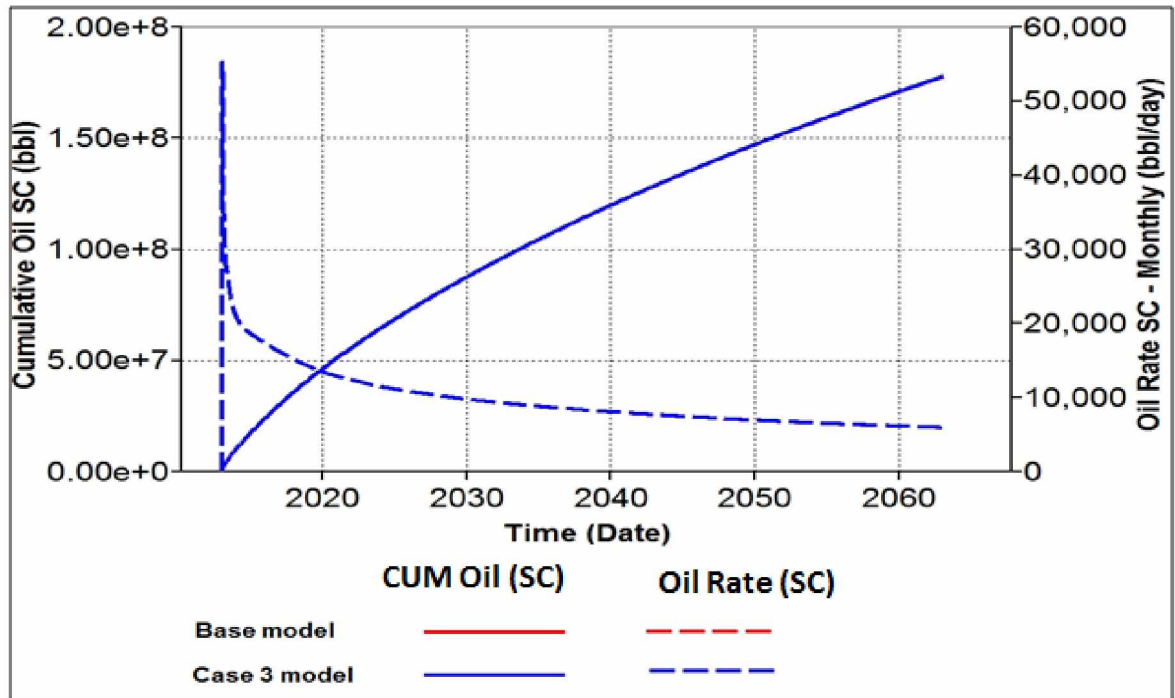


Figure 65. Field cumulative oil production and field oil rate for case #3: change in K_{rg} for the rock types #1. The red curves underlie the blue curves.

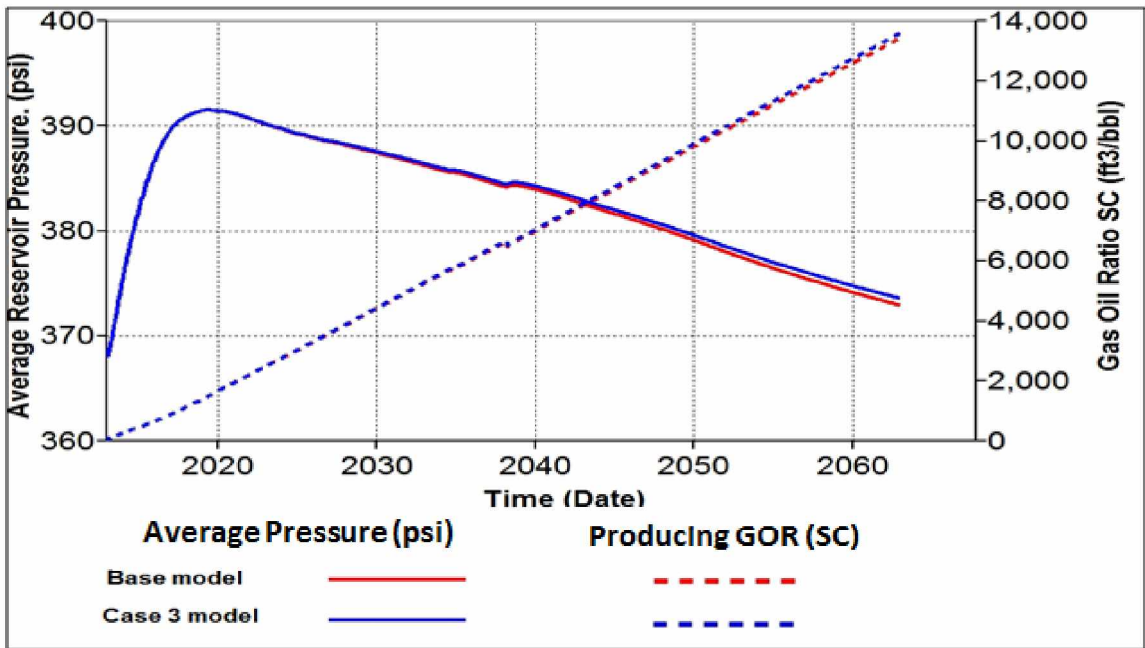


Figure 66. Average reservoir pressure and field producing gas oil ratio for case #3: change in K_{rg} for the rock types #1

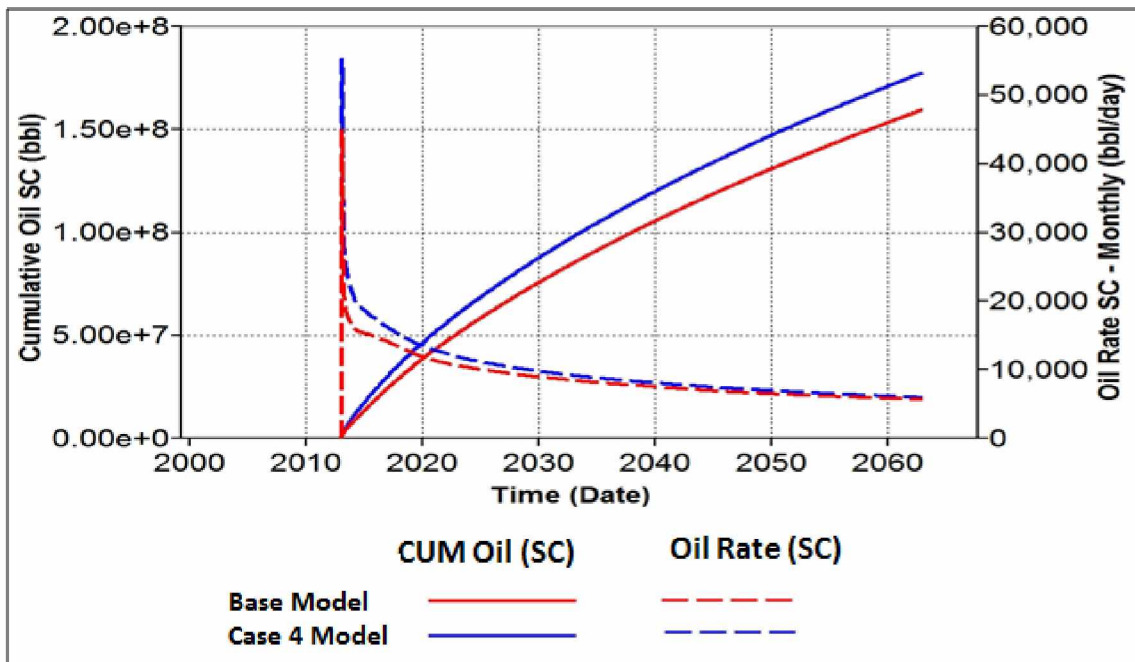


Figure 67. Field cumulative oil production and field oil rate for case #4: change in K_{rg} for the rock types #2 and #3

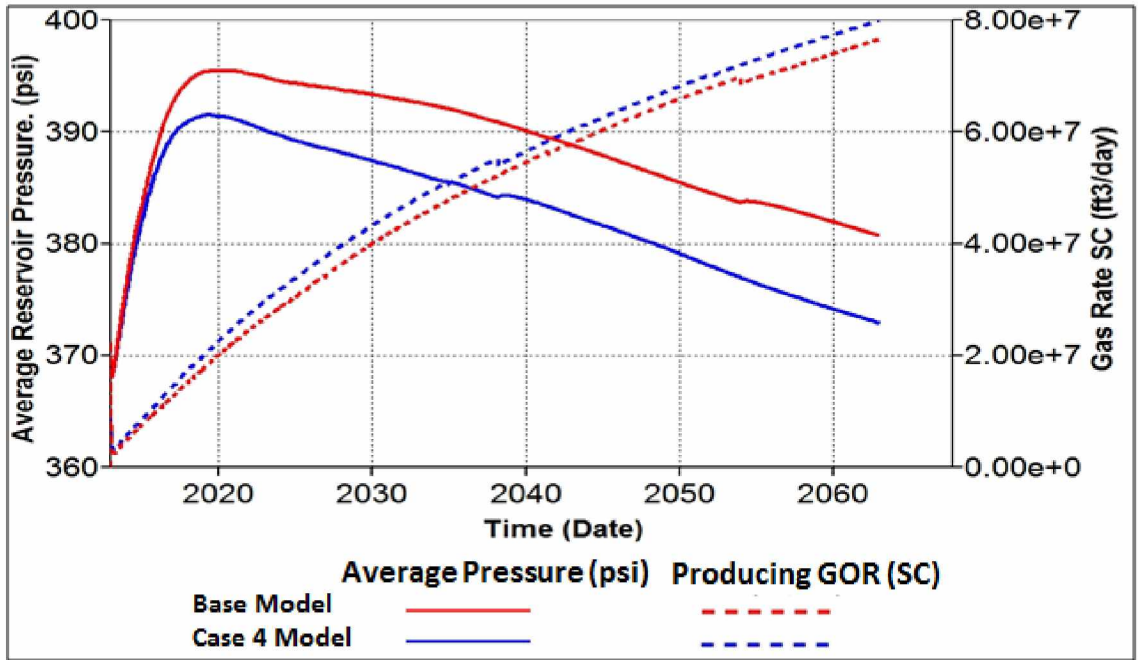


Figure 68. Average reservoir pressure and field producing gas oil ratio for case #4: change in K_{rg} for the rock types #2 and #3

To have a better picture of the impact of changes in residual saturation and the end point relative permeability have on the cumulative oil recovery, a summary of their cumulative oil production vs. time is presented in Figure 69.

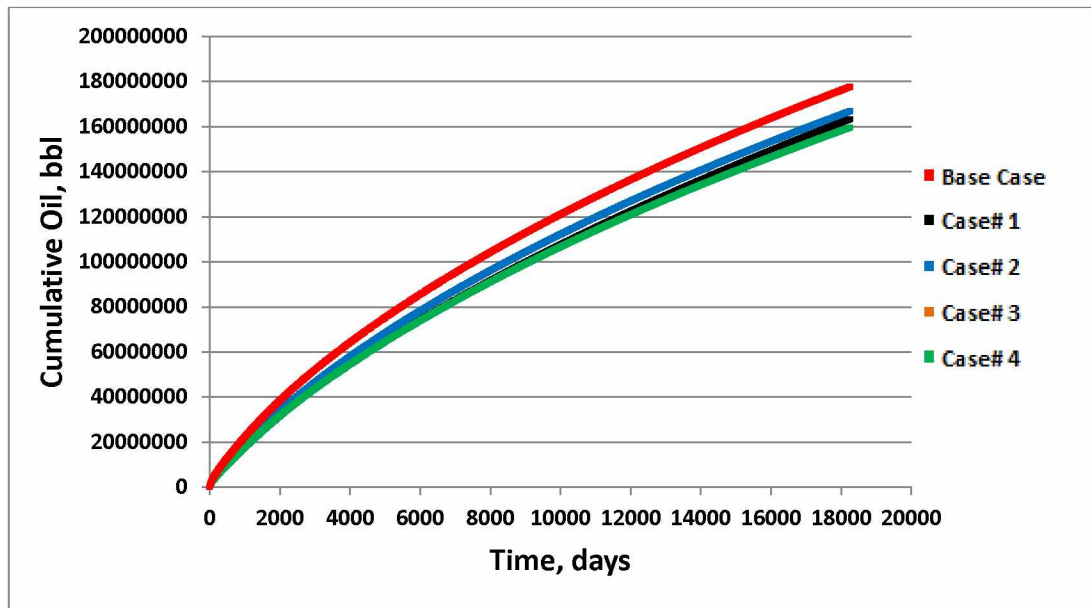


Figure 69. Comparison of the cumulative oil productions for Case#1 through Case# 4 with the base case. The base case and Case# 3 are overlying each other. Case 1: change in S_{or} for all the rock types. Case 2: change in S_{gc} for the rock types #2 and #3. Case 3: change in K_{rg} for the rock types #1. Case 4: change in K_{rg} for the rock types #2 and #3

5.4.3 Producing GOR

For every reservoir subject to gas injection and production, there is always a concern about gas handling capacity and impact to environment (Pillai, 2012). To address this, we considered different limitations on the field producing GOR and their impacts on the oil recovery, oil rate, and average reservoir pressure (Figures 70 and 71).

The case with no GOR constraints gives the highest cumulative oil recovery (Figure 70). When the reservoir is constrained by a smaller value of a producing GOR (5000 ft^3/bbl), the cumulative oil recovery decreases. When the reservoir is not constrained by producing GOR (the base case), the oil recovery is about 12%. With 5,000 scf/STB and 10,000 scf/STB constraints on the producing GOR, the oil recoveries decrease by about

18% and 6% respectively. This can be interpreted to indicate that putting any constraints at the field level on the producing GOR will cause a reduction in the oil recovery. In terms of oil production rates, the general trend is similar to the previous cases. (Figure 70). There is a sudden increase in the oil rates in the few first months when the system is opened to production and then gradual decline as the simulation continues.

The GOR increases as the constraint on the producing GOR is removed (Figure 71). For the case with no constraint, the GOR reaches as high as 13,000 ft³/bbl after 50 years. This value is less than 6000 ft³/bbl and 4000 ft³/bbl for the cases with producing GOR constraints of 10,000 ft³/bbl and 5000 ft³/bbl, respectively.

The average reservoir pressure follows an expected trend (Figure 70). The case with no GOR constraint maintains a lower average pressure than the other two cases. The lower the constraint, the more gas volume in the reservoir and the higher average reservoir pressure (Figure 71).

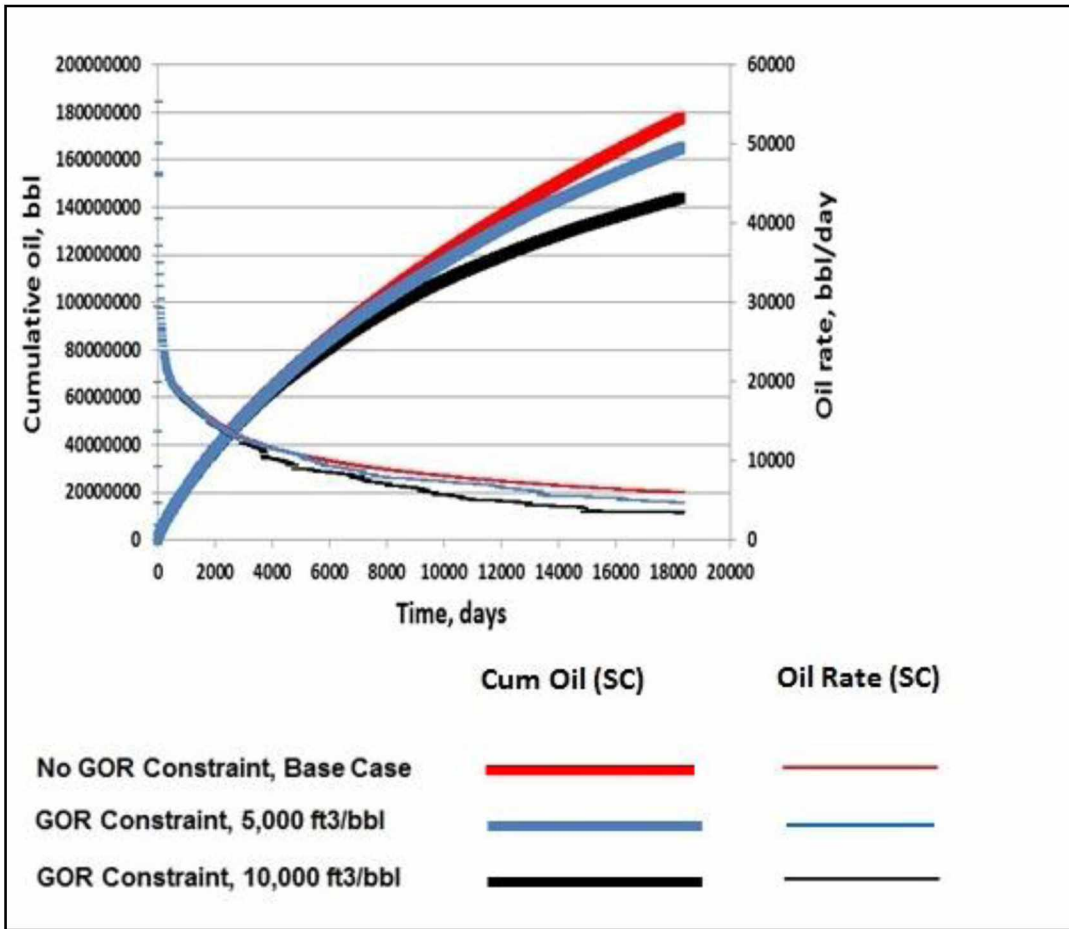


Figure 70. Field cumulative oil production and field oil rate for different GOR constraints

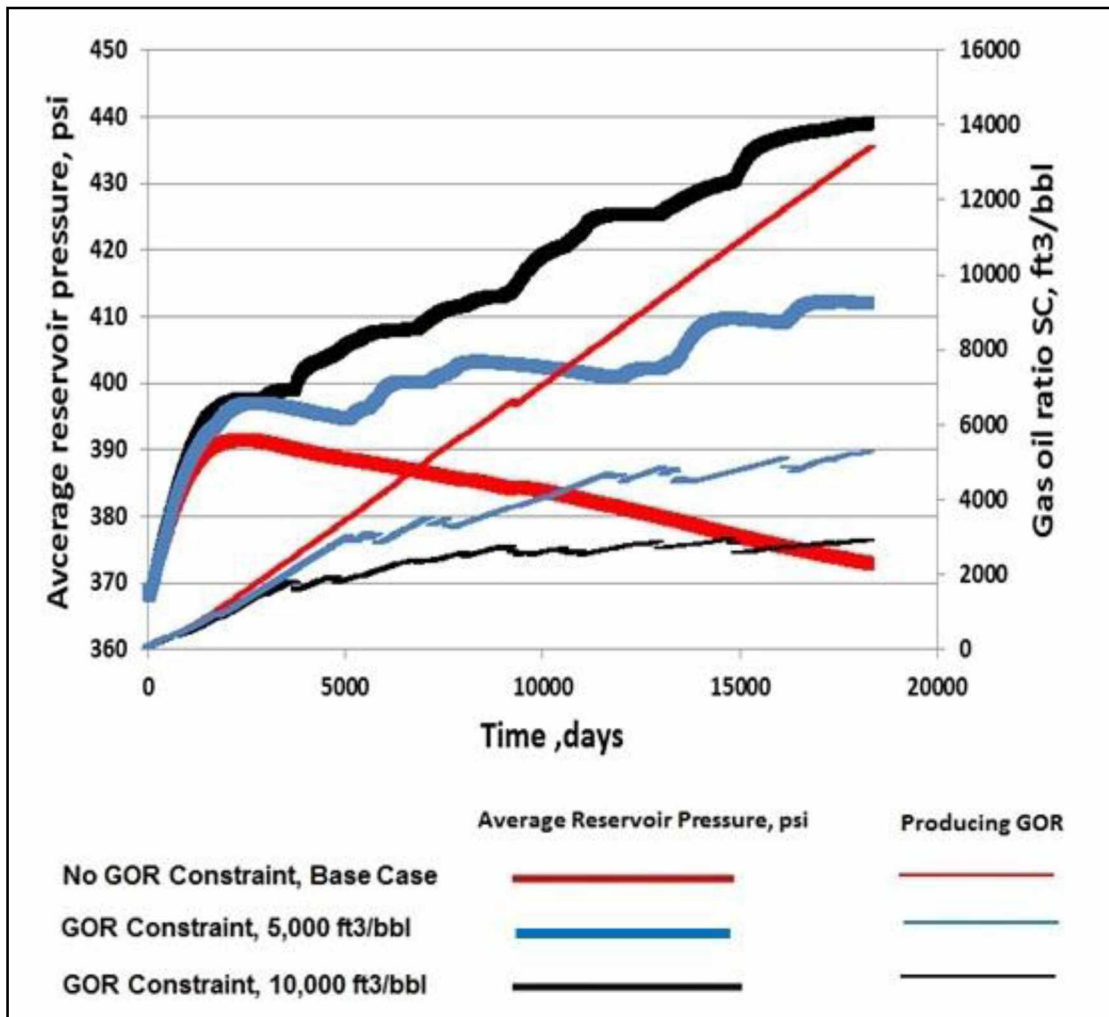


Figure 71. Average reservoir pressure and producing GOR for different GOR constraints

5.5 Discussion

Because of the low reservoir pressure at Umiat, the flowing bottom-hole pressure should be kept at a minimum in order to have maximum pressure drawdown for oil production. By using this minimum pressure (80 psi here), the fluid cannot be delivered in the vertical section of the wellbore and raise the fluid up to the surface. Consequently, the reservoir energy should be supplemented by using an artificial lift method. A loss of production

wells due to insufficient artificial lift would result in increasing operating cost and reducing overall field productivity.

The preferred lift method is an ESP (Electrical Submersible Pump) (Watt et al., 2010). The ESP should be placed at the deepest straight horizontal section of the wellbore provided that the wellbore radius is large enough for the selected ESP (r_w is 4 inch). This would improve gravity drainage and the efficiency of gas injection. With low volumes of water production and shallow depth of the wells, a low horsepower ESP could even be sufficient. The only concern about using ESP is that with gas injection as the current development plan, high rates of GOR are expected (as high as 13,000 ft³/bbl in the base case) and the ability or capacity of ESPs for such conditions is unknown (Watt et al., 2010). An extensive volume of gas causes unstable flow which ultimately leads to pump failure.

Another type of artificial lift method that can be implemented at Umiat is gas lift. Since gas lifts are less capital-intensive than ESP, it may be a viable candidate for decreasing the hydrocarbon weight and increasing well production rates, provided that sufficient gas compression infrastructure is available.

Based on the results of this study, the LGS reservoir contains a significant amount of oil in place (1550 STB bbl). Nine geologic models and 15 simulation models were built to model production of the reservoir over a projected 50 year lifespan. The simulation cases with gas injection from the start of the production life of the reservoir were run with all the lateral horizontal wells producing and injecting against bottom hole pressures and oil economic limit (5 bpd). The oil recoveries ranged from 5% to about 15% in all the prediction simulation cases. The range of cumulative oil production was from 80 MM STB to 230 MM STB and the oil production rates ranged from as low as 2500 bpd to as high as 80,000 bpd.

Injecting gas will supplement the reservoir pressure and maintain the energy in the system. In the simulations, gas injection at the start of the production maintained the energy in the system and, in effect, avoided a sharper rapid decline in the pressure and cumulative oil as observed in the primary production (no gas injection).

In the base case with a gas injection pressure of 400 psi, a total of 9.5×10^{11} ft³ gas (methane) is needed to support the 177 MMM STB of oil during the 50 years of the injection operation. Higher bottom hole injection pressures that would lead to higher ultimate recoveries will require an additional volume of gas. Some portion of the required injection gas can be provided by the produced gas and some of it can be from other resources. In the case with injection pressure of 600 psi, an additional 4.4×10^{11} ft³ of gas will be needed to support the of oil incremental recovery. However, for selecting the actual injection pressure, the actual fracture gradient must be determined to ensure successful design of injection systems and prevent fracturing the reservoir rocks.

The presence of natural fractures could provide a supportive production mechanism but only if they could provide extra flow channel to oil in addition to that of lower permeability matrix. However, additional geologic and production data are needed to help characterize the fractures more efficiently.

With all of the engineering and geologic constraints, the decision to implement gas injection as the development plan also depends on economic conditions and the price of oil. If the price of oil falls below a certain limit or if the operation costs increases to a certain amount, the project may not be profitable. A simple economic model covering different economic metrics for operation costs was developed and is presented in Appendix D.

Chapter 6 Conclusions and Recommendations

6.1 Conclusions

Current high oil prices and availability of new technologies allow re-evaluation of oil resources previously considered uneconomic. The Umiat oil field in National Petroleum Reserve of Alaska (NPRA), discovered in 1946, is located north of the Arctic Circle, 140 miles southwest of Prudhoe Bay and 80 miles west of Trans Alaska Pipeline System (TAPS). It is a promising oil reservoir, with 37° API gravity crude and an estimated 1.5 billion barrel of STOOIP. This unique, shallow (275–1055 ft), low-pressure (200–400 psi) reservoir lies mostly within the permafrost zone and is now considered an attractive development target.

A static model was built based on reinterpretation of original log and core data, new outcrop data and new seismic data. Water saturations were also mapped in the model using new capillary pressure data. Based on new permeability data, an anisotropy ratio of 0.45 was incorporated into the geologic model.

A geological uncertainty study was conducted to quantify the impact of different input parameters on reserve estimation such as facies, porosity, permeability anisotropy, variogram characteristics and water saturation. Based on a Monte Carlo simulation that incorporated the potential range in these parameters, OOIP estimates for the primary reservoir interval of interest, the Lower Grandstand, range from 790 MM STB to 2474 MM STB with a P50 value of 1550 million bbl oil.

Based on the wide variation in the permeabilities in the field (0–500 md), three rock types were defined for permeabilities less than 1 md, between 1 md and 50 md and higher than 50 md and were included in a dynamic model along with measured PVT data and gas-oil relative permeabilities in the presence of ice. Oil recovery was evaluated using a

wagon wheel well pattern and immiscible gas injection. Variables included well length, permeability anisotropy, production and injection constraints and economic metrics.

100 multiple realizations of the geologic model were run and degrees of uncertainty associated with each geologic realization were identified. The combinations of input parameters (depth of WOC, variogram uncertainty in porosity and permeability in normal and parallel direction, water saturation, porosity, and NTG) were tested to assess their impact on the STOOIP volumes and the top 4 contributors to geological uncertainty were determined. The highest-ranked contributor was found to be depth of the oil/water contact. Variogram uncertainty in porosity and permeability in both normal and parallel range was ranked next. This implies a large degree of uncertainty in the spatial distribution of the data. Water saturation, porosity, and NTG (Net To Gross) ratio were found to be the subsequent most important parameters. B_o was the lowest-ranked uncertainty parameter.

Cold gas injection was proposed as the development plan and simulation studies focused on the LGS that has the greatest thickness and lies mostly below the permafrost zone. With no distinguishable trends in the porosity and permeability data and due to wide variations in permeability, three sand groups (rock types) were defined. A mechanistic simulation model was built to show the effect of gas injection in the LGS reservoir of Umiat field. Rock and fluid data measured in presence of ice were either measured or calculated and were imported into a simulation model. Due to environmental concerns, a wagon wheel dual lateral well configuration with 80 producers and 25 injections was designed on 5 pads and incorporated into the simulation model. Grid sizes of 200 ft by 200 ft in x and y directions and 1 to 45 ft in vertical direction were determined to be the optimal grid sizes for computational speed and simulation accuracy.

The optimum horizontal well length and injection pressure were found to be 1500 ft and 400 psi, respectively.

Based on gas injection over 50 years and 400 psi bottom-hole gas injection pressure, the predicted recovery is about 12%. For a 600 psi bottom-hole gas injection pressure, the recovery is 15%. The recovery for the case with no gas injection (primary production) is about 8% of OOIP.

The simulations indicate that the higher the injection pressure, the higher the average reservoir pressure and the greater the recovery. However, higher injection pressures lead to the danger of exceeding the formation fracture gradient. Overpressuring the reservoir rock may result in fracturing the reservoir that may cause reduction in oil recovery due to early breakthrough of gas. An optimized injection pressure depends on the matrix fracture gradient, which is not currently well constrained at Umiat.

The simulation results demonstrate reduction in oil recovery by 18%, when producing GOR is limited to 5000 scf/STB. When the limit of produced GOR is increased to 10,000 scf/STB, the oil recovery is reduced by 6%.

Since the Umiat reservoir pressure is significantly low compared to other conventional reservoirs, a small increase or decrease in the reservoir pressure causes thousands of barrels difference. Simulation results also indicate that the average reservoir pressure and ultimate recovery are very sensitive to the endpoint relative permeability assigned to the more permeable sands. This effect emphasizes the need to use accurately measured relative permeability data (especially the relative permeability to oil and gas) to produce accurate results.

The impact of potential fractures was evaluated by testing the sensitivity of the reservoir performance to permeability anisotropy (K_v/K_h). Resulting simulations indicate that higher anisotropy ratios (> 0.5) results in higher oil production and lower average reservoir pressures after 50 years of gas injection. When the anisotropy ratio drops from 0.25 to 0.1, the average reservoir pressure increases by more than 6% and cumulative oil

production decreases by more than 45%. This suggests that less fluid has been displaced in the reservoir.

With minimum flowing bottom hole pressure for higher drawdown, the use of an artificial lift method is necessary to supplement the energy in the system. Selection of the right artificial lift method would result in less shut-offs and facilitate the production operations. However, many factors such as depth of the pump, diameter of the pump and economic considerations against gas lift option have to be evaluated prior to implementation of the development plan.

Despite limited data and lack of production history to tune the model, the simulation results indicate the areas where the proposed development plan has the highest degree of uncertainty and therefore risk. These findings strongly encourage the operator to include in their development plan strategies to reduce uncertainty by collecting additional data about reservoir properties.

6.2 Recommendations

The following are recommendations for future work:

- This study only focused on LGS reservoir. For a complete understanding of behavior of the Umiat reservoir, it would be beneficial to see how the UGS reservoir behaves under the same development plan (gas injection).
- During the course of this study, it was observed that gas hydrate could be forming under reservoir temperature and pressure conditions. It is recommended that formation of hydrate should be more comprehensively studied and in the case of its formation, prevention methods should be evaluated.
- This study focused on methane as the immiscible gas injection. The effect of other injection gases such as CO₂ or N₂ should also be evaluated.

- This study focused on immiscible gas injection. It would be helpful to see what range of recoveries would be obtained by implementing some other EOR processes such as waterflooding or polymer flooding.
- Although cold gas injection has been proposed as the main development plan for this study, the adjustment of injection temperature can be made in such a way that by injecting gas at a few higher degrees than reservoir temperature, near-wellbore ice melting might melt some of the ice around the wellbore and increase the relative permeability to oil to flow. It is recommended as future study to use a simulator that can handle this process for near-wellbore stimulation.
- This study did not consist of history matching. When production data becomes available, it is recommended history matching analysis be done to validate the results of this study.

References

Ahlbrandt, T. S., Preliminary geologic, petrologic and paleontologic results of the study of Nanushuk Group rocks, North Slope, Alaska, U.S. Geological Survey Circular 794 163 p [1979].

Ahmed, T., Reservoir engineering handbook, Gulf Professional Publishing, [2001].

Amyx, J., Bass, M.D., Whiting, L.R., Petroleum reservoir engineering physical properties, McGraw-Hill Companies, pp 155, [1960].

Ayan, C., Colley, N., Cowan, G.; Ezekve, E., Wannell, M., Goode, P., Halford, F., Joseph, J., Mongini, A., Obondoko, G., and Pop, J., Measuring permeability anisotropy, Oilfield Review, Schlumberger, p.p. 24-35, [1994].

Baptist, O.C., Oil recovery and formation damage in permafrost, Umiat field, Alaska, [Washington] U.S. Dept. of the Interior, Bureau of Mines, [1960].

Beal, C., The viscosity of air, water, natural gas, crude oil and its associated gases at oil field temperatures and pressures, SPE 946094-G, Journal of Transactions of the AIME, Vol. 165, No. 1, [1964].

Beliveau, D., Heterogeneity, geostatistics, horizontal wells and blackjack poker, SPE 30745, [1995].

Brooks, R.H. and Corey, A.T., Hydraulic properties of porous media, Hydrology Papers, No. 3, Colorado State University, Ft. Collins, Colo, [1964].

Brosge, W. P., Geology of Umiat-Maybe Creek region Alaska, U.S. Geological Survey Vol 638, [1966].

Cho, H, Shah, S.N., Prediction of specific productivity index for long horizontal wells, SPE 67237, SPE Production and Operations Symposium, [2001].

Collins, F.R., Test Wells, Umiat area, Alaska: U.S. Geological Survey Professional Paper 305-B, p.71-206, [1958].

Corey, A.T., The interrelation between gas and relative permeabilities, Producers Monthly, pp. 38–41, [1954].

Cronquist, C., Estimation and classification of reserves of crude oil, natural gas and condensates, GSLIB user's manual, Applied Geostatistics, second edition, Oxford University Press. [2001].

Dachang, L., Myra, D., Cut-off or Separation? A new approach to distinguish reservoir rock from non-reservoir rock for reservoir modeling and simulation, SPE 38380, SPE Rocky Mountain Regional Meeting, [1997].

Dandekar, A.Y., Petroleum reservoir rock and fluid properties: CRC Press, Boca Raton, Florida, [2006].

Darche, G., Grabenstetter, G.E., and Sammon P.H., The use of parallel processing with dynamic gridding, SPE 93023, Reservoir Simulation Symposium, [2005].

Espach, R.H., Recoverable petroleum reserves in the Umiat Structure, Naval Petroleum Reserve No.4, Alaska, U.S. Bureau of Mines Petroleum and Natural Gas Branch Open-file report [1951].

Fanchi, J.R., Principles of applied reservoir simulation, Second Edition, Gulf Professional Publishing, [2001].

Fylling, A., Quantification of petrophysical uncertainty and its effect on in-place volume estimates: numerous challenges and some solutions, SPE 77637-MS, SPE Annual Technical Conference and Exhibition, [2002].

Gates, G.L., and Caraway W.H., Well productivity related to drilling muds national petroleum reserve No 4 Alaska, U.S Department of the Interior, Bureau of Mines [1960].

Geerstma, J., Estimating the coefficient of inertial resistance in fluid flow through porous media, Society of Petroleum Engineers. J Oct, 445. [1974].

Ghedan, S.G., Bertrand, M.T., and Douglas, A.B., Modeling Original Water Saturation in the Transition Zone of a Carbonate Oil Reservoir, Journal of Reservoir Evaluation and Engineering, SPE 88756, [2006].

Godabrelidze, V., Characterization and fluid flow Properties of frozen rock systems of Umiat oil field, Alaska, M.S. thesis, University of Alaska Fairbanks. 115 pp, [2010].

Hagedorn, A.R., Brown, K.E., Experimental study of pressure gradients occurring during continuous two phase flow in small-diameter vertical conduits, April, Journal of Petroleum Technology, Pages 475- 484., [1964].

Hanks, C.,; Shimer, G., Ahmadi, M., Oraki Kohshour, I., McCarthy, P., Dandekar, A., Mongrain, J., Wentz, R., and Davis, J, Can a shallow frozen reservoir be successfully exploited? A Predevelopment Case Study Of The Umiat Oil Field, Northern Alaska, SPE 159249-MS, [2012].

Hinderaker, L., Utseth, R., Hustad, O., Akervoll, I., Dalland, M., Kvanvik, B., Paulsen, T., and Eric, J., RUTH - A comprehensive norwegian R & D program on IOR, European Petroleum Conference, SPE 36844, [1996].

Joshi, S.D., Horizontal Well Technology, [1990].

Joshi International Technologies, Inc., Umiat Field, Alaska: Development with horizontal wells, prepared for Renaissance Alaska LLC, [2008].

King, M.J., Karam S.B., Wangh, P., Muralidharan, V., Alvarado, F., Optimal coarsening of 3D reservoir models for flow simulation, SPE Reservoir Evaluation & Engineering, Vol. 9, No. 4, pp. 317-334, [2006].

Krajewski, S.A., and Gibbs, B.L., Understanding contouring: A practical guide to spatial estimation using a computer and Variogram Interpretation, [2001].

Levi-Johnson, O., Petrophysical property modeling of Umiat field, a frozen Reservoir, M.S. thesis, University of Alaska Fairbanks. 129 pp [2010].

Linc Energy Report [2012]. web link:
<http://www.lincenergy.com/data>

Lindley, D.V., Understanding uncertainty, Published by John Wiley & Sons, Inc, [2006].

Mattax, C.O., Dalton, R.L., Reservoir simulation, SPE Monograph, volume 13, Henry L. Doherty series, [1960].

Masoudi, R., Halim, M.H.A, Karkooti, H., Othman, M., On the concept and challenges of water saturation determination and modeling in carbonate reservoirs, SPE International Petroleum Technology Conference, ISBN 978-1-61399-148-0, [2011].

McCain, W.D., The Properties of petroleum fluids, Second edition, PennWell Publishing Company, [1990].

Meisingset, K.K., Uncertainties in reservoir Fluid description for reservoir modeling, SPE Reservoir Evaluation & Engineering, Vol. 2, No. 5, pp. 431-435, [1999].

Molenaar, C. M., Umiat field, an oil accumulation in a thrust-faulted anticline, North Slope of Alaska, in Powers, Geologic studies of the Cordilleran thrust belt, Rocky Mountain Association of Geologists, p.537-548 [1982].

Novy, R.A., Pressure Drops in horizontal wells, when can they be ignored?, SPE 24941, [1995].

Oil & Gas Journal, March 20, 2000, web link:
<http://www.ogi.com/ogi-survey-downloads.html>

Pedersen, K.S., Thomassen, P., and Fredenslund, A., Properties of oils and natural gases. Gulf Publishing Company, [1989].

Pillai, R.G., Oil production optimization for fields with sensitive wells and gas handling limitation, SPE 161780-MS, [2012].

Poete, N., Quantitative Petrophysical Uncertainties Modeling and its Impact on Reserves Estimates, SEWL-Kuwait Presentations, [2012].

Pooladi-Darvish, M., and Gerami, S, Use of Analytical Models and Monte-Carlo Simulation for Quantification of Uncertainties Associated With Gas Production From Hydrate-Capped Gas Reservoirs, Offshore technology Conference, SPE 19568-MS, [2008].

Potter, C. J., and Moore, T.E., Brookian structural plays in the National Petroleum Reserve, Alaska, U.S.G.S. Open-File Report 03-266, [2003].

Roebuck, I.F., Petroleum Engineering Handbook, Chapter 43, Gas-Injection Pressure Maintenance in Oil Reservoirs, Society of Petroleum Engineers, [1987].

Roxar, RMS Manual Guide, [1994-2008].

Schneider, J.H., Empirical capillary pressure relative permeability correlation, consulting reservoir engineering, [2003]. Web link:
http://www.jhschneider.com/Empirical_Capillary_Relationship

Shimer, G., McCarthy, P., Hanks, C., Core-based interpretation of parasequence stratigraphy within the Cretaceous Nanushuk formation, Umiat, Alaska: in program with Abstracts joint AAPG Pacific Section/SPE Western Regional meetings, Anchorage, Alaska, [2011].

Shukla, C., Fluid characterization and phase behavior studies of oil from the frozen reservoir of Umiat Oil Field, Alaska, M.S. thesis, University of Alaska Fairbanks. 103 pp [2011].

Sloan, E.d., Koh, C.A., Clathrate Hydrates of Natural Gases, Taylor & Francis Group, [2007].

Van Golf-Racht, T.D., Fundamentals of Fractured Reservoir Engineering, Elsevier Publishing Company, [1981].

Venepalli, K., Implication of the Pore-scale Distribution of Frozen Water for Production of Hydrocarbon Reservoirs Located in Permafrost, M.S. thesis University of Alaska Fairbanks, 95 pp, [2011].

Watt, J., Huckabay, A., and Landt, M.R. Umiat: a North slope giant primed for oil development, Oil and Gas Journal, [2010].

Zeybek, A.D., Onur, M., and Tureyen, O.I., Assessment of uncertainty in saturation estimated from Archie's equation, SPE 120517-MS, SPE Middle East Oil and Gas Show and Conference, [2009].

Zhang, J, Song, K, Dong, B, Chen, D, Prevention and control of gas hydrates for foam combination flooding, SPE Asia Pacific Oil and Gas Conference and Exhibition, SPE 77875-MS, [2002].

Zhang, K., Ghanbari, S., and Chelak, R., Introduction to simulation grid design and upscaling methods, The CSPG CSEG CWLS Joint Annual Convention, [2009]

Nomenclature

Actnum	Active number of cells
Bo	Oil formation volume factor
Bpd	Barrel per day
CIR	Cell Impact Ratio
EOS	Equations of state
EOR	Enhanced oil recovery
FCF	Free cash flow
FCOP	Field cumulative oil production
FOR	Field oil rate
FVF	Formation volume factor
GOC	Gas oil contact
GOR	Gas-oil ratio
GOGD	Gas oil gravity drainage
HCPV	Hydrocarbon pore volume
IOR	Improved Oil Recovery
IPL	Internal programming language
IRR	Internal rate of return
Kx	Permeability in x direction
Ky	Permeability in y direction
Kz	Permeability in vertical direction
Kr	Relative permeability
LGS	Lower Grandstand
MC	Monte Carlo
MMB	Million barrels
MMSCF	Thousands standard cubic feet
NPRA	National Petroleum Reserve of Alaska
NPV	Net Present Value

NTG	Net to gross
OOIP	Original oil in place
POR	Porosity
Pc	Critical pressure
PVT	Pressure, volume and temperature
Rs	Solution gas-oil ratio
RMS	Reservoir management system
RIR	Resource Impact Ratio
Sg	Gas saturation
So	Oil saturation
STBD	Standard tank barrel per day
STOOIP	Standard tank original oil in place
Sw	Water saturation
Swi	Irreducible water saturation (Initial water saturation)
TAPS	Trans Alaska Pipeline System
Tc	Critical temperature
UGS	Upper Grandstand
USGS	U.S. Geological Survey
Vb	Bulk volume
Visg	Gas viscosity
Viso	Oil viscosity
WGOR	Well producing gas oil ratio
WOC	Water oil contact
WOR	Well oil rate
Φ	Porosity

APPENDIX A. Optimal Layer Design Algorithm

Objective: A practical workflow was designed to create and optimize the heterogeneity of the irregular grid in K directions by utilizing:

- Algorithm based on SPE 95759 (King, et al. 2006)
- RMS 2011
- IPL programming
- Help from Roxar support

The basic idea is based on the fact that the variation inside a geobody is small, so a coarser cell is enough. The challenge was how to quantify the variation inside the geologic model to observe the impact of layer coarsening on overall heterogeneity. The idea of the proposed solution is to preserve the maximum heterogeneity on the geological grid by applying non-uniform proportional layering scheme. Since the porosity data were more consistent and accurate, the algorithm was only applied to porosity modeling.

Methodology: A RMSipl script is executed and it exports the combination sequence and the remaining total heterogeneity of the current grid scheme. Then the script loops through all the two-layer pairs of a grid, and finds the pair with the minimum variation. When combining that pair (of layers), the heterogeneity change is the smallest at that stage; in other words, the reservoir heterogeneity is maximum preserved. The optimal number of layers is picked from the plot of heterogeneity versus model layers. The executed workflow is shown in Figure A1.

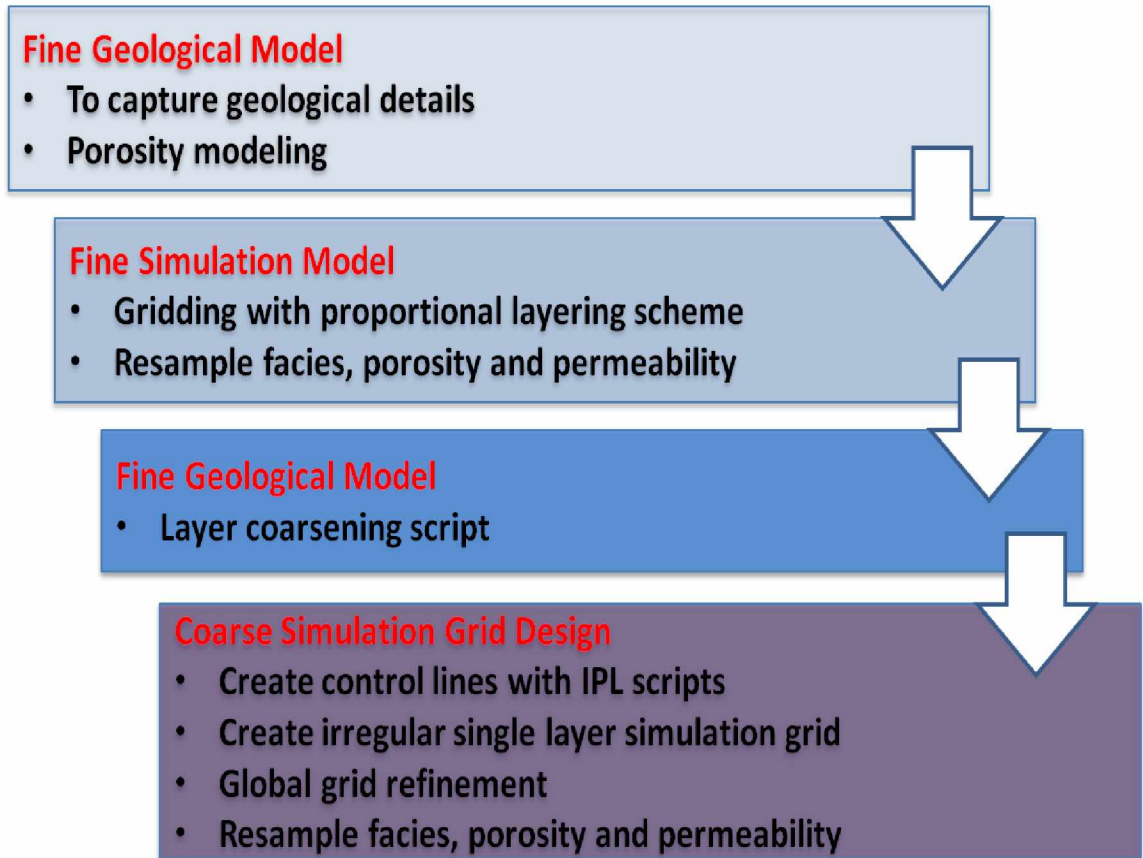


Figure A1. Workflow for layer coarsening scheme in the geologic model

The most similar layers have the smallest variation change ΔW_k , $K=1, \dots, NZ-1$, so if the two layers are merged, total variation change is the smallest. In other words, maximum heterogeneity is kept. As described by the equation 10:

$$\Delta H_{\text{new}} = \Delta H_{\text{old}} - \Delta W_{\text{smallest}} \quad (10)$$

The algorithm consisted of three steps (Figure A2):

Step 1: For a given fine simulation grid, the IPL script loops through all layer pairs ($NZ - 1$) and determine the most similar pair with the smallest variation change

Step 2: Step 2: Merge the pair and update the total number of layers to ($NZ = NZ - 1$)

Step 3: Repeat step 1 and 2 until there is only a single layer left



Figure A2. Step by step illustration of layer coarsening algorithm

The Optimal Number of Layers: At each step (merging two layers), the remaining heterogeneity is calculated and for convenience, the remaining heterogeneity is converted to a percentage ($H_{\text{current}} / H_{\text{original}}$). The heterogeneity is plotted versus model layers (Figure A3). Another parameter that should be considered is the total number of cells that

can be handled by the available computational capacity. A compromise has to be made if the total cell numbers exceeds the computational limit. The optimal number of layers was picked as $Z=78$ for the whole reservoir from the plot of heterogeneity versus model layers which corresponded to 100% heterogeneity.

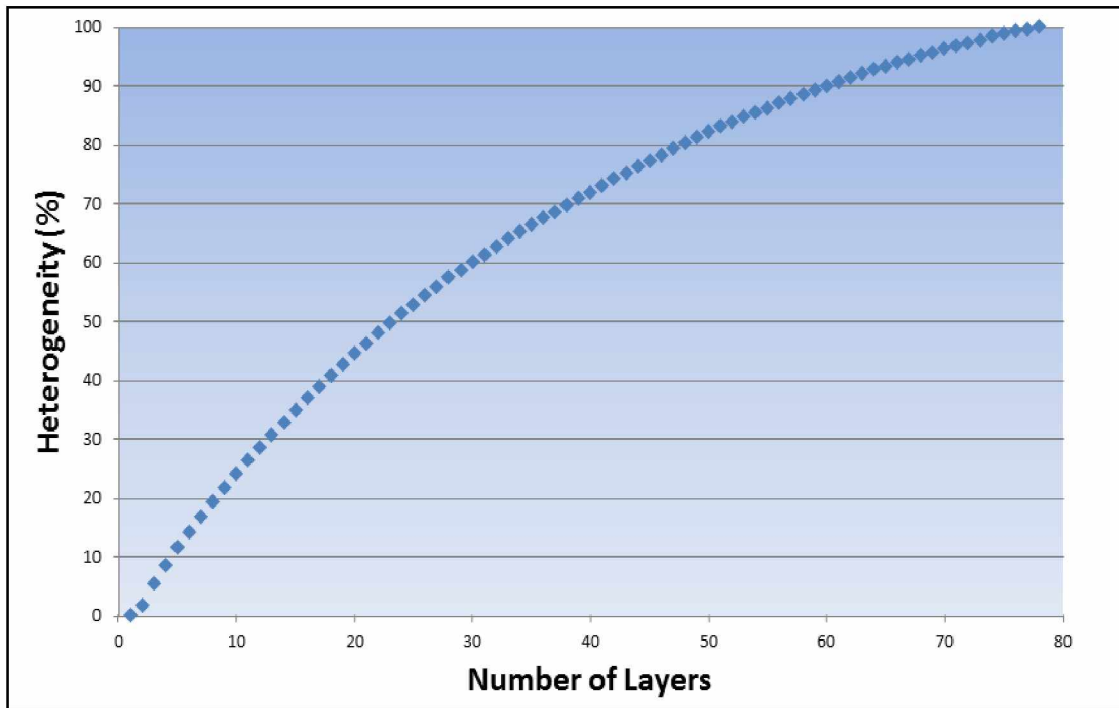


Figure A3. The relationship between degree of heterogeneity and the layer coarsening based on porosity modeling

APPENDIX B. New Well Pick Data

Table B.1. Well pick data for Chandler horizon in the updated model geometry

MD, Ref RKB (ft)	Well	Horizon	Trajectory
390.16	UMIAT-06	Chandler	Drilled
419.99	SEABEE-01	Chandler	Drilled
544.99	UMIAT-07	Chandler	Drilled
810.08	UMIAT-10	Chandler	Drilled
1060.19	UMIAT-01	Chandler	Drilled
2189.99	UMIAT-11	Chandler	Drilled

Table B.2. Well pick data for UGS horizon in the updated model geometry

MD, Ref RKB (ft)	Well	Horizon	Trajectory
360.45	UMIAT-05	UGS	Drilled
377.00	UMIAT-09	UGS	Drilled
385.00	UMIAT-02	UGS	Drilled
651.17	UMIAT-08	UGS	Drilled
655.19	UMIAT-06	UGS	Drilled
701.00	SEABEE-01	UGS	Drilled
815.99	UMIAT-07	UGS	Drilled
1055.19	UMIAT-10	UGS	Drilled
1330.18	UMIAT-01	UGS	Drilled
1880.00	UMIAT-11	UGS	Drilled

Table B.3. Well pick data for Shale barrier horizon in the updated model geometry

MD, Ref RKB (ft)	Well	Horizon	Trajectory
366.26	UMIAT-03	Shale barrier	Drilled
448.96	UMIAT-04	Shale barrier	Drilled
455.00	UMIAT-05	Shale barrier	Drilled
468.50	UMIAT-02	Shale barrier	Drilled
527.18	UMIAT-09	Shale barrier	Drilled
701736.65	UMIAT-06	Shale barrier	Drilled
767.00	SEABEE-01	Shale barrier	Drilled
883.50	UMIAT-07	Shale barrier	Drilled
1065.20	UMIAT-08	Shale barrier	Drilled
1178.27	UMIAT-10	Shale barrier	Drilled
1438.82	UMIAT-01	Shale barrier	Drilled
2526.50	UMIAT-11	Shale barrier	Drilled

Table B.4. Well pick data for Upper LGS horizon in the updated model geometry

MD, Ref RKB (ft)	Well	Horizon	Trajectory
642.36	UMIAT-03	Upper LGS	Drilled
740.00	UMIAT-04	Upper LGS	Drilled
780.00	UMIAT-05	Upper LGS	Drilled
790.00	UMIAT-02	Upper LGS	Drilled
870.00	UMIAT-09	Upper LGS	Drilled
1000.16	UMIAT-06	Upper LGS	Drilled
1020.03	SEABEE-01	Upper LGS	Drilled
1200.00	UMIAT-06	Upper LGS	Drilled
1260.00	UMIAT-06	Upper LGS	Drilled
1313.20	UMIAT-06	Upper LGS	Drilled
1740.00	UMIAT-06	Upper LGS	Drilled
2800.01	UMIAT-06	Upper LGS	Drilled

Table B.5. Well pick data for Middle LGS horizon in the updated model geometry

MD, Ref RKB (ft)	Well	Horizon	Trajectory
830.00	UMIAT-04	Middle LGS	Drilled
860.00	UMIAT-05	Middle LGS	Drilled
880.00	UMIAT-02	Middle LGS	Drilled
950.00	UMIAT-09	Middle LGS	Drilled
1790.00	UMIAT-01	Middle LGS	Drilled
2940.00	UMIAT-11	Middle LGS	Drilled

Table B.6. Well pick data for Lower LGS horizon in the updated model geometry

MD, Ref RKB (ft)	Well	Horizon	Trajectory
880.00	UMIAT-05	Lower LGS	Drilled
900.00	UMIAT-02	Lower LGS	Drilled
960.00	UMIAT-09	Lower LGS	Drilled
1820.00	UMIAT-09	Lower LGS	Drilled
2960.00	UMIAT-11	Lower LGS	Drilled

Table B.7. Well pick data for Base of Grandstand horizon in the updated model geometry

MD, Ref RKB (ft)	Well	Horizon	Trajectory
1002.00	UMIAT-03	Base of Grandstand	Drilled
1040.00	UMIAT-05	Base of Grandstand	Drilled
1050.00	UMIAT-02	Base of Grandstand	Drilled
1080.00	UMIAT-09	Base of Grandstand	Drilled
1347.81	UMIAT-06	Base of Grandstand	Drilled
1383.67	SEABEE-01	Base of Grandstand	Drilled
1970.00	UMIAT-01	Base of Grandstand	Drilled
3090.00	UMIAT-11	Base of Grandstand	Drilled

APPENDIX C. Kelly Bushing depths and Tie-in Points

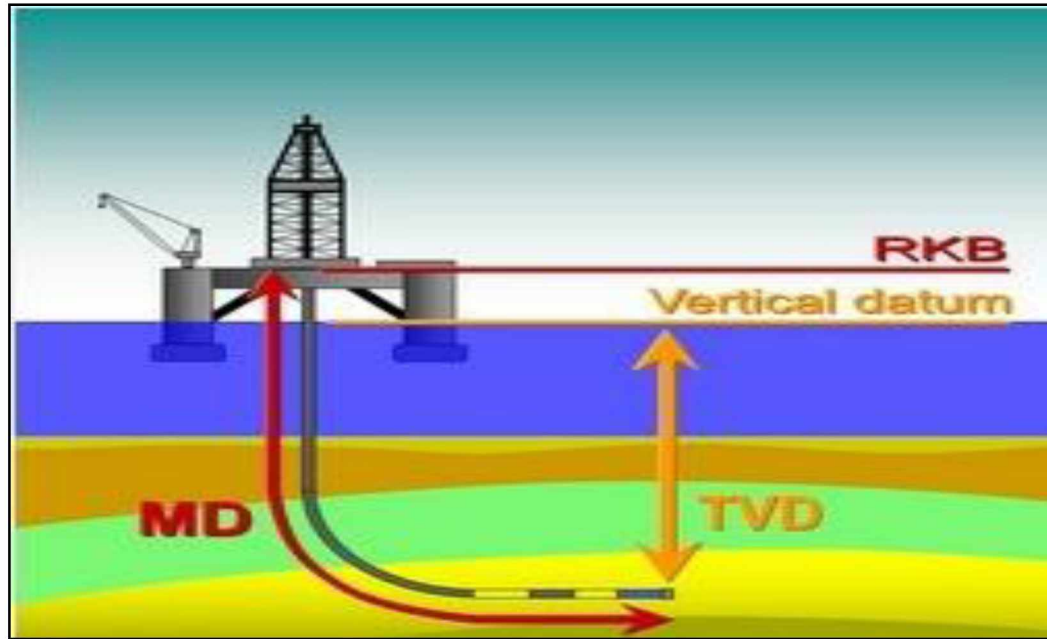


Figure C.1 RKB configuration with respect to well pad

Table C.1 RKB depth and tie-in points for each well pad used in the model

	Pad #1	Pad #2	Pad #3	Pad #4	Pad #5
RKB (ft)	241	249	230	241	260

Table C.2 Tie-in depth for different wells used in the well designing

Well	Tie-in point (ft) Measured Depth	Well	Tie-in point (ft) Measured Depth	Well	Tie-in point (ft) Measured Depth
2	-150	i13L	-170	26L	-169
i2	-152	14	-156	i26L	-170
3	-154	i14	-161	27	-158
i3	-156	14L	-172	i27	-160
4	-150	i14L	-174	27L	-168
i4	-152	16	-150	i27L	-170
4L	-162	i16	-152	28	-156
i4L	-163	17	-154	i28	-161
5	-154	i17	-156	28L	-172
i5	-158	18	-150	i28L	-174
5L	-164	i18	-152	30	-150
i5L	-166	18L	-166	i30	-152
6	-158	i18L	-168	31	-154
i6	-160	19	-154	i31	-156
6L	-168	i19	-156	32	-150
i6L	-170	19L	-169	i32	-152
7	-156	i19L	-170	32L	-166
i7	-161	20	-158	i32L	-168
7L	-172	i20	-160	33	-154
i7L	-174	20L	-168	i33	-156
9	-150	i20L	-170	33L	-169
i9	-152	21	-156	i33L	-170
10	-154	i21	-161	34	-158
i10	-156	21L	-172	i34	-160
11	-150	i21L	-174	34L	-168
i11	-152	23	-150	i34L	-170
11L	-166	i23	-152	35	-156
i11L	-168	24	-154	i35	-161
12	-154	i24	-156	35L	-172
i12	-156	25	-150	i35L	-174
12L	-169	i25	-152		
i12L	-170	25L	-166		
13	-158	i25L	-168		
i13	-160	26	-154		
13L	-168	i26	-156		

Appendix D. Economic Model

Many aspects of projects must be analyzed and approved before project execution. Alaska is a stable domestic environment with lots of investment incentives. Nevertheless, drilling and operating costs in Alaska are more expensive compared to other locations in the world. From a business perspective, without financial viability the project cannot go forward. In order to evaluate the fiscal parameters involved in the business aspects of Umiat field, it is essential to develop an economic model to provide information about economic performance of the field that can be expected from the project and justify the qualitative and quantitative measure for project rejection or acceptance.

The Microsoft Excel program was utilized to build the model. The model used the simulation results from the base case model for a 50 year economic evaluation (2013 to 2063). Some of the financial metrics and model parameters used in the model are listed in Table D.1.

Injection gas required to achieve desired simulated oil rates is provided from the Torok Formation at no cost (Linc Energy Report 2012).

Table D.1. Financial metrics and economic model parameters

Parameter	Value
Oil price per barrel	\$90
Labor salary per year	\$4,000,000
Labor salary change per year	2%
Biennial well interventions	\$6,000,000
Upfront costs (divestment, sucker rods, etc.)	\$35,000,000
Production cost per barrel	\$13
Small producer credit (less than 100,000 bpd)	\$12,000,000
Primary credit	20% of capital expenditures
Discount rate *	10%
Federal Royalty	12.5%
Base tax rate	25%

*Base case

The procedure for calculating tax liability for the economic model is as follows:

- 1) Calculate wellhead price.
- 2) Calculate production tax value (wellhead price less deductible capital and operating expenditures).
- 3) Calculate production tax value per barrel (production tax value divided by barrels produced in state, including royalty barrels).

4) Calculate tax rate (25% base tax, plus 0.4% for every \$1 per barrel that PTV exceeds \$30, up to \$92.50, then 0.1% for every \$1 per barrel that PTV exceeds \$92.50. Example, at \$50 / barrel PTV the tax rate will be 33%).

5) Calculate liability before credits (tax rate times production tax value)

6) Calculate credits (20% of capital expenditures is primary credit, and small producer credit).

After tax liability was calculated, the net present value (NPV) was calculated by using Equation 11.

$$NPV = \frac{FCF}{(1+i)^t} \quad (11)$$

Where:

FCF = Free Cash Flow

i= Discount rate

t= time

Discount rate: A key component of NPV analysis is the selection of the discount rate, the i in the equation above. It is defined as the “risk-adjusted cost of capital” for a specific project at hand. Since the discount rate of a function of company capital asset and there was no data available, a value was selected as the base case and sensitivity analysis was done to provide different outputs for the economic evaluations.

Internal Rate of Return: The internal rate of return is the discount rate that results in the NPV of the expected cash flow stream having a value of exactly zero. A project with an IRR greater than the minimum rate of return (discount rate) is an acceptable investment.

Table D.2 shows the NPV as a function of discount rate and their corresponding IRR values.

Table D.2. Project NPV and IRR for case with available gas supply

Discount rate (%)	NPV (\$)	IRR (%)
6	2,982,159,234	12
8	2,484,800,262	11.73
10	2,134,045,358	11.40
12	1,874,237,360	10.74
14	1,674,012,671	10.34
16	1,514,726,148	10.15
18	1,384,732,514	10.01
20	1,276,428,299	9.75

Appendix E. Digital Project Archive

The simulation model data files for this research are archived on the attached CD. It includes two separate folders for geologic modeling and reservoir simulation. The geologic data files can be run on RMS IRAP™ to update the geologic structures and petrophysical property modeling workflows. The simulation modeling files can be run on CMG IMEX™ simulation software to predict various production strategies at different time step in the life of the reservoir. The CD also includes an Excel file that explains each simulation run and the economic model parameters. The results can be directly incorporated into reservoir engineering model by generating a respective output file. The Non-Darcy effects on gas injections are also included in the CD.